REGULATION OF WNT DELIVERY AT INTESTINAL STEM CELL NICHE

by

SOUMYASHREE DAS

A dissertation submitted to the Graduate School-Newark

Rutgers, The State University of New Jersey

In partial fulfillment of the requirements

For the degree of

Doctor of Philosophy

Graduate Program in Biological sciences

Written under the direction of

Nan Gao, Ph.D.

And approved by

_____

_____

_____

_____

_____

Newark, New Jersey

January 2016

ABSTRACT OF THE DISSERTATION

REGULATION OF WNT DELIVERY AT INTESTINAL STEM CELL NICHE

By SOUMYASHREE DAS

Dissertation Director:

Nan Gao, Ph.D.

Communication between stem cells and its niche-supporting cells maintains the homeostasis of adult tissues. Wnt signaling is a critical regulator of stem cell niche, but the mechanism that governs Wnt-ligand delivery in this compartment has not been fully investigated. We identified that Wnt secretion is partly dependent on Rab8a-mediated anterograde transport of Gpr177/Wntless, a Wnt-specific transmembrane transporter. Gpr177 binds to Rab8a, depletion of which compromises Gpr177 traffic thereby weakening the secretion of multiple Wnts. Analyses of generic Wnt/β-catenin targets in *Rab8a* knockout mouse intestinal crypts indicate reduced signaling activities. There, maturation of Paneth cell–a Wnt-dependent cell type is severely affected. *Rab8a* knockout crypts show an expansion of Lgr5+ and Hopx+ cells in vivo. However, in vitro, the knockout enteroids exhibit significantly weakened growth that can be partly restored by exogenous Wnts or GSK3β inhibitors. Immunogold labeling and surface protein isolation identified decreased plasma membrane localization of Gpr177 in *Rab8a* knockout Paneth cells and fibroblasts. On stimulation by exogenous Wnts, *Rab8a* deficient cells show ligand-induced Lrp6 phosphorylation and transcriptional reporter

activation. Rab8a thus controls Wnt exocytosis in ligand producing cells and is critical for Paneth cell maturation. Additionally, deletion of *Gpr177* alone from epithelium and underlying mucosal layer of intestine showed only subtle changes in stem cell number in vivo. However interestingly, significant deterioration in stem cell activity led to death of all *Gpr177* null organoids within 4 days in culture. Taken together our data highlight profound tissue plasticity in vivo in response to stress induced by depletion of a stem cell niche signal.

ACKNOWLEDGEMENTS

I would first like to thank Nan, my thesis advisor, who always encouraged me to work hard (and smart!) and helped me realize my highest potential. I also thank him for providing me the opportunity to be a part of many collaborative projects and several conferences that helped me hone my technical and intellectual skills.

I would also like to thank Ed, my co-advisor, for being a mentor who was of great help at every step of my PhD career- starting from useful scientific feedback in lab meetings to easing administrative hassles. But more importantly, his love for basic science has been a constant source of inspiration.

Special thanks to the rest of my thesis committee- Dr. Haesun Kim, Dr. Gregory Weber and Dr. Ron Ferraris for their tremendous help and useful suggestions in the thesis committee meetings. I thank every member for the committee for being so approachable and patient with me throughout.

Thanks Alex, for taking me in as a mentoring and rotation student during my initial days in the PhD program and introducing me to "RE"-search. I admire your humorous scientific (and non-scientific) comments in the lab meetings which always lightened me up if experiments did not work.

I additionally thank all faculty members in cell and molecular biology community at Rutgers Newark for their comments and suggestions during my presentations at Biology colloquium and the annual research day(s).

Thank you Larry, Kay, Steve and Robert at the mouse facility who have helped me manage numerous mouse-lines and kept me informed even on weekends.

Most importantly (BIG!) thanks to all former and present members of LSC who have been great friends throughout. Ryo- who helped me settle down in the lab when I initially joined as a PhD student; Connie, Xiao, Kavya, Chaitali, Pavan, Rucha, Jiji, Ming, Natasha and Lissette for your constant love and support; The newbies- Brian, Justin and Huri, I have always drawn inspiration from your enthusiasm; Richard and Qiang for all the technical help; the talented undergraduates- Addie, Sreya and Lauren for their assistance and finally Juan- an all-rounder lab technician with skills that ranges from ordering lab reagents to performing sophisticated experiments. Thank you all for the beautiful people you are.

My friends abroad- Rasi, Pal and Su thank you for the love and moral support.

I would now like to thank my family in the States and back home for being patient with me and not disowning me for my absence in most of the family functions and trips. I love you all.

Special thanks to the greatest friend, philosopher and guide- Tarun. Thank you for being my sink.

My sister-Sudha, brother-in-law- Himanshu and my adorable nephew- Aarush, thank you for the unconditional love.

Finally, I would like to dedicate this work to my dearest parents. Thank you for your (overwhelming!) love and support throughout- at every step of my life. Thank you for being the rock of my life. I love you guys.

TABLE OF CONTENTS

Page

LIST OF ILLUSTRATIONS

Figure **Page**

LIST OF TABLES

Table **Page**

LIST OF APPENDICES

Page

CHAPTER 1

BACKGROUND AND INTRODUCTION

Information included in this chapter is taken from and are published in Das et al., Development (2015) ;142(12):2147-62 and Das et al., Fron. of Bio. (2012); *7*, 587-593.

Organization of intestinal epithelium in mouse

Fast regeneration, presence of entire generative hierarchy of cell population and integration of critical morphogenetic signaling pathways makes intestine an outstanding model to study tissue development and its maintenance. Additionally, the capability of intestinal tissue to be cultured in vitro in three dimensions, allows researchers to study and manipulate genetic as well as micro-environmental factors that maintain them in functional organs. Such in vitro cultures of intestinal crypts are called mini-gut, organoid or enteroid and are conveniently maintained in presence of few critical growth supporting supplements such as EGF, Noggin and R-Spondin (ENR, discussed later).

Adult intestinal epithelium has primarily two structural components as discussed below- the upward projections into intestinal lumen called villi and downward invaginations into the mesenchyme called crypts of Liberkuhn or crypts (**Fig. 1C**). In early embryonic stage E14.5 in mice, remodeling of endodermal sheet into stratified epithelium gives rise to a tube like structure of digestive tract. At this stage the embryonic gut is lined by multiple layers of undifferentiated proliferating cells. At E15, geometric changes in mesenchyme underlying the intestinal epithelium lead to villus morphogenesis and restriction of proliferative cells to the inter-villus regions. Unlike villus morphogenesis event, crypts are formed after birth. Crypts originate due to invagination of inter-villus epithelium into the mesenchyme around postnatal day 7 (**Fig. 1A**).

In adult mice, the intestinal epithelium is continuously renewed by stem cells residing at the crypts (**Fig. 1C**). These stem cells are otherwise called as crypt base columnar stem cells (CBCs) that give rise to proliferative population of multi-potent progenitor cells known as transit amplifying (TA) cells. There are majorly four types of differentiated cell population arising from the TA cells (**Fig. 1B**). Firstly, absorptive cells (enterocytes) function to intake nutrients from the intestinal lumen and compose a significant portion of villi. Secondly, goblet cells secrete mucin and protect the epithelial layer of intestine from microbial invasion. Next are enteroendocrine cells that secrete neuropeptides and hormones in response to dietary or bacterial stimuli. Finally, Paneth cells secrete anti-microbial peptides and growth factors that support the CBCs. As the TA cells divide and differentiate, the daughter cells migrate upwards along the villi and are eventually shed into the lumen as their life cycle completes. An exception however is Paneth cell that escapes the usual trend of upward migration and instead co-occupies the crypt base with intestinal stem cells (**Fig. 1C**).

Combination of molecular signals maintain intestinal crypt cells

The remodeling of mammalian intestine from endoderm to organized crypt-villus structure and maintenance of adult intestines are dependent on several cues derived from epithelial and mesenchymal cells. In particular, the intestinal stem cell (ISC) microenvironment consists of several signaling molecules provided by Paneth cells and underlying fibroblasts in close proximity of stem cells. Thus the intestinal crypt compartment is a hub of signaling events that together maintain proliferation and self-

renewal of ISCs. Due to its high turnover, ISCs are likely to accumulate mutations that make them sensitive to the precise regulation of their niche composition.

Wnt is an essential growth factor in intestinal stem cell niche

Among various cell types that produce distinct cohorts of Wnts surrounding intestinal stem cell niche (Gregorieff et al., 2005), Paneth cells are the major epithelial Wnt producers that produce Wnt3 and co-occupy the crypt bottom with stem cells (Sato et al., 2011). The self-renewal of fast-cycling $Lgr5^+$ stem cells (Barker et al., 2007), which emerges as organoid-forming capacity in culture, is enhanced by their close association with Paneth cells or by addition of exogenous Wnt ligands (Sato et al., 2011). Although depletion of Paneth cells is indispensable for organoid survival ex vivo, the same does not seem to be the case in vivo. Ablation of Paneth cells in several mouse models caused recoverable loss of $Lgr5^+$ stem cells in vivo (Kim et al., 2012). For instance, Atoh1 deficient mouse intestines with an absence of Paneth cell differentiation preserved functional intestinal epithelia (Durand et al., 2012; Kim et al., 2012), suggestive of high plasticity demonstrated by crypt cells (Tetteh et al., 2014). In addition to Paneth cells, subepithelial stromal cells express Wnt2b, Wnt4, and Wnt5a (Farin et al., 2012; Gregorieff et al., 2005; Miyoshi et al., 2012). $Wnt5a^+$ mesothelial cells contribute to regenerating nascent crypts after tissue injury (Miyoshi et al., 2012). Intestinal epithelia-specific ablation of Wnt3 (Farin et al., 2012), or Porcupine (a Wnt specific enzyme that post-translationally modifies and facilitates Wnt secretion) deletion in both epithelia and myofibroblasts (Kabiri et al., 2014; San Roman et al., 2014) did not cause detectable

tissue degeneration. In culture, Wnt3-deficient intestinal organoids fail to propagate, whereas administration of Wnts is able to restore the growth (Farin et al., 2012), collectively suggesting that multiple sources of Wnts redundantly support the stem cell niche. Based on Reverse transcription PCR (RT-PCR) and in-situ hybridization analysis, **Table 1** and **Table 2** summarize gene expression levels of different Wnts and Wnt receptors (Frizzleds) in small intestinal tissue (Farin et al., 2012; Gregorieff et al., 2005). In addition to Paneth cells and sub-epithelial fibroblasts there might exist other source(s) of Wnts that supports stem cell activity in absence of Paneth or mucosal fibroblasts; such as endothelial cells, immune cells or neurons.

Hedgehog-BMP relay maintain Wnt signaling at crypt base

In adult mice, epithelial cells at the crypt compartment secrete Sonic Hedgehog (Shh) and Indiana Hedgehog (Ihh) that through long range signaling activate Bone Morphogenetic Protein (BMP) in the mesenchyme underlying villi (Madison et al., 2005). BMP activity in the villi region inhibits Wnt/β-catenin signaling in proximity thus limiting the proliferative zone to crypt bases (He et al., 2004). Note that, gradient of Wnt is exactly opposite to the gradient of BMP (**Fig. 1D**). Presence of another signaling molecule Noggin, a BMP inhibiter, at mesenchyme underlying crypt epithelial cells ensures inactivation of BMP signaling at the crypt base hence indirectly maintaining Wnt signaling in the crypt compartment (Haramis et al., 2004; He et al., 2004; Karlsson et al., 2000). Additionally, Wnt is not only produced by crypt epithelial cells (such as Paneth cells) but also by a population of fibroblasts underlying the crypt epithelium (Farin et al.,

2012). This autocrine and paracrine Wnt signaling at crypt compartment maintains epithelial (Paneth and stem cells) and mesenchymal (fibroblasts) cells.

Wnt and Notch cooperatively maintain CBCs

Presence of both Wnt and Notch activity is essential to drive stemness in CBCs (Yin et al., 2014). For instance, when a transcription factor in Notch pathway (Recombination Signal Binding Protein for Immunoglobin kappa J region (RBP/J)) is deleted in mice, secretory cells especially goblet cells are overproduced at the expense of proliferative cells (van Es et al., 2005). Interestingly, inhibition of Notch in Wnt-hyperactive mice $Apc^{min/+}$ mice using γ-secretase led to reduced proliferation in microadenomas where canonical Wnt signaling is hyper-active (van Es et al., 2005). Hyperactivation of Notch was unable to drive proliferation in villi where Wnt activity is low but was able to enhance proliferation in intervillus regions in mouse embryos where Wnt activity is high (Fre et al., 2005). Thus, data suggest that Notch activity is capable of driving proliferation only in presence of canonical Wnt activity but the converse is not true and hence the following model may be deduced. Differentiation of TA cells into either absorptive or secretory precursors is determined by the presence or absence of Delta protein, a known ligand for Notch signaling, in these cells. Expression of Delta leads to Notch deactivation and absence of Delta leads to Notch activation. The precursor cells that escape Notch activation differentiate into secretory cells (Paneth, enteroendocrine or goblet cells). In contrast, progenitor cells with active Notch signaling

give rise to enterocytes. Thus, ISCs and TA cells respond to Wnt and Notch jointly, the combination of which ultimately decides their fate.

Intestine demonstrates profound plasticity

CBCs are actively cycling stem cells marked by several proteins such as Lgr5 and Olfm4. It has been proposed that upon quantitative loss of $Lgr5^+$ stem cells, a typically quiescent "reserve" stem cell pool rejuvenates the epithelia (Tian et al., 2011). These stem cells are considered to be slow-cycling, predominantly found at "+4" crypt positions, irresponsive to Wnt perturbation and identified by several markers, including Bmi1 (Sangiorgi and Capecchi, 2008), Hopx (Takeda et al., 2011), Lrig1 (Powell et al., 2012) and mTert (Montgomery et al., 2011). Lineage conversion from these alleged quiescent cells to $Lgr5^+$ cells were observed during homeostasis or epithelial injury (Takeda et al., 2011; Tian et al., 2011; Yan et al., 2012). However, all these markers were found highly expressed in $Lgr5^+$ cells (Munoz et al., 2012; Wong et al., 2012), and also in a subset of $Lgr5^+$ label retaining cells (LRCs) (Buczacki et al., 2013). This subset of $Lgr5^+$ cells were recently proposed to be secretory precursors for Paneth and enteroendocrine cells, and could be reactivated by injury for epithelial regeneration (Buczacki et al., 2013; Roth et al., 2012). In a parallel study, $Dll1^+$ secretory precursors were shown to revert to stem cells upon injury to regenerate the epithelia (Farin et al., 2012). These secretory precursors are postulated to represent the alleged +4 quiescent cells (Tetteh et al., 2014). However, different from $Lgr5^+$ cells, $Bmi1^+$ cells were shown to resist Wnt

perturbation and radiation injury (Yan et al., 2012). Thus, whether a dedicated quiescent stem cell population truly exists is still under debate (Tetteh et al., 2014).

Canonical Wnt signaling is essential for intestinal crypt homeostasis

Wnt proteins are cysteine-rich glycolipoproteins acting as paracrine or autocrine ligands believed to engage in short-range signaling (Willert et al., 2003; Willert and Nusse, 2012). Signal transduction in Wnt-responding cells is initiated by binding of Wnts to their 7-pass transmembrane Frizzled (Fzd) receptors (Schulte, 2010; Schulte and Bryja, 2007; Wu and Nusse, 2002). Wnt-Fzd complex recruits cytoplasmic protein Dishevelled (Dvl) (Wong et al., 2003), in association with the Low-density lipoprotein receptor-related protein 5 and 6 (Lrp5/6), triggering the assembly of a multiprotein complex at plasma membrane (Bilic et al., 2007). This plasma membrane localized protein complex, sometimes referred to as the "Wnt signalosome" (Bilic et al., 2007), inactivates a cytoplasmic destruction machinery consisting of Casein kinase 1, Glycogen synthase kinase 3 (GSK3), Axis inhibitor (Axin), Adenomatosis polyposis coli, and an E3 ubiquitin ligase β-Trcp, causing β-catenin stabilization (Cadigan and Peifer, 2009; Huang and He, 2008; MacDonald et al., 2009) and transcriptional activation of Wnt targets (Gerges et al., 2004; MacDonald and He, 2012; Tamai et al., 2000; Wehrli et al., 2000). This signaling cascade, often referred to as the canonical Wnt pathway, plays fundamental role in fetal development and adult tissue homeostasis (Clevers, 2006; Clevers and Nusse, 2012).

Global or intestine specific deletions of several genes associated with canonical Wnt pathway have been reported to disrupt intestinal homeostasis leading to lethality in mice. Tcf4 and β-catenin are two such well-studied genes, the conditional deletion of which leads to lack of proliferation in crypt compartments eventually leading to death of mice (Fevr et al., 2007; Korinek et al., 1998; van Es et al., 2012a). A similar phenotype was observed when Wnt signal transduction was inhibited with adenoviral expression of a secreted Wnt antagonizer, Dkk1, in adult mice (Kuhnert et al., 2004). In all three instances, severe architectural degeneration followed loss of crypts and villi in the intestine, establishing the essential role of Wnt pathway in maintaining adult tissue homeostasis. Additionally, inappropriate activation of this pathway in diseases especially colon cancers has highlighted its profound influence on cellular behavior (Angers and Moon, 2009; Clevers and Nusse, 2012; de Lau et al., 2007; MacDonald et al., 2009; Nusse et al., 2008; Polakis, 2007; Reya and Clevers, 2005). Hyper-activation of Wnt signaling pathway can be achieved by either stabilizing β-catenin (Andreu et al., 2008; Romagnolo et al., 1999) or deactivating APC (Andreu et al., 2008) which leads to adenoma formation in intestine and eventual death of mice. In concurrence, 90% of human colorectal cancer cases have been linked to genetic mutations associated with Wnt pathway including *β-catenin, APC or Axin1/2* (Cancer Genome Atlas, 2012). Extensive studies have been performed to understand the role of Wnt pathway members involved in signal transduction, and intestine specific perturbation of these gene-functions, even for an acute period, is sufficient to generate such severe consequences (Reviewed in (van Amerongen and Berns, 2006)).

Gpr177 is a unique Wnt ligand transporter conserved across species

Wnts are acylated and glycosylated secretory proteins with established roles in embryonic development and tissue homeostasis (Logan and Nusse, 2004; Sato et al., 2011). Extensive studies have been performed on Wnt downstream signaling events, which regulate target gene expression in signal-receiving cells (Clevers, 2006; Logan and Nusse, 2004; MacDonald et al., 2009). However, less is known about Wnt trafficking in ligand-producing cells, and a great amount of interest is now dedicated to dissecting the Wnt secretory pathways completely.

Wntless: biochemical and molecular characteristics.

Discovered in 2006, Wntless (Wls or Evenness Interrupted/Sprinter in *Drosophila*, MOM-3/Mig-14 in *C. elegans,* and GPR177 in mammals) is an evolutionarily conserved trans-membrane protein, indispensible for the secretion of multiple Wnt proteins (Banziger et al., 2006; Bartscherer et al., 2006; Belenkaya et al., 2008; Franch-Marro et al., 2008; Goodman et al., 2006; Port et al., 2008; Silhankova et al., 2010; Yang et al., 2008). Studies to date show that depletion of Wntless in both vertebrates and invertebrates gives rise to Wnt loss-of-function phenotypes (Barrott et al., 2011; Belenkaya et al., 2008; Carpenter et al., 2010; Franch-Marro et al., 2008; Port et al., 2008; Silhankova et al., 2010; Yang et al., 2008), thus illustrating a fundamentally conserved function of Wntless in Wnt secretion (MacDonald et al., 2009).

Structural details of Wntless protein have provided the first piece of evidence in support of its role in intracellular Wnt trafficking. Through amino acid sequence analysis

Wntless is predicted to contain a long N-terminal region, seven or eight transmembrane segments and an intracellular C-terminus similar to the member of G-protein coupled receptor (GPCR) superfamily. Indeed, Wntless has been proposed as a putative orphan GPCR (Yu et al., 2010). However, there is a lack of evidence supporting whether or not Wntless may signal as a GPCR. As great structural and functional diversities lie within the GPCR superfamily, it is difficult to speculate function of Wntless purely based on our classic GPCR knowledge. In addition, Wntless contains almost no known motifs that are homologous to existing GPCRs, greatly impeding our understanding of its molecular function and regulation.

Like most GPCRs, Wntless is N-linked glycosylated (Yu et al., 2010). However, whether this glycosylation is essential for the interaction between Wntless and Wnts, or for the trafficking of Wntless itself, is not clear. In terms of the structural property of Wnts for the recognition by Wntless, a conserved serine residue within most of Wnts (e.g. Ser239 in *Drosophila* Wg) has been elucidated to be indispensable for their interaction with Wntless (Gasnereau et al., 2011). Substitution of this serine residue with alanine significantly affects the physical association of Wnts with Wntless. However, the detailed mechanism and the signal that triggers the recognition and binding of Wnts to Wntless still remain elusive.

Similar to many known GPCRs, Wntless can be internalized from the cell membrane through endocytosis (Harterink et al., 2011; Pan et al., 2008; Port et al., 2008). Indeed, a conserved YXXΦ endocytotic motif has been identified in the third intracellular loop of Wntless. This motif serves as an endocytic signal for recognition by

a clathrin adaptor protein 2 (AP2), and is critical for recycling Wntless from the plasma membrane (Gasnereau et al., 2011). Site-directed mutation of a YEGL motif in Wntless results in its accumulation on the cell surface. But this sequestration of Wntless on the outer cellular membrane can be restored via the addition of classic YXXΦ motif to its C terminal tail. Interestingly, although this key motif is missing in the *C. elegans* Wntless homolog, a similar YNRI motif is found within the second intracellular loop instead.

Two independent studies have identified the interaction between Wntless and Vps35, a core subunit of retromers responsible for retrograde transport of Wntless from plasma membrane to Golgi (discussed in details below). These studies have promoted the discovery of FLM tripeptide motif at the end of the third intracellular loop of Wntless. This motif is required for retromer-dependent transportation. Immunofluorescence and co-immunoprecipitation studies indicate that Wntless localizes with yet another subunit of retromer, a cargo sorting protein Sortin Nexin 3 (SNX3) (Harterink et al., 2011; Zhang et al., 2011). Unfortunately, no further experiment have verified whether this interaction between Wntless and SNX3 is direct.

Taken together, further structural analysis of Wntless is needed to understand whether this GPCR-like protein can indeed recruit heterotrimic G-proteins and subsequently initiate related signaling pathways in the process of Wnt secretion.

Protein modifications of Wnts: Wntless-Wnts interplay

The posttranslational modifications of Wnts are critically coupled with their secretion and activity. Wnts are produced and then modified in ER by a membrane-

bound acyltransferase, Porcupine **(Figure 28A,iv)**, Porcupine is believed to facilitate the lipidation of Wnt proteins on at least two distinct sites: the N-terminal cysteine rich residues (Tanaka et al., 2002; Tanaka et al., 2000) and a C-terminal serine 209 residue (Coombs et al., 2010). The conserved cysteine residues at the N-terminus of Wnts are subjected to addition of palmitate groups (Takada et al., 2006). This cysteine rich locus creates a binding site for Porcupine (Tanaka et al., 2002), however whether Porcupine itself adds or merely facilitates addition of palmitate group to this locus, through other proteins, is less clear.

In contrast to uncertain role of Porcupine in Wnt palmitoylation at the cysteine rich residues, Porcupine is strongly believed to directly catalyze addition of palmitate group to the Serine 209 (Galli et al., 2007; van den Heuvel et al., 1993; Zhai et al., 2004). Mutation in *Porcupine* leads to impaired Wnt secretion suggesting the necessity of these lipid modifications for Wnt secretion (van den Heuvel et al., 1993).

Wntless has been found to be localized to ER, Golgi, vesicles and plasma membrane (Banziger et al., 2006; Bartscherer et al., 2006; Coombs et al., 2010; Fu et al., 2009), covering the entire Wnt-secretory route **(Figure 28A,iv)**. Having a lipocalin-like structure (Fu et al, 2009) makes Wntless capable of binding to hydrophobic regions like the palmitate groups in mature Wnts . The affinity of Wntless towards the hydrophobic regions in Wnts might facilitate the physical association of Wnts with Wntless. Indeed, palmitoylation at Ser209 in Wnt3a by Porcupine, but not at cysteine residues, is required for its physical interaction with Wntless (Coombs et al., 2010), and its release

from ER (Komekado et al., 2007; Takada et al., 2006; Willert et al., 2003). Consistently, reduced Ser209 palmitoylation of Wnt3a demonstrates ER retention (Takada et al., 2006), which reflects a defective Wnt secretion probably due to disrupted Wnt-Wntless association.

On the other hand, as impaired Wnt secretion likely affects downstream Wnt signaling as well, different interpretations of the experimental findings exist on whether a specific Wnt lipidation promotes only its secretion, signaling, or both (Sato et al., 2011). For example, absence of cysteine rich residues in Wnt1, Wnt3a and Wnt5a results in depleted Wnt signaling in vertebrates (Galli et al., 2007; Kurayoshi et al., 2007), whereas absence of palmitoylation at cysteine residue in *Drosophila* Wg causes ER retention (Franch-Marro et al., 2008). Whether it is the amino acid itself altering protein folding, or the lipid modification on the amino acids affecting Wnt secretion and signaling is yet to be established. Furthermore, the *Drosophila* Wnt D is recently identified as the only Wnt protein that neither requires lipid modification nor an association with Wntless for its secretion (Gasnereau et al., 2011; Henry and Sheff, 2008).

Another posttranslational modification undergone by the Wnts in the ER is N-terminal glycosylation. In *Drosophila*, N-terminal glycosylation at Ser239 is stimulated by Porcupine, and this modification is found to be indispensable for its interaction with Wntless (Tanaka et al., 2002). Overall, these data suggest that the posttranslational modifications of Wnts contribute to their transport and secretion from the ligand-

producing cells; however whether these specific modifications provide opportunities for precise regulation of Wnt trafficking and exocytosis via Wntless or other secretory pathway components awaits definitive studies.

Wnt-Wntless dissociation

Apart from post translational modifications, an interesting physical parameter that seems to have a strong impact on Wnt secretion is the environmental pH. Endosomal pH gradient plays an important role in the secretory pathway of proteins. An acidic pH ~ 5.5 of secretory vesicle appears to promote dissociation of Wnt3a from Wntless and facilitates Wnt secretion out of the cell (Coombs et al., 2010). The precise role of the endosomal pH gradient in Wnt secretory pathway is yet to be explored.

Retrograde trafficking of Wntless.

The fate of Wntless is distinct from Wnts after the Wnt-Wls protein complex reaches the plasma membrane. Wntless is recycled back into the Wnt-producing cells and reutilized for yet another round of Wnt secretion (Belenkaya et al., 2008; Franch-Marro et al., 2008; Port et al., 2008; Silhankova et al., 2010; Yang et al., 2008) **(Figure 27A,iv)**. Wntless is retrieved from the plasma membrane by early endosomes in clathrin coated (Harterink et al., 2011; Port et al., 2008) and Rab5 positive vesicles (Harterink et al., 2011; Rojas et al., 2008). This transport is also demonstrated to be AP2 and dynamin dependent (Belenkaya et al., 2008; Franch-Marro et al., 2008; Pan et al., 2008; Port et al., 2008; Silhankova et al., 2010; Yang et al., 2008).

From early endosomes, Wntless is carried to the Golgi in a Retromer-dependent manner in small vesicles (Belenkaya et al., 2008; Franch-Marro et al., 2008; Port et al., 2008; Silhankova et al., 2010; Yang et al., 2008) **(Figure 27A,iv)**. Retromer is a macromolecular complex of different protein subcomplexes including a cargo recognition Vps26-Vps29-Vps35 heterotrimer (Attar and Cullen, 2010; Seaman, 2005) and a cargo sorting, SNX-BAR (Sorting Nexin Protein with Carboxyl terminal Bin amphiphysin Rvs) hetero or homodimer (Carlton et al., 2004; Carlton et al., 2005; Wassmer et al., 2007). These SNX proteins contain BAR domains that tether them to specific regions of endosomal membrane, in this case phosphatidylinositol 3-phosphate (PI3P) rich region (Seaman, 2005). Hence the functionality of SNX proteins is also dependent on the overall lipid composition of the vesicular membrane and the activity of enzymes like PI3P phosphatases (Seaman, 2005). The Vps subcomplex identifies and binds to the cargo whereas SNX-BAR sorts out proteins into tubular structures, which are directed constitutively to different cellular subcompartments (Belenkaya et al., 2008; Franch-Marro et al., 2008; Harterink et al., 2011; Port et al., 2008; Silhankova et al., 2010; Yang et al., 2008).

In contrast to the above studies, it was recently found that SNX-BAR is dispensable for a retromer dependent Wntless recycling. Instead, Wntless retrieval is found to require SNX3, yet another nexin family protein without BAR domains (Harterink et al., 2011; Zhang et al., 2011). The absence of BAR domains in SNX3 facilitates formation of small endosomal vesicles rather than larger tubular structures. Probably this is how Wntless traffic is sorted from other housekeeping proteins in a

more regulated manner. SNX3 sorts Wntless traffic to the trans-Golgi network (TGN) by preventing it from degradation in lysosomes and hence promoting its stabilization. This sorting action is possibly achieved by SNX3 via recruitment of Vps26 to the endosomal membrane containing Wntless (Harterink et al., 2011).

Other experimental data from invertebrates illustrate the inevitability of Vps complex components Vps26 and Vps35 in the retrograde trafficking of Wntless from plasma membrane to the TGN (Belenkaya et al., 2008; Franch-Marro et al., 2008; Port et al., 2008; Silhankova et al., 2010; Yang et al., 2008). Hence overall it is believed that the retromer complex maintains the stability of Wntless (Belenkaya et al., 2008; Franch-Marro et al., 2008; Harterink et al., 2011; Port et al., 2008; Silhankova et al., 2010; Yang et al., 2008). How SNX3 recruits the Wntless-recognition retromer component to the endosomal membrane and the precise underlying mechanism that prevents the degradation of Wntless and instead retrieves it to TGN is still unclear.

Synaptic transmission of Wnts via Wntless

Till date it is known that Wntless is associated with Wnt secretion as discussed above, and is believed to be present in all Wnt-producing cells. Nonetheless, the precise function of Wntless in Wnt-receiving cells is obscure. RNAi studies in Drosophila neuromuscular junction show that Wnt1 travels through the synapse via exocytic vesicles containing multivesicular bodies (Korkut et al., 2009). The transport of Wnt1 from the cell body to the presynaptic terminal and further trans-synaptic transport to the post-synaptic terminal are found to be Wntless dependent. These vesicles are

endocytosed and the Wnt-Wntless complex is internalized by the post-synaptic neuron. Furthermore, Wntless appears to target a Wnt receptor interacting protein, dGRIP, to the post-synaptic plasma membrane (Korkut et al., 2009). This study demonstrates the role of Wntless in the post-synaptic terminal, which is comparable to Wnt-receiving non-neuronal cells. However, whether the same is true for vertebrates is yet to be established.

Gpr177 knockout mouse models: genetic insights into Wnt/Wntless function.

To investigate the role of Wntless in mammalian development, two independent groups have generated *Gpr177* knockout mouse models using different gene targeting strategies. Homozygous *Gpr177* knockout mice in both studies exhibited embryonic lethality (Carpenter et al., 2010; Fu et al., 2009). *Gpr177* knockout mice developed by Fu et al. survived through E10.5 while the ones by Carpenter et al. survived through E8.5. At E7.5-8.5 $Gpr177^{-/-}$ embryos lacked primitive streak and mesoderm hence morphologically appearing as an egg cylinder (Carpenter et al., 2010; Fu et al., 2009).

Studies of E6.5-7.5 embryos demonstrate that Gpr177-knockout affects β-catenin activation, hence the canonical Wnt-signaling pathway. This advises three possibilities: Gpr177 affects Wnt production, its secretion, or both. The first possibility is unlikely as Western blots for Wnt3 showed increased protein levels in E7.5 knockout embryos (Fu et al., 2009). This also suggests an accumulation of Wnt3 possibly due to a defective secretion. Alternatively, this Wnt protein accumulation may attribute to an autocrine regulatory mechanism that compensates for the reduced extracellular Wnts,

thus producing more Wnts within the cell. Absence of Gpr177 at E7.5 affects the accumulation of Wnt3 more severely than any other time point (E6.5 or E9.5) (Barrott et al., 2011; Fu et al., 2009). In contrast, absence of Gpr177 at E9.5 does not affect Wnt1 or Wnt5a levels (Barrott et al., 2011). These results advocate the presence of a narrow developmental window when individual Wnt proteins are actively secreted and hence are more sensitive to the availability of Gpr177. This calls for further studies to define this "window" for individual Wnts and characterize their dependability on Gpr177 for their secretion during this time period.

Wnt3 signaling is required for formation of anterior-posterior embryonic axis, which makes it essential for early embryonic development (Liu et al., 1999). The *Gpr177* knockout mouse phenotype resembles *Wnt3* knockouts, β-catenin mutants (Brault et al., 2001), as well as Wnt1 and Wnt3 double knockouts (Ikeya et al., 1997). The overall phenotypes in Gpr177 knockouts appear more severe than the phenotypes observed by knocking out Wnt1 alone (McMahon and Bradley, 1990; Thomas and Capecchi, 1990). Together, these observations further affirm the role of Gpr177 in secreting multiple Wnts in mammals (Carpenter et al., 2010; Fu et al., 2009).

In situ hybridization and immunostaining analysis show that Gpr177 is expressed in organs, such as inner ear (Yu et al., 2010), the development of which depends on both canonical and non-canonical Wnts. Loss of Gpr177 in mice clearly affects canonical Wnt signaling pathway suggested by the depletion of active β-catenin (Fu et al., 2009). Mouse Gpr177 is also associated with non-canonical Wnts such as Wnt5a that co-

immunoprecipitates with Gpr177 (Fu et al., 2009). Recently, it has been established that Gpr177 affects angiogenesis regulated by Wnt5a/11 secreted by retinal myeloid cells (Barrott et al., 2011; Stefater et al., 2011). Hence there is a possibility that Gpr177 might also affect cell polarity formation and epithelial to mesenchymal transition.

Gpr177 heterozygous mice are fertile but demonstrate certain developmental defects suggesting an essential Gpr177 dosage dependency (Carpenter et al., 2010; Fu et al., 2009). The phenotypes such as defects in the brain regions (i.e., telencephalon) observed by Carpenter et al. are more severe than those observed by Fu et al. The difference in mortality rate of embryos and severity of phenotypes between these models could be due to their gene targeting strategies.

Rab8a is an important regulator of post-golgi vesicular transport

Rabs are small GTPases that switch between a cytosolic (inactive) GDP bound form and membrane associated (active) GTP bound state. The property of membrane insertion and extraction of small GTPases allows them to act as molecular switches with spatial and temporal regulation of their function. This family of proteins belongs to Ras super family and usually classified based on their association with intracellular membrane compartments or specific signaling pathways (Hutagalung and Novick, 2011; Schwartz et al., 2007). Rabs are considered master regulators of vesicular trafficking and believed to facilitate several aspects of vesicular trafficking including budding of a vesicle from donor membrane, transport of vesicles as well as docking and fusion of vesicles on to target membrane (Stenmark, 2009). This property of Rabs allows them to

shuttle between compartments and interact with specific effectors to carry out their function. Rab8a is one such Rab that regulates vesicle trafficking from golgi to plasma membrane (Das and Guo, 2011; Hutagalung and Novick, 2011; Seabra et al., 2002).

Like most other Rabs, Rab8 is modified with a prenyl group at its C-terminus causing an increase in hydrophobicity which targets it to membrane compartments. Once delivered to the membrane Rab8 is activated by exchange of GDP for GTP by its Guanine nucleotide exchange factor (GEF) Rabin8 or MSS4 (Burton et al., 1994; Hattula et al., 2002). After one round of transport is performed, the GTP is hydrolyzed to GDP by its GTPase-activating protein (GAP) (TBC1D14 in mammalian cells (Vaibhava et al., 2012)) allowing it to be recognized by GDP dissociation inhibitor (GDI) which sequesters it in the cytosol. Thus an up or down regulation of GEFs, GAPs or GDIs in response to several stimuli may lead to activation of deactivation of these Rabs.

Rab8 has two isoforms namely Rab8a and Rab8b; that may co-exist with non-overlapping functions (Das et al., 2015; Demir et al., 2013). Rab8 is involved in post-golgi transport of several cargoes to the apical, basolateral or dendritic plasma membrane (Ang et al., 2003; Bryant et al., 2010; Haubruck et al., 1990; Henry and Sheff, 2008; Huber et al., 1993a; Huber et al., 1995; Huber et al., 1993b; Salminen and Novick, 1987; Sato et al., 2007) and is known to be essential for polarized transport in several cell types such as photoreceptor cells, neurons and melanocytes and transporting diverse cargoes including rhodopsin, melanosome, AMPA receptors and β-amyloid precursor in these cells (Chabrillat et al., 2005; Chakraborty et al., 2003; Deretic et al., 1995; Gerges

et al., 2004; Huber et al., 1995; McConlogue et al., 1996). Several other examples are available supporting the role of Rab8 in anterograde protein transport which include its involvement in transport of Huntington, Glut4, Transferrin, VSV-G, adherens junction components (del Toro et al., 2009; Hattula et al., 2006; Huber et al., 1993b; Sun et al., 2014).

One of the few known effectors of Rab8a is FIP-2 (also called Optineurin) which links membrane associated with Rab8a with actin cytoskeleton via Myosin VI and potentially promotes movement of vesicles on actin tracks (Hattula and Peranen, 2000; Sahlender et al., 2005). Additionally, all three isoforms of Myosin V are also known to act downstream of Rab8 (Hume et al., 2001; Rodriguez and Cheney, 2002; Roland et al., 2009).

Rab8 localizes to centrosomes/ciliary sheath and is believed to have potential role in ciliary membrane formation and elongation during early stages of ciliogenesis (Hsiao et al., 2009; Kim et al., 2008; Kobayashi et al., 2011; Murga-Zamalloa et al., 2010; Nachury et al., 2007; Tsang et al., 2008). However, when cells lacking Rab8a or/and Rab8b are nutrient starved no significant changes were observed in cilia length or their number in vivo suggesting that role of Rab8 in ciliogenesis is dependent on the physiological environment (Sato et al., 2014). Thus polarized membrane transport by Rab8 determines diverse important cellular functions including ciliogenesis, maintaining cell polarity and nutrient absorption; the absence of which has been associated with serious diseased conditions such as angle glaucoma, human microvillus inclusion

disease and Bardet biedl syndrome (Nachury et al., 2007; Rezaie et al., 2002; Sato et al., 2007).

Introduction to Thesis Project

Vesicular trafficking influences Wnt signaling capacities in both ligand-producing and -receiving cells (de Groot et al., 2013; Feng and Gao, 2014; Kabiri et al., 2014; San Roman et al., 2014). During intestinal differentiation, the intestinal cell fate activator Cdx2 transcriptionally regulates the expression of Rab8 small GTPases, (Gao and Kaestner, 2010). Rab8 directly binds all isoforms of Myosin V motor (Hume et al., 2001; Jin et al., 2011; Rodriguez and Cheney, 2002; Roland et al., 2009), facilitating exocytic cargo movements on actin tracks in epithelial and non-epithelial cells (Ang et al., 2003; Bryant et al., 2010; Gerges et al., 2004; Hattula et al., 2006; Henry and Sheff, 2008; Huber et al., 1993a; Sato et al., 2009; Sun et al., 2014). Complete *Rab8a* ablation in mice impaired apical delivery of peptidases and nutrient transporters to enterocyte brush borders. As a consequence, these proteins are transported into lysosomes, causing nutrient deprivation and postnatal death of knockout mice (Sato et al., 2007). This phenotype however might be a result of defective crypt cell function as all differentiated villi cells arise from crypt compartments prompting us to explore the less defined contribution of Rab8 vesicles to intestinal crypt homeostasis.

A recent screening for Rab modulators of Wnt pathway identified RAB8B, but not RAB8A, as a crucial regulator for canonical Wnt signaling in receiving cells by directly interacting with LRP6 and CK1γ (Demir et al., 2013). We provide evidence here that in Wnt producing cells, Rab8a regulates Gpr177 anterograde traffic and Wnt secretion.

Significance of the study

The establishment and maintenance of intestinal stem cell population is extremely critical for its constant tissue regeneration, nutrient absorption, and the secretion of antimicrobial agents. Adult stem cell research so far has provided therapeutic progression in cancer and several developmental disorders. Vesicular trafficking is long known as a major player in intracellular trafficking and secretion of ligands that control stem cell behavior and niche. The current research explores molecular mechanism(s) involving Wnt ligand secretion giving us insights into the critical regulation of Wnt secretion during development and adult tissue homeostasis. The study sheds light on stem cell maintenance and has potential to open up new prospects in therapeutic advancement of regenerative medicine to treat intestinal disorders such as congenital intestinal disorders, gastrointestinal diseases and colon cancer. Knowledge gathered from this study could also be applied to other organ systems where Wnt signaling primarily drives development and tissue homeostasis, for instance the mammalian nervous system or mammary gland.

A

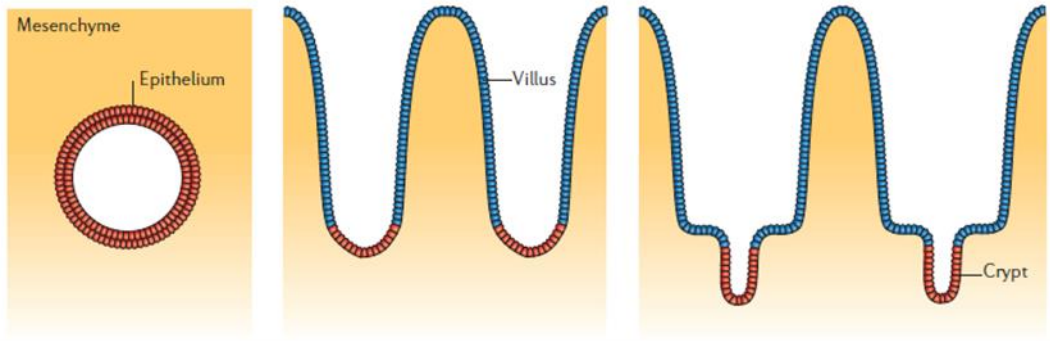
Mesenchyme
Epithelium
Villus
Crypt
E14.5
P7
Early embryo
Adult

B

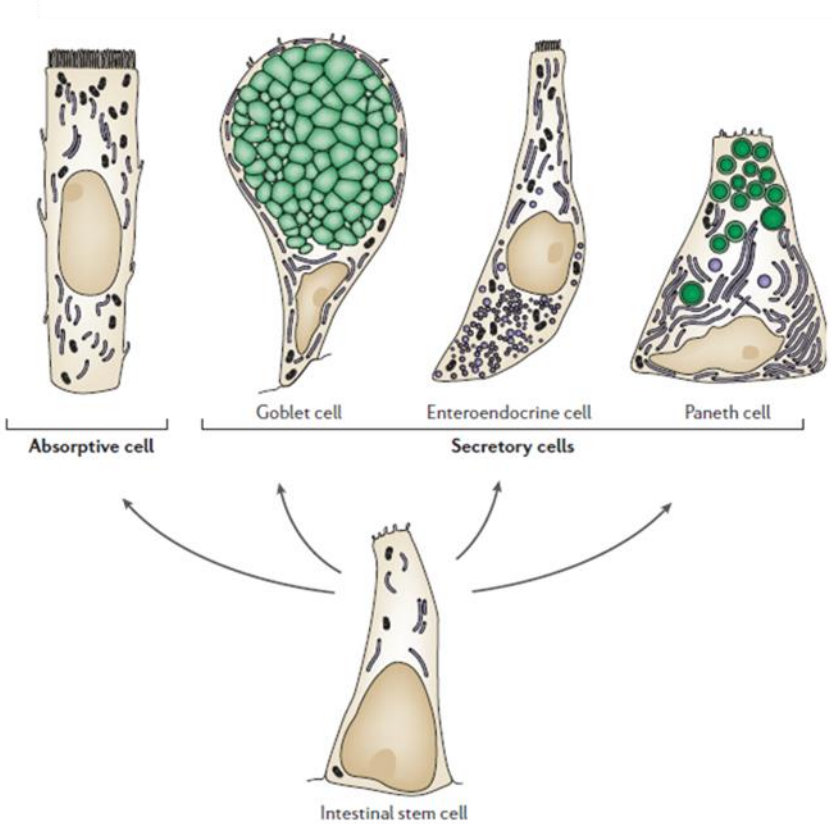
Goblet cell
Enteroendocrine cell
Paneth cell
Absorptive cell
Secretory cells
Intestinal stem cell

C

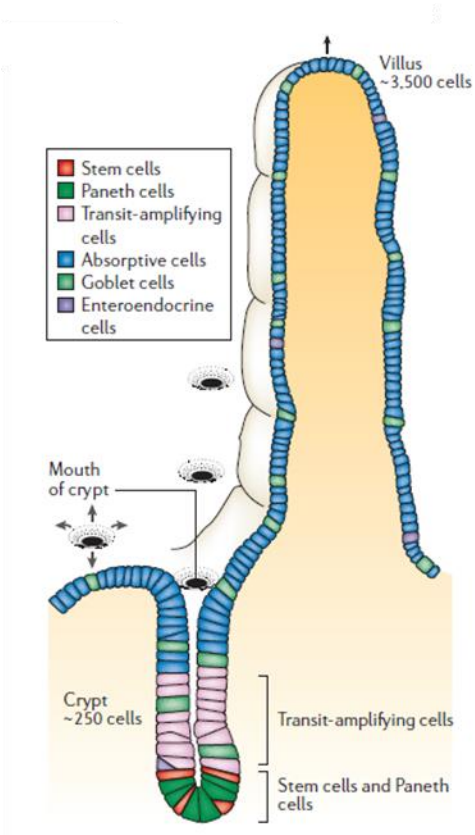
Villus
~3,500 cells
Stem cells
Paneth cells
Transit-amplifying cells
Absorptive cells
Goblet cells
Enteroendocrine cells
Mouth of crypt
Crypt
~250 cells
Transit-amplifying cells
Stem cells and Paneth cells

D

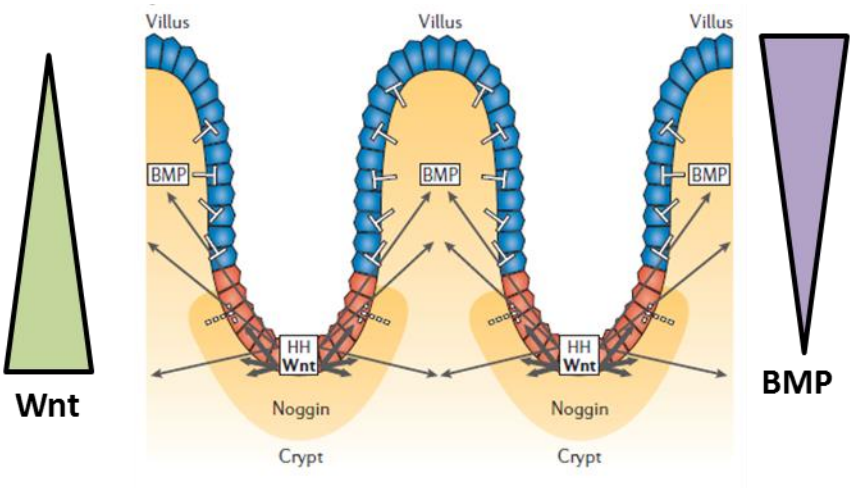
Wnt
Villus
Villus
Villus
BMP
BMP
BMP
HH
Wnt
HH
Wnt
Noggin
Noggin
Crypt
Crypt
BMP

Figure 1: Organization of intestinal stem cell niche in mice (Images are adapted and modified from (Crosnier et al., 2006))

A. At early embryonic stage (E14.5), the digestive tract in mice originates from folding of an endodermal sheet that undergoes remodeling to form a tube like structure lined with multiple layers of proliferating, undifferentiated epithelial cells (**red**). Villus forms at around E15 as a result of reshaping mesenchyme that underlies the epithelia (**orange**). During villus formation the epithelial stratification is lost and proliferative cells are restricted only to the inter-villus regions (**red**). Cells in **blue** represent differentiated cells. Crypts form at a later stage of development, postnatal day 7 (P7), due to the invagination of inter-villus regions into the underlying mesenchyme.

B. Intestinal stem cells give rise to majorly four types of differentiated cells- absorptive enterocytes and secretory goblet, enteroendocrine and Paneth cells.

C. In adult intestine, proliferating stem cells (**red**) reside at the crypt base and give rise to multi-potent TA cells (**pink**). TA cells further differentiate into enterocytes (**blue**), goblet (**light green**), enetroendocrine (**purple**) and Paneth cells (**dark green**). Except Paneth cells that reside at the crypt bottom with stem cells, other three differentiated cells migrate upwards as they are formed and are eventually shed into the lumen.

D. In adult intestine, multiple signaling pathways cross-talk to maintain intestinal stem cells at the crypt base. Hedgehog via long range signaling maintains BMP activity in

mesenchyme underlying villi epithelium. Active BMP inhibits formation of proliferative crypts in villi region. Presence of Noggin inhibits BMP in crypt area. Absence of BMP and active Wnt signaling promote crypt cell proliferation at the crypt compartment. Note that Wnt (**green**) and BMP (**purple**) have exactly opposite gradients.

Wnts	Source cells		
	Crypt cells	Villi cells	Mesenchymal cells
Wnt 2			+
Wnt2b			+++
Wnt 3	+++		
Wnt 4			+++
Wnt 5a			+++
Wnt 5b			+
Wnt 6	+	+	
Wnt 9b	+	+	+

Table 1: Analysis of Wnt gene expression in small intestinal tissue from mice

Out of 19 known Wnt genes, 8 of them (Wnt2, 2b, 3, 4, 5a, 5b, 6, 9b) were detected in small intestinal tissue using RT-PCR and in-situ hybridization (Farin et al., 2012; Gregorieff et al., 2005). “+”, “++” and “+++” refer to low, medium and high mRNA levels detected in corresponding cell compartments in small intestine.

Frizzleds	Source cells		
	Crypt cells	Villi cells	Mesenchymal cells
Fzd 1	+		++
Fzd 2	+		+
Fzd 4	+	++	+++
Fzd 5	+++	+++	
Fzd 6	++	+	++
Fzd 7	+	+	+
Fzd 8	++	++	+++
Fzd 9	++	+	
Fzd 10			+

Table 2: Analysis of Frizzled gene expression in small intestinal tissue from mice

Out of 10 known Frizzled genes, 9 of them (except Frizzled 3) were detected in small intestinal tissue using RT-PCR (Farin et al., 2012). “+”, “++” and “+++” refer to low, medium and high mRNA levels detected in corresponding cell compartments in small intestine.

CHAPTER 2

MATERIALS AND METHODS

Information included in this chapter is taken from and are published in Das et al., Development (2015);142(12):2147-62

Mice and Cells.

Rab8a$^{-/-}$, *Rab8a*$^{\Delta IEC}$, *Lgr5*$^{EGFP\text{-}IRES\text{-}\ CreERT2}$, *Gpr177*$^{fl/fl}$ and *Axin2*$^{LacZ/+}$ mice have been described previously (Barker et al., 2007; Fu et al., 2011; Lustig et al., 2002; Sato et al., 2007). SMAcre transgenic mouse line was kindly provided by Dr. Timothy C. Wang (Department of Medicine, Columbia University, NY) and Transgelin Cre was obtained from Jackson Laboratories. *Rab8a*$^{-/-}$ and *Rab8a*$^{\Delta IEC}$ mice die around 4 weeks; all comparisons were made between littermates of at least 3 mice for each genotype unless stated otherwise. All experiments were repeated at least 3 times; only representative results are shown. Animal handling procedures were approved by Rutgers University Institutional Animal Care and Use Committee. Procedures for derivation of *Rab8a*$^{-/-}$, *Rab8b*-Knockdown, and *Gpr177*$^{-/-}$ MEFs, and molecular phenotypic analyses of cells and tissues have been described previously (Das et al., 2012; Gao et al., 2009; Okamoto et al., 2014) and described below (page 36).

Quantifications and statistical analyses

Quantifications were performed using either 2-tailed, unpaired or paired one-tailed student t-test on the basis of experimental setups. All graphs show mean values, with error bars representing S.E.M., p-values less than 0.05, 0.01 and 0.001 were denoted as "*","**" and "***" respectively to indicate significance. Western blots were quantified using NIH Image J. β-gal staining areas and intensities were measured and quantified with "colour deconvolution" plug-in provided by NIH Image J. All graphs were constructed using Graph-pad Prism 5.

Antibodies.

Antibodies used for immunofluorescence staining are as follows. Wnt5a (Cell Signaling, 2530), Frizzled (1-10) (Santa cruz, 9169), Lrp6 (Cell Signaling, 3395), p-Lrp6 (Cell Signaling, 2568), N-Cadherin (BD Transduction 610920), Lysozyme (Biogenex, AR024-5R), Hopx (Santa-Cruz, sc-30216), GFP (Invitrogen, A11122 and Abcam, ab6673), E-Cadherin (BD Transduction Laboratories, 610182), Histone H3 (Cell Signaling, 12648), Phospho-Histone H3 (Millipore, 06-570), 5-Bromodeoxyuridine (Abdserotec, OBT0030), β-catenin (Abcam, ab16051), β-actin (Santa Cruz, sc-47778), C-myc (Millipore, CBL 430), Rab8 (BD Transduction Laboratories, 610845), Sox9 (Millipore, AB5535), Mmp7 (Santa Cruz, 8832), Flag (Sigma, F1804), Tcf-1 (Cell Signaling, 2203S), Tcf-4 (Cell Signaling, 2565S), Gpr177 (Fu et al., 2009), Rab5 (abcam, ab13253), Rab7 (Cell Signalling, 9367P), Rab9 (Cell Signalling, 5118), Rab11 (BD Tansduction, 610656), Vps35 (abcam, ab10099), LAMP1 (abcam, ab25630). Nuclei were stained with Topro-3 (Invitrogen, T3605), and 5-ethynyl-2'-deoxyuridine (EdU) staining was performed using Click-iT EdU Alexa Fluor 555 Imaging Kit (Invitrogen, C10338) using the manufacturer's protocol.

Cell culture

HeLa and Caco2 cells were obtained from American Type Culture Collection (ATCC) and maintained according to the animal cell culture guideline provided by the company. HeLa, 293T and MEF cells were maintained and passaged in Dulbecco's Modified Eagle Medium (DMEM) supplemented with 10% Fetal Bovine Serum (FBS) and 0.1X Penicillin/Streptavidin (P/S). Caco2 cells were cultured in Minimum Essential

Media (MEM) supplemented with 10% FBS and 0.1X P/S. Wild-type and *RAB8AKD* Caco2 cells were treated with 0.1 µM of Bafilomycin A1 (Sigma, B1793) for 18 hours. *RAB8A* knockdown procedure is described below (page 36).

Plasmids and transfections

Renilla luciferase (pRL-CMV), Wnt3a-Guassia luciferase, pEGFP-RAB8A, and pGEX-KG-RAB8A have been described previously (Chen et al., 2009; Gao et al., 2003; Knodler et al., 2010; Sakamori et al., 2012). Truncated (ΔC44, 44 amino acids at C-terminus) GPR177 coding sequences were tagged with 3×Flag by inserting the CDS into pQCXIP retroviral vector pre-engineered to carry N-terminal 3×Flag. GPR177-mCherry was constructed by inserting the GPR177 cDNA into pmCherry-N1 vector to carry mcherry tag at the C-terminus. Topflash plasmid (12456), pcDNA-WNT5A (35911) pcDNA3-ShhN-Ren (37677) and pGEX4T-1-CDC42 (12175) were obtained from Addgene. SEcreted Alkaline Phosphatase (SEAP) and Metridia luciferase constructs were provided with the Great EscAPe Fluorescence detection kit (Clontech, 631704). Transient transfections were performed with Lipofectamine 2000 (Life Technologies) using manufacturer's recommendations for plasmid concentrations except Renilla-luciferase which was used at a concentration of 5-10 ng per 500µl of transfection system. Stable cell lines expressing Flag- or mCherry-tagged GPR177 in pQCXIP vector were established using lentiviral transduction under puromycin selection pressure. Live cell images were acquired by a Zeiss LSM 510 confocal or a Zeiss Cell Observer Spinning Disk confocal microscope. pGEX4T-1, pGEX4T-1-RAB8A, pGEX4T-1-CDC42 and pGEX4T-1-JFC1D1

plasmids are described elsewhere (Feng et al., 2012; Sakamori et al., 2012) pQCXIH-Cre was made by inserting cDNA of Cre into pQCXIH (Clontech, 631516). Cell experiments were performed in triplicates, repeated multiple times, and only representative results were shown.

Lentiviral shRNA knockdown

A detailed protocol can be found in **appendix 6**. Efficiency of RAB8A knockdown was determined by western blot.

Lentiviral shRNA transduction particles against human *RAB8A* were obtained from Sigma, TRCN0000048213.

ShRNA sequences against mouse *Rab8b* are shown below**.**

shRab8b1 CCGGGCCAAGAACTAACAGAACTTTCCATGGAAAGTTCTGTTAGTTCTTGGCTTTTTG

shRab8b2 AATTCAAAAAGCCAAGAACTAACAGAACTTTCCATGGAAAGTTCTGTTAGTTCTTGGC

Derivation of wild type, Rab8a$^{-/-}$, Rab8b-Knockdown, and Gpr177$^{-/-}$ MEFs

The trunk of E12.5-13.5 wild type, *Rab8a*$^{-/-}$, or *Gpr177* $^{fl/fl}$ embryos were diced into small pieces with fine aseptic scissors and treated with Trypsin-EDTA at 37°C for 20 mins. The tissue remnants were pipetted up and down, centrifuged at 1,000 rpm for 3 mins. Pellets were plated in 1× DMEM (Dulbecco's Minimal Essential media) with 10% FBS, 5% Penicillin/Streptomycin and 10 μg/mL Gentamycin. To knockdown *Rab8b*, wild type or *Rab8a*$^{-/-}$ MEFs were infected with lentiviral shRab8b particles (see sequence in

page 36) and selected by Puromycin (3μg/ml) for 2 days. To derive *Gpr177*$^{-/-}$ MEFs, *Gpr177*$^{fl/fl}$ MEFs were infected with retroviral CMV-Cre and selected by Hygromycin B (500 μg/ml) for 3 weeks. For Cre retroviral production, pQCXIH-Cre and pVSV-G (Clontech, 631457) were co-transfected into GP2-293 cells (Clontech 631458). After 48 hrs, cell culture medium was harvested and ultracentrifuged at 30,000 g for 2 hrs to concentrate retroviral Cre particles.

Intestinal organoid culture

Procedures were adapted and modified from original report (Sato et al., 2011). Proximal one third of the intestines were dissected and flushed with 1× Phosphate Buffer Saline (PBS), cut open and fragmented into smaller pieces (~2 cm sizes). Tissue fragments were then rinsed 3 times in cold 1× PBS followed by 2 washes in cold chelating buffer (2 mM EDTA in PBS) at 4°C for 5 minutes and 40 minutes respectively. Intestinal fragments were then vigorously re-suspended in cold chelation buffer and allowed to flow through 70 μm filter (BD Falcon, 352350) into pre-cooled 1× PBS. A pellet of crypts was obtained by centrifuging this flow-through suspension at 200 g for 3mins at 4°C. The pellet was then washed twice and resuspended in cold 1× PBS for counting. 100~200 crypts suspended in matrigel (BD Biosciences, 356231) were plated into each well of pre-warmed (at 37 °C) 24-well plates. After allowing the matrigel to solidify at 37°C for 10 minutes, 500 μl of ENR organoid culture medium was added to each well (Sato et al., 2011). Working ENR medium contains 2× N2 supplement (Life Tech Gibco. 17502-048), 0.5× B27 (Life Tech Gibco. 17504-044), 1 mM N-Acetyl Cysteine

(Sigma, A9165), 0.05 μg/ml of EGF (Life Technologies, PMG8043), 0.1 μg/ml of Noggin (Peprotech, 250-38) and 1μg/ml of R-Spondin (R & D Systems, 3474-RS-050)] made in Basal Culture medium [Advanced DMEM/F12 (Life Technologies, 12634-010) with 1× Penicillin/Streptomycin (Life Technologies, 15140-122), 1× Glutamax (Life Technologies, 35050-061) and 10mM HEPES Buffer (Life Technologies, 15630-080)]. To rescue *Rab8a*$^{-/-}$ organoids, culture medium with 100 ng/mL mouse recombinant Wnt3a (R & D Systems, 1324-WN-002) or 3μM of CHIR99021 (Stemgent, 04-0004) was added daily to the culture. Organoid survival results and images of β-galactosidase staining of organoids are from 3 independent experiments. Wnt3a and CHIR99021 rescue experiments were repeated twice.

Dual luciferase assay, and fluorescent SEAP assay

To measure Wnt3a-Gluc, ShhN-Ren and Metridia luciferase secretions, MEF cells of various genotypes were transiently co-transfected with Wnt3a-Gluc, ShhN-Ren or Met-Luc and Firefly luciferase which serves as transfection control. 24 hours after transfection, the supernatants and cell lysates were collected and subjected to dual luciferase assay (Promega, E1980), using Glomax multi-detection system (Promega). Each reaction consisted of 50 μl media or 10 μl cell lysates, and 50 μl of luciferase assay substrate and 50 μl of Stop & Glo reagent. The SEAP assay was performed using the Great EscAPe Fluorescence detection kit (Clontech, 631704). 25 μl of supernatants or cell lysates were diluted with same volume of 1×dilution buffer in a 96-well plate, mixed gently on rotating platform for 5 mins at room temperature, and incubated at 65°C for

30 mins. The samples were then cooled to room temperature. 97 μl of assay buffer was added and incubated for 5 mins at room temperature. 3 μl of 1mM MUP (substrate) was added and incubated with the samples at room temperature for 1 hour in dark. Fluorescent units were read using Glomax multi-detection system. Luminescence units from Guassia luciferase, Renilla luciferase and Metridia luciferase were normalized against intracellular Firefly luciferase. Assays were repeated 3 or more times with 3-6 technical replicates for individual cell line each time.

Topflash reporter assay

To compare Wnt3a responsiveness in wild type, *Rab8a*$^{-/-}$ and *Rab8bKD* MEF cells, cells were co-transfected with Topflash and Renilla luciferase for 24 hours. The cells were then serum starved for 3 h in Wnt-free DMEM media and treated with 20 ng/ml recombinant murine Wnt3a (Peprotech, 315-20). After 5 hours media was removed, cells were washed with 1X PBS, lysed and luciferase activity was detected using dual-luciferase assay (Promega, E1980), using Glomax multi-detection system (Promega). To compare Wnt5a secretory abilities by wild-type and *Rab8a*$^{-/-}$ MEFs, cells were simultaneously transfected with pcDNA-WNT5A, Topflash and Renilla luciferase in Wnt-free Lactalbumin hydrolysate (SAFC Biosciences, 58901-C) in DMEM for 16-18 hours. Topflash activity was then detected in cell lysates and normalized to intracellular Renilla luciferase. Data represent 3 independent experiments with comparable transfection efficiencies.

Co-immunoprecipitation and GST pull-down assays

Immunoprecipitations were performed with anti-Flag M2 affinity gel (Sigma, A2220) using 2 mg total lysates extracted from 3×Flag-GPR177 stable HeLa cells. Reactions were incubated for 8 hrs at 4° C, washed 3 times with buffer containing 1% Triton X-100, and eluted with 40 μl of 3× Flag peptides. Western blot and GST pull-down procedures have been described earlier (Das et al., 2012; Gao and Kaestner, 2010; Gao et al., 2009). The wash buffer contained 50 mM Tris HCl (pH 7.5), 150 mM NaCl, 1 mM EDTA and 1% TritonX-100. For GST pull-down, GST, GST-RAB8A, GST-CDC42 and GST-JFC1D1 fusion proteins were expressed in BL21 cells induced by 0.5mM IPTG and cultured at room-temperature for 18 hours (Das et al., 2012). The bacterial cells were then resuspended in 2ml of 1× PBS with 1% Triton X-100, 0.1mg/ml Lysozyme (Sigma, L6876), 1mM PMSF and 1× Bacterial protease inhibitors (Sigma, P8465), incubated on ice for 30 minutes followed by sonication. GST protein-containing lysates hence collected were then incubated with pre-swollen glutathione–agarose beads (Molecular probes, G-2878) at 4°C for 1 hr. The beads were washed three times with 1X PBS. To check GST-protein expression, a portion of GST-protein conjugated beads was denatured in 4× LDS (Life Technologies, NP0007) at 70ºC for 15 minutes and subjected to SDS-PAGE followed by comassie blue staining (Invitrogen, LC6060). Comparable amounts of beads were incubated with 1 mg cell lysates from 3×Flag-GPR177 stable HeLa for 1 hr at 4°C. Beads were washed with PBS containing 1% Triton X-100 and mammalian protease inhibitors (Roche, 11 697 498 001) , denatured in 4×LDS (Life Technologies, NP0007) at 70°C for 15 minutes, and subjected to anti-Flag Western blot analysis. Data represent 3 independent experiments.

β-galactosidase staining

For β-galactosidase staining, tissue sections or whole organoids in chamber slides were rinsed with 1X PBS, fixed in 1X PBS containing 1% formaldehyde, 0.2% glutaraldehyde, 2mM $MgCl_2$, 5mM EGTA and 0.02% NP40 for 15 mins, washed in PBS for 3 times at room temperature, and stained with staining solution containing 5 mM $K_3Fe(CN)_6$, 5 mM $K_4Fe(CN)_6$, 2 mM $MgCl_2$, 0.01% sodium deoxycholate, 0.02% NP-40, 1 mg/ml X-Gal (Fisher Scientific, 50-213-181) overnight at 37°C. The samples were then rinsed with 1X PBS and mounted for imaging with a Nikon TE2000 microscope. Data represent 3 independent experiments.

Immunofluorescence and immunohistochemical staining

Procedures for immunofluorescence staining of histological sections, organoids or cells and immunohistochemistry on histological sections have been described earlier (Das et al., 2012; Gao and Kaestner, 2010; Gao et al., 2009) and detailed in **appendices 1-5**. **Fig. 2A, 5, 7E,F, 8A, 11, 25 and 26B** show staining on paraffin sections. **Fig. 7A,B, 9, 12A and 23** show staining on cryo-sections.

Quantitative RT-PCR

Procedure for quantitative RT-PCR has been described earlier (Das et al., 2012; Gao and Kaestner, 2010; Gao et al., 2009; Sakamori et al., 2014). RNA was extracted from ~30mg snap frozen total intestinal tissue using RNAeasy mini kit (Qiagen, 74104)**.** 30µl total volume of cDNA was prepared from 2µg of extracted RNA on the same day

using Maxima first strand cDNA synthesis kit (Fermentas, K1661)**.** 1µl of 10 times diluted cDNA with 2X Maxima SYBR green/ROX qPCR Master Mix (Thermo Scientific, FERK0222) and mRNA specific primers (**Table 3**, see below) was amplified in Light Cycler 480 (Roche).

Threshold cycle (C_t) values obtained for each gene were normalized to C_t values obtained for either *β-actin* or *Hypoxanthine-guanine phosphoribosyl transferase*. Data was obtained from 3 or more independent biological samples with 3 technical replicates.

Quantitative RT-PCR primers: (Table 3)

Gene	**Forward**	**Reverse**
c-Myc	GTGCTGCATGAGGAGACACC	CAGGGGTTTGCCTCTTCTCC
Tcf4	AGCCCGTCCAGGAACTATG	TGGAATTGACAAAAGGTGGA
Tcf1	AGCCTCAACCCCCGCTGCAT	CTTGCTTCTGGCTGATGTCC
Axin2	TGAGATCCACGGAAACAGC	GTGGCTGGTGCAAAGACAT
Gpr177	CAAATCGTTGCCTTTCTGGT	CGCCAGCCATCTTGTTTTAT
Lyz	GGTGGTGAGAGATCCCCAAG	CAGACTCCGCAGTTCCGAAT
Mmp7	CTTACAAAGGACGACATTGCAG	AGTGCAGACCGTTTCTGTGAT
Defa5	TATCTCCTTTGGAGGCCAAG	TTTCTGCAGGTCCCAAAAAC
Wnt3	CTTCTAATGGAGCCCCACCT	GAGGCCAGAGATGTGTACTGC
Wnt3a	GGAATGGTCTCTCGGGAGTT	CTTGAGGTGCATGTGACTGG

Wnt2b	CCGTGTAGACACGTCCTGGT	TGATGTCTGGGTAGCGTTGA
Wnt5a	GACAGGCATCAAGGAATGC	GTCTCTCGGCTGCCTATTTG
Wnt9a	GGCGCTCTAGCAAGGATTT	CCAGACACACCATGGCATT
Wnt6	CGTGGAGATATCCGTGCAT	CCCATGGCACTTACACTCG
Ascl2	TCCAGTTGGTTAGGGGGCTA	GCATAGGCCCAGGTTTCTTG
Tert	AGCGGGATGGGTTGCTTTTAC	CACCCATACTCAGGAACGCC (Munoz et al., 2012)
Bmi1	GAGCAGATTGGATCGGAAAG	GCATCACAGTCATTGCTGCT (Sakamori et al., 2012)
Lrig1	AAGGGAACTCAACTTGGCGAG	ACGTGAGGCCTTCAATCAGC (Munoz et al., 2012)
Hopx	CATCCTTAGTCAGACGCGCA	AGGCAAGCCTTCTGACCGC (Munoz et al., 2012)
Olfm4	GCCACTTTCCAATTTCAC	GAGCCTCTTCTCATACAC
β-actin	TTGCTGACAGGATGCAGAAG	CCACCGATCCACACAGAGTA
Hprt	AAGCTTGCTGGTGAAAAGGA	TTGCGCTCATCTTAGGCTTT

Biotinylation Assay

Cells were grown to ~90% confluency in 10-cm dishes, washed three times with pre-cooled 1X PBS and incubated with 10ml of cold Biotin solution with gentle rocking at 4°C. Biotinylation was quenched after 30 minutes and cell lysates were collected as per

manufacturer's instructions (Pierce, 89881). 300µg of cell lysates were added to 100µl of Neutravidin beads for 1 hour at room-temperature, washed four times with the wash buffer provided by the manufacturer and eluted in 4× LDS containing 50mM DTT at 70°C for 15 minutes. The supernatant was then collected and immunoblot analysis was performed using anti-Frizzled (1-10), anti-Lrp6, anti-phospho Lrp6 (Ser1490), anti-N-Cadherin and anti-Gpr177. Data represent 3 independent experiments.

Wnt5a/b secretion assay

MEFs were grown to ~90% confluency in 10cm dishes, washed three times with 1× PBS and cultured in 10ml of 1X Lactalbumin hydrolysate (SAFC Biosciences, 58901-C) in DMEM. After 24 hours, media was collected in 50ml falcon tubes and centrifuged at 10,000g for 10 minutes. Supernatant was then loaded to Amicon Ultra-15 Centrifugal filter system (Millipore, UFC 901024, 10K MWCO) and centrifuged at 5000g at room-temperature for an hour. The concentrate (~100 µl) was collected and subjected to immunoblot analysis using anti-Wnt5a/b and anti-Histone 3.

Transmission EM analysis and Gpr177 immunogold labeling.

TEM procedures have been described previously (Gao and Kaestner, 2010; Sakamori et al., 2012). For Gpr177 immunogold labeling and EM analysis, duodenal and jejunal tissues were dissected from wild type (n=3) and *Rab8a*$^{-/-}$ mice (n=2) and immediately fixed as ~1 mm fragments in 2.5% paraformaldehyde in cacodylate buffer, pH 7.4 overnight. The tissue was then sliced to 100-200 microns thickness on a vibratome and frozen between two brass "top-hats" in a HPM010 (Abra Fluid AG.

Widnau, Switerlan) at 5,000 P.S.I. at -180 °C. Next, the frozen tissue was transferred to frozen glass-distilled 100% acetone and dehydrated at -90 °C for 48 hours. The tissue was then infiltrated with HM-20 lowicryl and polymerized with 360 nm light at -50 °C in a dry nitrogen environment. Tissue sections cut 60 nm thick containing Paneth cells were immunolabeled with Gpr177 antibody (Fu et al., 2009) at 1:250 to 1:50 in 5% BSA, 0.1% cold water fish gelatin in PBS pH 7.4. No primary antibody control and *Gpr177*-deficient cells were used in initial tests to optimize labeling conditions. Images shown were immunolabeled with 1:100 dilution of primary antibody. Stable antigen-antibody complexes were detected with protein A conjugated to either 15nm gold colloids or 20nm gold colloids. Imaging was performed with a FEI Tecnai-12 microscope at 80 keV using a nominal magnification of 6500×. Montage images were collected using Serial EM and stitched together with the IMOD subroutine Blendmont (Kremer et al., 1996; Mastronarde, 2005). Each image has a pixel dimension of ~3 nm such that each spherical gold particle should fill 5 pixels and resizing of the images should provide information to reveal the approximate volume the gold would occupy in the images. Immunogold particles were counted manually, excluding particles within nuclear area. Area and perimeter of individual Paneth cells were measured using Photoshop CS. Number of immunogold particles in each subcellular compartment per unit area (for ER and Golgi) or per unit length (for plasma membrane) were calculated and compared by t-test. Data were collected from 3 independent labeling experiments, twice performed on 2 pairs of independent wild type and knockout tissues, and once on a wild type mouse tissue.

RNA in situ hybridization

The protocol is modified from an earlier published method (Gregorieff and Clevers, 2010). RNase protected 8µm mouse intestinal cryo-sections were thawed at room temperature (RT) for 15 minutes followed by treatment with 4% para-formaldehyde (made in DEPC PBS). The slides were then washed sequentially with 1X DEPC PBS for 5 minutes, 0.2N hydrochloric acid for 15 minutes and 30µg/ml Proteinase-K for 20 minutes. The action of Proteinase K is stopped by transferring the slides to 0.2% glycine solution for a minute after which the slides are washed twice in 1X DEPC PBS followed by post-fixation with 4% PFA for 10 minutes. Next, the slides were washed with 1X DEPC PBS thrice and rinsed in 0.25% acetic anhydride solution (in Triethanolamine buffer) twice for 5 minutes each. The slides were then washed with 1X DEPC PBS 5 times followed by two washes in 5XSSC (pH=7.5) solution for a minute. Following this, the slides were pre-hybridized with hybridization solution (50% Formamide, 5X SSC (pH=4.5), 5X Denhardt's buffer, 2.5mg/ml of yeast t-RNA, 0.05% CHAPS buffer, 0.5mg of Heparin, 5mM EDTA added in DEPC water) for 3 hours followed by incubation with 500µl of 1µg/ml of *Olfm4* probe and 2µg/ml *Gpr177* probe (in hybridization solution) overnight at 65°C. Preparation of probes is mentioned elsewhere (Gregorieff and Clevers, 2010). During this incubation, the slides were kept in a chamber humidified with 5XSSC (pH=7.5)/50% Formamide. 5XSSC is prepared from 20XSSC (Ambion, AM9763). The next day, the slides were rinsed in 2XSSC (pH=7.5, prepared from 20XSSC) for 1 minute and kept in 2XSSC/50% Formamide at 65°C for 20 minutes. The slides were then washed 5 times with 0.1% Tween-20 in Tris-NaCl buffer (pH=7.5), blocked with blocking solution

(1g blocking powder from Roche catalog# 11 096 176 001 dissolved in 1X Tris-NaCl buffer of pH=7.5) for an hour and followed by incubation in 500µl of (1:1500) anti-Digoxygenin-AP primary antibody (Roche, 1109327490) made in block) over night at 4̊C. On the third day, the slides were rinsed 5 times in 0.1% Tween-20 in Tris-NaCl buffer for 1 minute followed by rinsing with NTM buffer (0.1M Tris-Cl (pH=9.5), 0.1M NaCl, 0.05M $MgCl_2$ in DEPC water) twice for a minute each. Next, 500µl of BM-Purple/AP substrate (Roche, 11 442 074 001) was applied to the slides and the slides were incubated until an intense blue color for *Olfm4* or *Gpr177* (3-6 hours) was seen under a dissecting microscope. After the color has developed, the slides were rinsed once in 1X PBS, 70% (v/v in water), 90% (v/v in water), twice in 100% ethanol and twice in Xylene respectively followed by mounting in xylene-based mounting media. All steps were performed at room temperature unless mentioned otherwise. All washing steps with 1X DEPC PBS were performed for a minute unless mentioned otherwise. Steps other than application of probes, primary antibody and BM-Purple/AP substrate were performed on a rocker.

CHAPTER 3

RAB8A MAINTAINS INTESTINAL CRYPT CELLS IN VIVO AND EX VIVO

Information included in this chapter is taken from and are published in Das et al., Development (2015);142(12):2147-62

During intestinal differentiation, the master regulator of epithelial morphogenesis of intestinal cells, Cdx2, transcriptionally regulates the expression of Rab8 small GTPases (Gao and Kaestner, 2010) indicating potential role of Rab8a in intestinal cell fate determination. Crypt cell maintenance is also dependent on several secretory products such as anti-microbial peptides, mucin, cytokines and several growth factors, which makes Rab8a dependent post-golgi transport important for intestinal homeostasis. Global *Rab8a* ablation in mice impaired apical delivery of peptidases and nutrient transporters to enterocyte brush borders. As a consequence, these proteins are transported to lysosomes, causing nutrient deprivation leading to postnatal death of knockout mice (Sato et al., 2007). However, the contribution of Rab8 vesicles to intestinal crypt homeostasis was not explored by Sato et al. This defect observed in *Rab8a*$^{-/-}$ enterocytes could be a result of loss of *Rab8a* in stem cells at crypt base from which the entire villi arises. Thus to understand the function of Rab8a in crypt compartment, we investigated the effect of *Rab8a* deletion on Paneth cells and intestinal stem cells.

Results

Impaired Paneth cell morphology in absence of Rab8a

Paneth cells are the major epithelial Wnt producers within the intestinal crypts (Sato et al., 2011). Lysozyme staining identified significant reduction of Lysozyme^{+} Paneth cells in *Rab8a*$^{-/-}$ crypts. 85% of *Rab8a*$^{-/-}$ intestinal crypts contained virtually no detectable Lysozyme^{+} Paneth cell, while the rest had a single Lysozyme^{+} cell **(Fig. 2A,B)**.

Interestingly, when compared to *Rab8a*$^{+/+}$, *Rab8a*$^{-/-}$ intestines transcribed similar or even higher levels of several Paneth cell-specific genes–*Lysozyme*, *Mmp7*, and *Defa5* **(Fig. 2C)**, suggesting that *Rab8a* deletion did not affect the fate determination of Paneth cells but have potentially blocked terminal differentiation of Paneth cells from the precursors. Such intermediate secretory precursors have been recently described (Buczacki et al., 2013; Clevers et al., 2014).

To analyze the ultra-structural details of *Rab8a*$^{-/-}$ Paneth cells, we performed Transmission Electron Microsocpy (TEM) using intestinal tissue samples from *Rab8a*$^{+/+}$ and *Rab8a*$^{-/-}$ mice. Analyses of *Rab8a*$^{-/-}$ intestinal crypts by TEM discovered substantial subcellular defects in these residual Paneth cells. Virtually all *Rab8a*$^{-/-}$ Paneth cells contained fewer electron-dense secretory granules typically found in this cell type **(Fig. 4A)**. *Rab8a*$^{-/-}$ Paneth cells also showed markedly expanded smooth ER cisternal stacks of approximately 2.5-fold expanded than those in *Rab8a*$^{+/+}$ Paneth cells **(Fig. 4B)** suggesting potential sorting defects in *Rab8a*$^{-/-}$ Paneth cells.

Having explored the morphological defects in Paneth cells in absence of Rab8a, a unique cell type that provides growth factor support to ISCs, we investigated whether *Rab8a*$^{-/-}$ crypts when isolated can be maintained in vitro. In cultured organoids, Lysozyme staining identified Paneth cells in small buds of surviving *Rab8a*$^{-/-}$ organoids **(green, Fig. 3)**, hinting that preservation of small number of Paneth cells in surviving knockout crypts might have facilitated their survival, whereas crypts lacking mature Paneth cell were arrested **(red line, Fig. 6B)**. When isolated and cultured ex vivo only

30% of *Rab8a*$^{-/-}$ organoids survived through day 7 in crypt culture media containing Epidermal Growth Factor (EGF), Noggin and R-Spondin1 (**Fig. 6B**). Even the surviving *Rab8a*$^{-/-}$ organoids showed smaller buds and larger lumen indicating growth defects in absence of Rab8a (**Fig. 6A**).

We next hypothesized that intestinal epithelial cell-specific *Rab8a* deletion (*Rab8a*$^{L/L}$*;Villincre*) would produce a milder phenotype than *Rab8a*$^{-/-}$ intestines. Indeed, compared to *Rab8a*$^{-/-}$ intestines, *Rab8a*$^{L/L}$*;Villincre* intestines exhibited less pronounced Paneth cell loss. Continuous stretches of *Rab8a*$^{L/L}$*;Villincre* crypts containing Paneth cells existed next to crypts without Paneth cells, suggesting an overall milder impact on Paneth cell maturation **(Fig. 5)**. This observation was echoed by organoid culture experiments. We observed two morphologically distinct clones of *Rab8a*$^{L/L}$*;Villincre* organoids: one resembled the wild-types with well-developed buds while the other mimicking *Rab8a*$^{-/-}$ organoids **(*Rab8a*$^{L/L}$*;Villincre* in Fig. 6A)**. The visibly improved epithelial budding in a fraction of *Rab8a*$^{L/L}$*;Villincre* organoids agreed with the observation that some *Rab8a*$^{L/L}$*;Villincre* crypts possessed more Paneth cells than others. Nevertheless, *Rab8a*$^{L/L}$*;Villincre* did not show an improved long-term survivability compared to *Rab8a*$^{-/-}$ organoids **(compare blue and red lines, Fig. 6B)**.

Expansion of Proliferative zone in absence of Rab8a

Essential growth factors and signaling molecules are expressed by Paneth cells such as EGF, Wnt3 and Delta that have potential role in maintenance of ISC niche. Having discovered the morphological defects in Paneth cells, we next examined the

status of proliferative and stem cell zone at crypt compartment. To do so, we examined the fast-cycling CBC cells in *Rab8a*$^{-/-}$ mice using Lgr5 as an indicator (Barker et al., 2007). We derived *Rab8a*$^{-/-}$*; Lgr5*$^{EGFP\text{-}IRES\text{-}CreERT2/+}$ mice, and analyzed proliferative Lgr5^{+} stem cells by EGFP and EdU labeling. Increased EdU^{+} Lgr5^{+} cells were detected in both small intestines and colons of *Rab8a*$^{-/-}$*; Lgr5*$^{EGFP\text{-}IRES\text{-}CreERT2/+}$ mice **(Fig. 7A-C)**. Total number of Lgr5^{+} cells per crypt in *Rab8a*$^{-/-}$ intestines also increased **(Fig. 7D)**. The numbers of transit-amplifying cell (BrdU^{+}) and mitotic crypt cell (pHH3^{+}) were also increased in *Rab8a*$^{-/-}$ crypts (**Fig. 7E and 7F**), which might explain the increased c-Myc in *Rab8a*$^{-/-}$ intestines **(Fig. 10A,B)**.

Tissue adaptation in Rab8a*$^{-/-}$ *intestine

Crypt cells demonstrate great plasticity (Tetteh et al., 2014). Tissue regenerative program could be activated by injury, in a number of slow-cycling or secretory precursor cell types (Buczacki et al., 2013; Farin et al., 2012; Powell et al., 2012; Tian et al., 2011; Yan et al., 2012). Bmi1^{+} cells were shown to be relatively resistant to Wnt signaling perturbation (Yan et al., 2012). By quantitative RT-PCR we surveyed several “quiescent” stem cell markers but only detected increased *Bmi1* mRNA level **(Fig. 8C)**. Using a Hopx antibody, we also analyzed this reported “+4” cell type that was shown to convert to Lgr5^{+} cells by lineage tracing (Takeda et al., 2011). *Rab8a*$^{+/+}$ intestinal epithelia contained approximately 3 Hopx^{+} cells (experimentally defined as strongly positive for nuclear immuno-reactivity) in every 10 adjacent crypts; whereas *Rab8a*$^{-/-}$ intestines showed 7~8 Hopx^{+} cells in same number of crypts **(Fig. 8A, B)**. *Rab8a*$^{-/-}$ intestines also

contained multiple Hopx^{+} cells in a single crypt, with generally stronger nuclear immuno-reactivity compared to *Rab8a*$^{+/+}$ intestines **(Fig. 8A,** arrows and arrowheads indicate strong and moderate staining, respectively**)**. Hopx^{+} cells were found in *Rab8a*$^{-/-}$ epithelium at positions other than "+4" **(Fig. 8A and Fig. 9A, B)**. One-hour EdU labeling of *Rab8a*$^{-/-}$ mice led to positive labeling of some Hopx^{+} cells; this was rarely found in *Rab8a*$^{+/+}$ crypts **(Fig. 9A)**. Additionally, co-immunofluorescent analyses of Lgr5^{+} cells and Hopx^{+} cells in *Rab8a*$^{-/-}$*; Lgr5*$^{EGFP\text{-}IRES\text{-}CreERT2/+}$ intestines showed increased number of both cell types **(Fig. 9B)**.

Discussion

Our data show that deletion of Rab8a had a significant impact on number and ultra-structure of Paneth cells. Despite the well-established role of Paneth cells as an essential component of intestinal stem cell niche (Sato et al., 2011), the $BrDU^{+}$, EDU^{+}, $pHH3^{+}$ proliferative compartment, actively cycling $Lgr5^{+}$ and relatively slow cycling "quiescent" $Hopx^{+}$ stem cell compartments expanded in *Rab8a*$^{-/-}$ crypts suggesting high tissue plasticity in absence of Rab8a function in vivo. However, when cultured ex vivo in absence of mucosal support, most of *Rab8a* null crypts (~70%) were growth arrested and dead by day 7 in ENR medium. Since organoid/crypt survival ex vivo is dependent on functional interaction between Paneth and stem cells, these data together indicate (but do not distinguish between) a direct (via stem cell) or indirect (via secretory function of Paneth cell) impact of Rab8a on organoid survival ex vivo.

Paneth cells provide Wnt3, an essential growth factor that maintains ISC niche and promotes growth and survival of organoids. Studies show that *Wnt3*$^{-/-}$ crypts in vivo did not demonstrate any phenotype in vivo however when cultured in vitro were unable to undergo multiple passages (Farin et al., 2012). Given the observed defects in Paneth cells, it will be interesting to examine if *Rab8a*$^{-/-}$ organoids are capable of being passaged and if *Rab8a* null stem cells show similar clonogenic activity as their wild-type counterparts. We speculate that *Rab8a*$^{-/-}$ stem cells will most likely illustrate reduced stem cell activity in absence of mucosal support, hence, reduced survival upon multiple passages.

Both *Rab8a*$^{-/-}$ and *Rab8a*$^{L/L}$*; Villincre* organoids showed similar morphological defects and mortality in culture. This data suggests that epithelial *Rab8a* is essential and most likely would be sufficient to establish and maintain organoid structures ex vivo. 30% survival of organoids isolated from these two knockouts also suggest that crypt cell (Paneth and stem cell) function in organoids is reduced significantly but only partially (and not abolished completely) in absence of epithelial *Rab8a*.

Increase in proliferating Lgr5^{+} cells indicate an independent pathway provided by non-Paneth intestinal epithelial cells maintaining proliferative zone in *Rab8a*$^{-/-}$ intestines. Even though the villi length is comparable to the wild-type counterparts; the crypt compartments are frequently larger in *Rab8a*$^{-/-}$ intestines (**Fig. 7E,F**). There are two possibilities that could result in expansion of proliferative zone at crypt compartment. Firstly, *Rab8a*$^{-/-}$ ISCs are continuously proliferating and differentiating at a higher rate than wild-type ISCs under the influence of a compensatory molecular signal. However this possibility is less likely to happen as the length of villi in *Rab8a*$^{-/-}$ intestine is similar to control intestines. Secondly, we postulate that a large population of *Rab8a* null Lgr5^{+} cells is unable to exit cell cycle resulting in larger crypt size. At the same time an independent population of proliferative (stem) cells is able to differentiate and maintain villi in *Rab8a* knockouts. However, if this small population of stem cells, that makes the intestine tolerant to elimination of *Rab8a*, is Hopx^{+} cells is yet to be determined. To check if the second possibility is true, lineage tracing Hopx^{+} cells in *Rab8a* knockout mice would be informative. Hopx^{+} cells have been earlier shown to give rise to all cell lineages including Lgr5^{+} CBCs (Takeda et al., 2011). If Hopx^{+} cells are giving rise to and

maintaining the villi in *Rab8a*$^{-/-}$ intestines, the abnormal morphology (characterized by enhanced proliferation and Lgr5^{+} cells) of *Rab8a*$^{-/-}$ intestinal epithelium could be an adaptive response rather than an immediate consequence to loss of Rab8a function in the intestine.

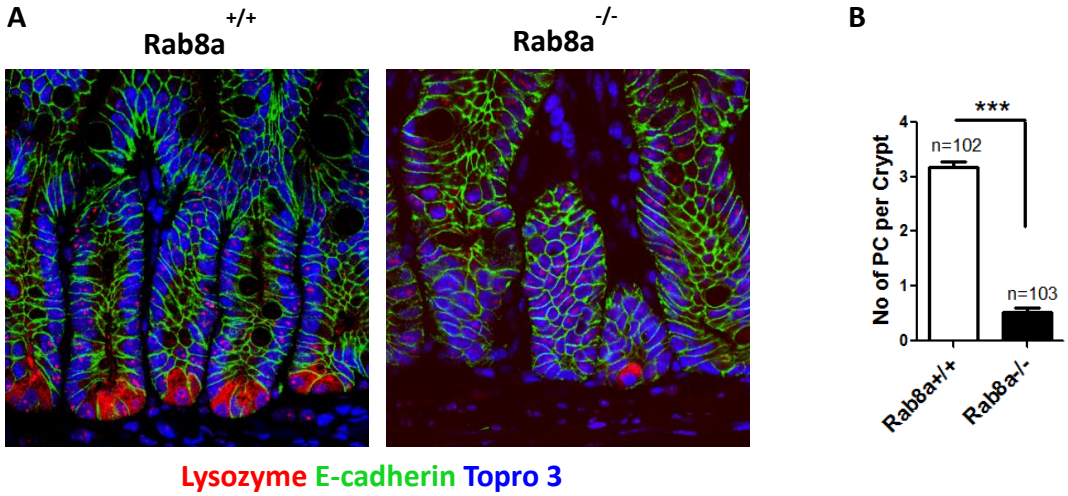
A
+/+
Rab8a
-/-
Rab8a
B
***
n=102
n=103
No of PC per Crypt
Rab8a+/+
Rab8a-/-
Lysozyme E-cadherin Topro 3

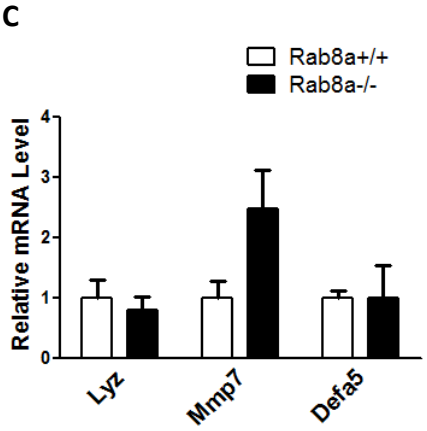
C
Rab8a+/+
Rab8a-/-
Relative mRNA Level
Lyz
Mmp7
Defa5

Figure 2: Analysis of Paneth cells using immunofluorescent staining and quantitative real-time PCR

A. Immunofluorescent (IF) staining on intestinal sections for Lysozyme showed reduced number of Lysozyme^{+} Paneth cells (**red**) in *Rab8a*$^{-/-}$ crypts. Most *Rab8a*$^{-/-}$ crypts did not show any staining for Lysozyme. Tissue morphology and nuclear staining is highlighted by immunofluorescent staining for E-Cadherin (**green**) and Topro-3 (**blue**) rspectively.

B. Quantification of 102 wild-type crypts and 103 *Rab8a*$^{-/-}$ crypts showed significant reduction in number of Lysozyme^{+} Paneth cells per crypt in *Rab8a*$^{-/-}$ intestines as compared to wild-type intestines that showed 3 Paneth cells per crypt on average. The quantifications were performed on IF stained intestinal sections as shown in **Fig. 2A**.

C. Quantitative RT-PCR showed no statistically significant change in genes specifically expressed by Paneth cells (such as Lysozyme, Matrix Metalloproteinase-7 (Mmp7) and Defensin- 5(Defa-5)) in *Rab8a*$^{-/-}$ intestinal tissue. Mmp7 gene expression was higher in *Rab8a* knockout intestines however was not statistically significant.

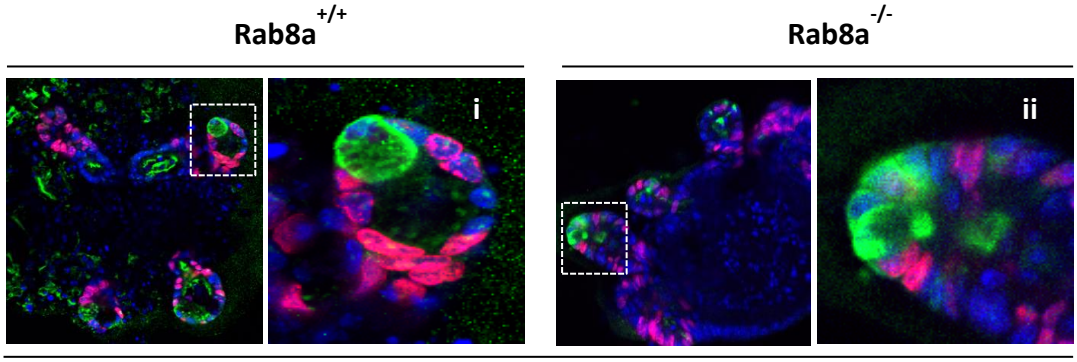
Rab8a+/+
Rab8a-/-
i
ii
EdU Lysozyme Topro 3

Figure 3: Analysis of Paneth cells using immunofluorescent staining of organoids

Lysozyme (**green**) and EdU (1 hr., **red**) staining of *Rab8a*$^{+/+}$ and *Rab8a*$^{-/-}$ organoids detected Lysozyme^{+} Paneth cells in proliferating buds of surviving organoids cultured for 7 days in ENR media. Representative organoid-buds are enclosed in **white boxes** and shown in (**i**) for wild-tye and in (**ii**) for *Rab8a*$^{-/-}$ organoids. Nuclear staining with Topro-3 is shown in **blue**.

A

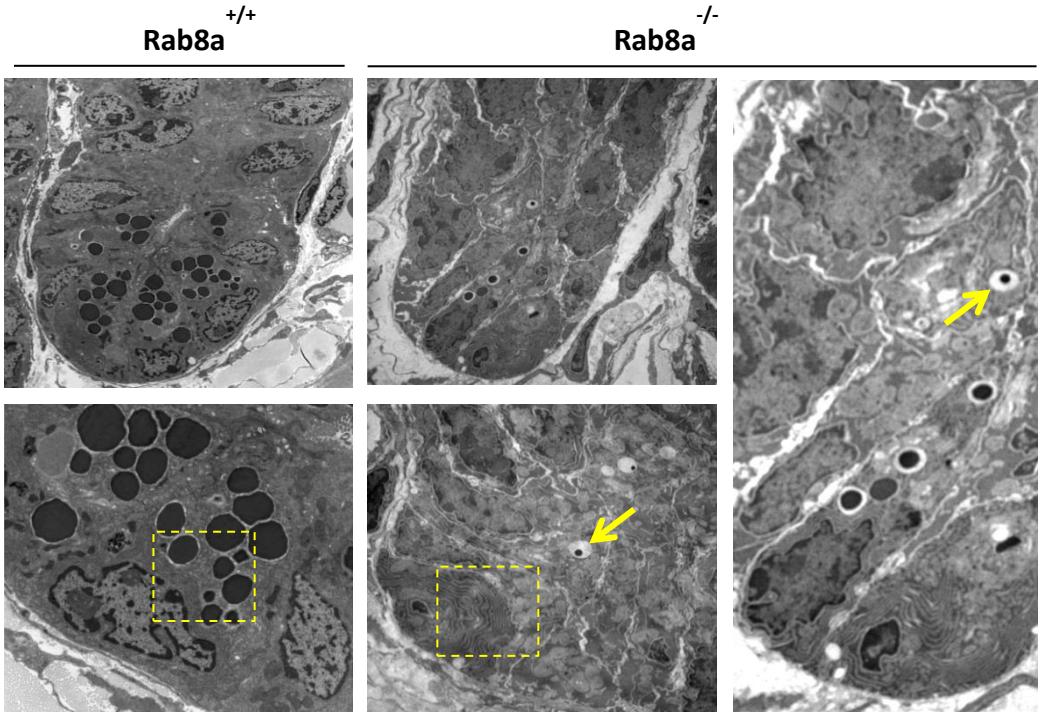

B

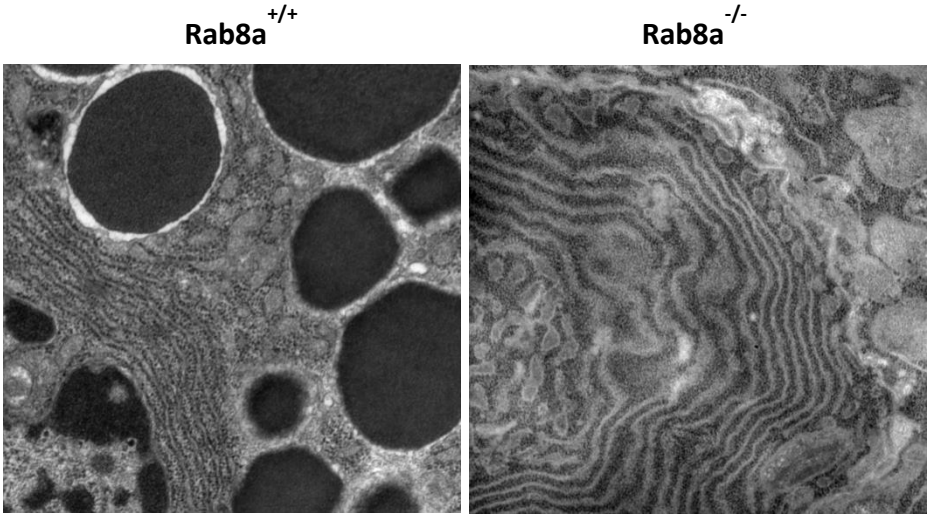

Figure 4: Examination of Paneth cell morphology using TEM

A. TEM micrographs showed reduction in number of Paneth cells in *Rab8a*$^{-/-}$ crypts. Paneth cells are easily identified by the presence of large secretory granules. Residual Paneth cells showed fewer and smaller granules. **Arrows** point at a secretory granule in *Rab8a*$^{-/-}$ crypt. Yellow boxed areas are described in **Fig. 4B**.

B. TEM micrographs of small intestines showed an expansion of smooth Endoplasmic reticulum in all remaining *Rab8a*$^{-/-}$ Paneth cells. The thickness of stacked ER cisternae was significantly expanded in *Rab8a*$^{-/-}$ (834±46 nm) than in *Rab8a*$^{+/+}$ (333±7 nm) Paneth cells. Images shown are magnified from **Fig. 4A** (**yellow boxes**).

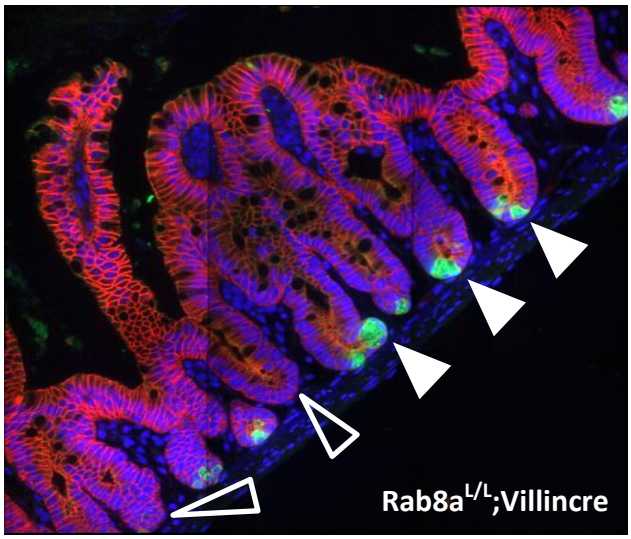

E-Cad Lysozyme Topro-3

Figure 5: Analysis of Paneth cells in *Rab8a$^{L/L}$;Villincre* intestines using immunofluorescent staining

Immunofluorescent staining showed occasional absence of Lysozyme^{+} Paneth cells (**green**) in histological sections from *Rab8a$^{L/L}$;Villincre* intestines. Continuous stretches of Paneth cell-containing crypts (**solid arrowheads**) were observed adjacent to Paneth cell-deficient crypts (**empty arrowheads**) in these sections. Morphology of intestine is highlighted by E-Cadherin (**red**) and nuclear staining (Topro-3) is shown in **blue**.

A

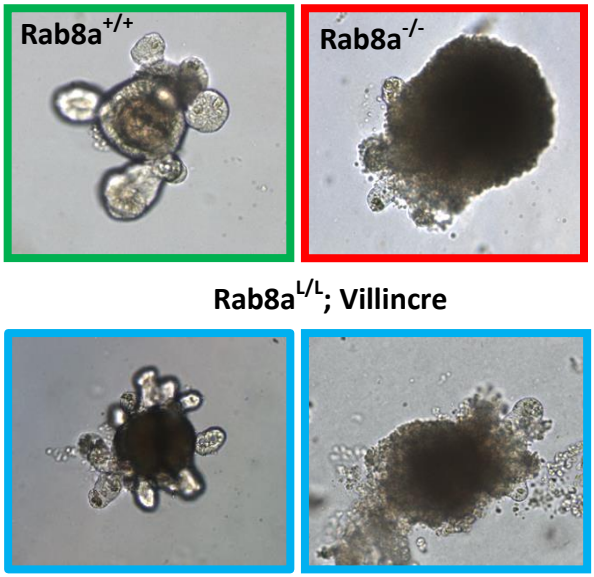
Rab8a+/+
Rab8a-/-
Rab8aL/L; Villincre

B

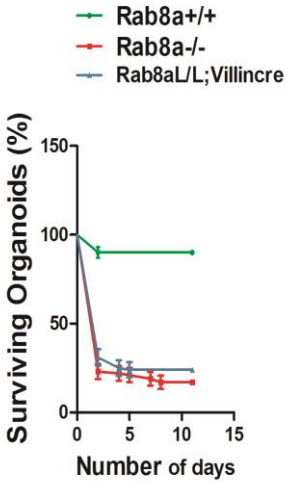
Rab8a+/+
Rab8a-/-
Rab8aL/L;Villincre
Surviving Organoids (%)
150
100
50
0
0
5
10
15
Number of days

Figure 6: Analysis of growth and morphology of organoids ex vivo

A. Representative bright-field images of organoids isolated from *Rab8a*$^{+/+}$, *Rab8a*$^{-/-}$ and *Rab8a*$^{L/L}$*; Villincre* intestines were cultured in vitro for 7 days in ENR media. As compared to wild-type organoids (boxed in **green**), *Rab8a*$^{-/-}$ organoids (boxed in **red**) showed smaller buds and larger central lumen. Organoids isolated from *Rab8a*$^{L/L}$*; Villincre* intestines showed morphology similar to both wild-type and *Rab8a*$^{-/-}$ organoids (boxed in **blue**).

B. Crypts (N=100) from each genotype were seeded in triplicates, and the number of surviving organoids were counted daily starting from day of seeding (Day 0). Growth of 80% *Rab8a*$^{-/-}$ intestinal organoids (**red line**) was arrested within the first 2 days. *Rab8a*$^{L/L}$*;Villincre* (**blue line**) did not show significant improvement in organoid survivability.

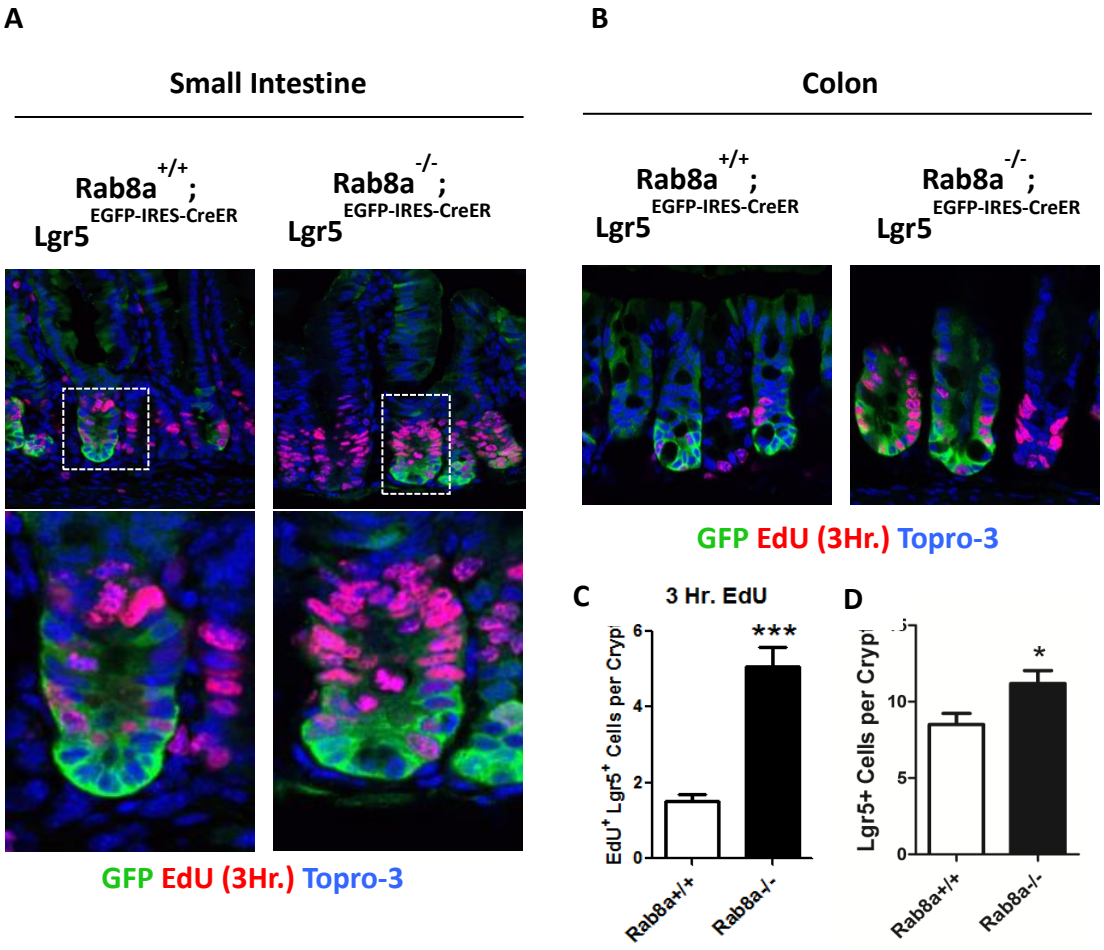
A
Small Intestine
Rab8a+/+; Lgr5EGFP-IRES-CreER
Rab8a-/-; Lgr5EGFP-IRES-CreER
GFP EdU (3Hr.) Topro-3
B
Colon
Rab8a+/+; Lgr5EGFP-IRES-CreER
Rab8a-/-; Lgr5EGFP-IRES-CreER
GFP EdU (3Hr.) Topro-3
C
3 Hr. EdU
EdU+ Lgr5+ Cells per Crypt
***
Rab8a+/+
Rab8a-/-
D
Lgr5+ Cells per Crypt
*
Rab8a+/+
Rab8a-/-
E
Rab8a+/+
Rab8a-/-
BrDU (1 hr.)
F
Rab8a+/+
Rab8a-/-
E-Cad pHH3

Figure 7: Analysis of intestinal stem and proliferative cell compartment using immunofluorescent and immunohistochemical staining

A. Immunofluorescent staining for Lgr5 (GFP, **green**) and EdU label (3 hrs, **red**) using mouse small intestinal cryo-sections showed a significant increase of proliferative $Lgr5^{+}$ cells in *Rab8a*$^{-/-}$*;Lgr5*$^{EGFP\ IRES\ CreERT2}$ mice. Nuclear staining (Topro-3) is shown in **blue**.

B. Immunofluorescent staining for Lgr5 (GFP, **green**) and EdU label (3 hrs, **red**) using mouse large intestinal cryo-sections showed a significant increase of proliferative $Lgr5^{+}$ cells in *Rab8a*$^{-/-}$*;Lgr5*$^{EGFP\ IRES\ CreERT2}$ mice. Nuclear staining (Topro-3) is shown in **blue**.

C. Quantification of $EdU^{+}Lgr5\text{-}GFP^{+}$ double positive cells in small intestinal sections (as shown in **Fig. 7A**) showed a significant increase in *Rab8a*$^{-/-}$*;Lgr5*$^{EGFP\ IRES\ CreERT2}$ mouse small intestines. 45 crypts from *Lgr5*$^{EGFP\ IRES\ CreERT2}$ or *Rab8a*$^{-/-}$*;Lgr5*$^{EGFP\ IRES\ CreERT2}$ mouse small intestines that contained $Lgr5^{+}$ (**green**) cells were examined for presence of EdU (**red**) and quantified as EdU^{+}-Lgr5-GFP^{+} double positive cells.

D. Quantification of Lgr5-GFP^{+} (**green**) cells in small intestinal sections (as shown in **Fig. 7A**) showed a significant increase in *Rab8a*$^{-/-}$*;Lgr5*$^{EGFP\ IRES\ CreERT2}$ mouse small intestines. 45 crypts that contained $Lgr5^{+}$ cells were analyzed in tissue sections from *Lgr5*$^{EGFP\ IRES\ CreERT2}$ or *Rab8a*$^{-/-}$*;Lgr5*$^{EGFP\ IRES\ CreERT2}$ mouse small intestines.

E. Immunohistochemistry for BrdU (1 hr., **brown**) detected an expanded transit amplifying epithelial cell compartment in *Rab8a*$^{-/-}$ small intestine.

F. Immunofluorescence staining showed increased number of $pHH3^{+}$ cells (**red**) in *Rab8a*$^{-/-}$ small intestines. Immunofluorescent staining for E-Cadherin (**green**) shows the morphology of small intestines.

A

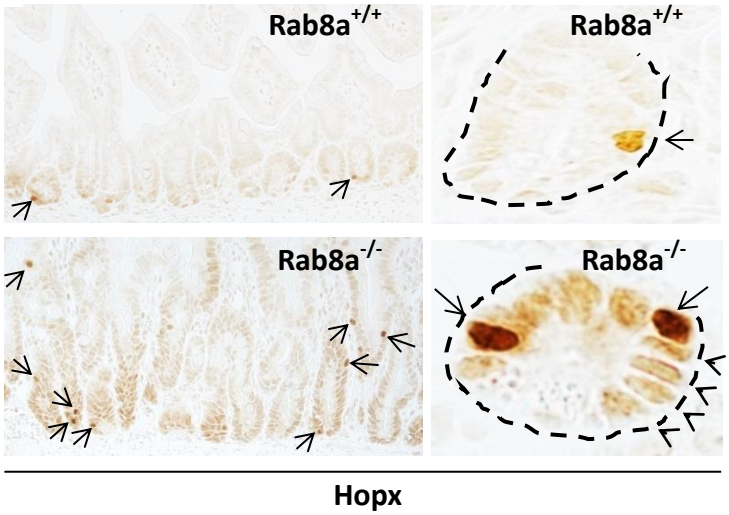
Rab8a+/+
Rab8a+/+
Rab8a-/-
Rab8a-/-
Hopx

B

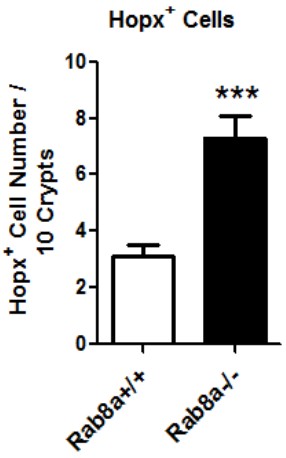
Hopx+ Cells
Hopx+ Cell Number / 10 Crypts
10
8
6
4
2
0
***
Rab8a+/+
Rab8a-/-

C

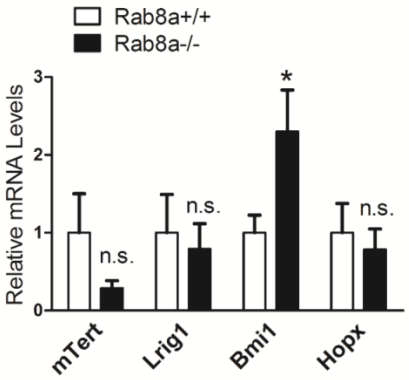
Rab8a+/+
Rab8a-/-
Relative mRNA Levels
3
2
1
0
n.s.
n.s.
*
n.s.
mTert
Lrig1
Bmi1
Hopx

Figure 8: Examination of Hopx^{+} cell compartment in mouse small intestines using immunohistochemical staining

A. Immunohistochemical staining showed increase in number of Hopx^{+} cells (**brown**) in *Rab8a*$^{-/-}$ small intestines. *Rab8a*$^{-/-}$ crypts contained more cells with the strong Hopx immunoreactivity (**arrows**). **Arrowheads** point to cells with moderate immunoreactivity seen in *Rab8a*$^{-/-}$ crypts.

B. Based on immunohistochemical staining (as shown in **Fig. 8A**), significant increase in Hopx^{+} cells was observed in *Rab8a*$^{-/-}$ small intestines. The graph shows number of Hopx+ cells in 10 continuous crypts. 100 crypts were quantified for presence of Hopx staining in each section of independent *Rab8a*$^{+/+}$ and *Rab8a*$^{-/-}$ mice.

C. Quantitative RT-PCR identified statistically significant increase in B Lymphoma Mo-MLV Insertion Region 1 Homolog (*Bmi1)* gene expression in *Rab8a*$^{-/-}$ intestines. Other genes expressed by "+4"/slow-cycling cells such as mouse telomerase reverse transcriptase (mTert), Leucine-rich repeats and immunoglobulin-like domains 1 (Lrig1) and Homeodomain protein X (Hopx) did not change significantly. n.s. stands for "not significant".

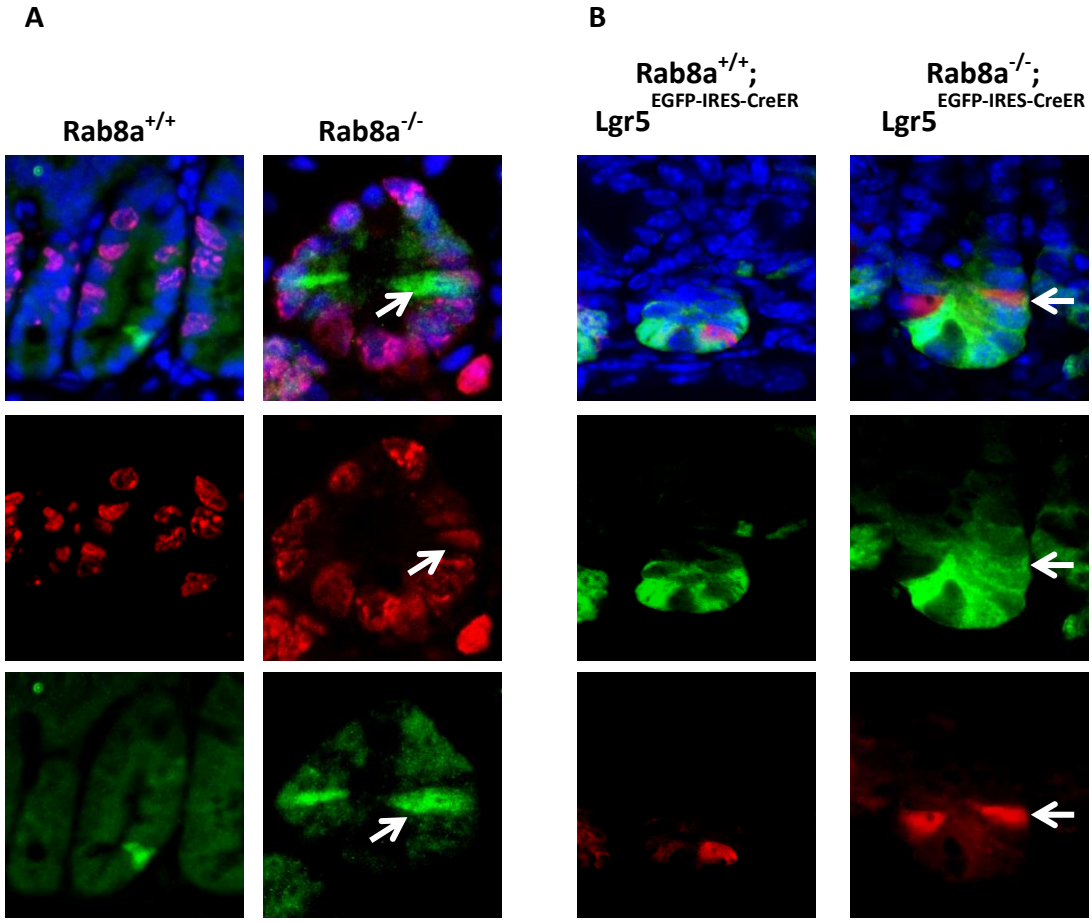
A
Rab8a+/+
Rab8a-/-
B
Rab8a+/+; EGFP-IRES-CreER Lgr5
Rab8a-/-; EGFP-IRES-CreER Lgr5
Hopx EdU (1 Hr.) Topro-3
Hopx GFP (Lgr5+) Topro-3

Figure 9: Analysis of intestinal stem cell compartment using immunofluorescent staining

A. Immunofluorescent co-staining for Hopx (**green**) and EdU (1 hr., **red**) (**arrows**) detected proliferative $Hopx^{+}$ cells in *Rab8a*$^{-/-}$ small intestinal cryo sections which were absent in wild type small intestines. Nuclear staining (Topro-3) is shown in **blue**.

B. Immunofluorescent co-staining for Lgr5 (EGFP, **green**) and Hopx (**red**) (**arrows**) showed increased number of double positive ($Lgr5^{+}$ $Hopx^{+}$) cell types in *Rab8a*$^{-/-}$ small intestinal cryo-sections. Nuclear staining (Topro-3) is shown in **blue**.

CHAPTER 4

RAB8A CONTRIBUTES TO CANONICAL WNT ACTIVITY AT INTESTINAL STEM CELL NICHE BY REGULATING WNT LIGAND SECRETION

Information included in this chapter is taken from and are published in Das et al., Development (2015), 142(12):2147-62

Rab8a is the master regulator of post-golgi vesicular trafficking through plasma membrane suggesting its potential role in secretory activity of crucial growth factors in stem cell niches such as the one that exists at crypt base. Paneth cells that co-occupy the crypt base with stem cells secrete (along with others) an essential morphogen named Wingless type mammary tumor virus integration site (Wnt) family members. These Wnt ligands are heavily dependent on regulated vesicular trafficking implicating a probable function of Rab8a in Wnt ligand secretion at intestinal stem cell niche. Thus we investigated the status of Wnt activity (both Wnt secretion and signaling) in *Rab8a*$^{-/-}$ mouse intestines.

Results

Reduced canonical Wnt signaling in Rab8a*$^{-/-}$ *crypts

Intestinal crypt homeostasis relies on proper Wnt signaling in the stem cell niche (Clarke, 2006; Gregorieff and Clevers, 2005; Haegebarth and Clevers, 2009). We took various approaches to check if Wnt signaling is affected in absence of Rab8a. Quantitative RT-PCR for canonical Wnt targets showed decreased *Axin2* and *Ascl2* expression in *Rab8a*$^{-/-}$ intestines **(Fig. 10A)**. Western blots detected reduced levels of total β-catenin, Tcf1, Tcf4, and Sox9 **(Fig. 10B)**. However, the level of c-Myc, a marker of transit amplifying cells (Gregorieff et al., 2005), increased in *Rab8a*$^{-/-}$ intestines **(Fig. 10B)**. Immunohistochemical analyses of β-catenin showed reduced number of crypts with nuclear β-catenin^{+} cells (only Paneth cell-containing crypts were compared, **Fig. 11**). Within a single *Rab8a*$^{-/-}$ crypt, the number of nuclear β-catenin^{+} cells was also

reduced compared to wild-types, collectively suggesting reduced Wnt/β-catenin signaling in knockout crypts.

We then used the *Axin2*$^{LacZ/+}$ reporter allele to determine the canonical Wnt signaling activity (Lustig et al., 2002). In this reporter mouse line, LacZ (β-galactosidase) expression is driven by Axin2 promoter, Axin2 being a downstream effector of canonical Wnt pathway. Thus, upon β-gal application Axin2 expressing (Wnt receiving) cells are stained blue. By establishing *Rab8a*$^{-/-}$*; Axin2*$^{lacZ/+}$ mice, we observed reduced *Axin2*$^{lacZ/+}$ reporter activities indicated by β-gal staining of mouse small intestines as compared to *Rab8a*$^{+/+}$*; Axin2*$^{lacZ/+}$ littermates **(Fig. 12A)** thus confirming reduced canonical Wnt activity in *Rab8a*$^{-/-}$ crypts.

We further analyzed *Axin2*$^{lacZ/+}$ reporter activity in cultured intestinal organoids. Similar to the above in vivo results, *Rab8a*$^{-/-}$*; Axin2*$^{lacZ/+}$ organoids also showed reduced β-gal activities in epithelial buds when compared to those in *Rab8a*$^{+/+}$*;Axin2*$^{lacZ/+}$ epithelial buds **(Fig. 12B, C)**. Remarkably, *Rab8a*$^{-/-}$ intestinal organoids, as well as the *Rab8a*$^{loxP/loxP;}$*Villin-Cre* organoids, showed severely compromised growth and budding capability, with nearly 70% of them arrested within 2 days **(Fig. 6 and Fig. 12C)**. The majority of surviving *Rab8a*$^{-/-}$ organoids showed tiny buds and large lumens **(Fig. 6A and 12B)** similar to *Wnt3*- or *Atoh1*-deficient enteroids (Durand et al., 2012; Farin et al., 2012) suggesting a possible Wnt dependent Paneth cell defect in knockout organoids that is unable to support organoid structure in vitro. Importantly, when we supplemented culture media with exogenous Wnt3a, the surviving and propagating

capacities of *Rab8a* deficient organoids were significantly improved by approximately 50% **(Fig. 13A, C)**. Wnt3a administration induced *Rab8a*$^{+/+}$ organoids into cyst-like morphology (Yin et al., 2014), an effect also observed for *Rab8a* deficient organoids. Treating *Rab8a* deficient organoids with CHIR99021, a GSK3β inhibitor improved survivability by 46% **(Fig. 13B and C)**, supporting the notion that the poor growth of *Rab8a*$^{-/-}$ organoids was due to insufficient Wnt proteins and *Rab8a* deficient cells can properly transduce Wnt signal.

Reduced Wnt protein secretion in absence of Rab8a

To check the function of Rab8a in Wnt protein secretion we took several different approaches. As Wnt5a is endogenously expressed by MEFs (Sato et al., 2004) and known to influence non-canonical and canonical Wnt pathways in mammalian cells (He et al., 1997; Mikels and Nusse, 2006; Okamoto et al., 2014), we compared Wnt5a/b secretion in *Rab8a*$^{+/+}$ and *Rab8a*$^{-/-}$ MEFs. . Using Wnt5a/b specific antibody, we detected significant reductions in secreted Wnt5a/b in media conditioned by *Rab8a*$^{-/-}$ MEFs **(Fig. 14)**. *Rab8a*$^{-/-}$ MEFs accumulated more intracellular Wnt5a/b indicated by cell lysates **(Fig. 14)**, suggesting that a blockage of Wnt5a/b secretion might have caused ligand accumulation. When an exogenous WNT5A was transiently transfected into *Rab8a*$^{+/+}$ MEFs, it enhanced Wnt Topflash reporter activity **(Fig. 15A)**, suggesting an elevated WNT5A autocrine signaling (Goel et al., 2012). However, similar overexpression of WNT5A in *Rab8a*$^{-/-}$ MEFs failed to augment Wnt reporter activity to the same extent

(Fig. 15A), suggesting that *Rab8a*$^{-/-}$ MEFs may not properly secrete the transfected WNT5A.

We asked whether Rab8a deficiency also impaired secretion of canonical Wnt ligands such as Wnt3a. MEFs do not detectably express endogenous Wnt3a. Wnt3a-Gluc, a fusion protein composing Wnt3a and Gaussia luciferase (Chen et al., 2009), has been shown to act as a functional ligand and been successfully used to screen for small molecular inhibitors of Porcupine (Chen et al., 2009). We transiently transfected *Rab8a*$^{+/+}$ and *Rab8a*$^{-/-}$ MEFs with Wnt3a-GLuc and assayed the conditioned media by luciferase assay (Chen et al., 2009). We detected an approximately 80% reduction of secreted Wnt3a-Gluc in *Rab8a*$^{-/-}$ MEF conditioned media compared to *Rab8a*$^{+/+}$ MEF conditioned media **(Fig. 15B)**. No reduction of Wnt3a-Gluc secretion was detected for MEFs with stably *Rab8b* depletion by a lentiviral ShRNA against *Rab8b* **(Fig. 15B)**. Combined depletion of *Rab8a* and *Rab8b* did not elicit additive inhibition on Wnt3a-Gluc secretion compared to *Rab8a* deletion alone **(Fig. 15B)**, suggesting that Rab8b neither by itself nor in combination with Rab8a influences Wnt3a-Gluc secretion. This was in agreement with the primary function of RAB8B in ligand-receiving cells (Demir et al., 2013). Stronger inhibitory effects on Wnt3a-Gluc secretion were observed with treatment of C59 (~93% reduction), a Porcupine inhibitor (Chen et al., 2009), or by *Gpr177* ablation in MEFs (~97% reduction) **(Fig. 15B)**. Notably, in contrast to a near complete abolishment of Wnt3a-Gluc secretion by C59 treatment or *Gpr177* deletion, 19% of Wnt3a-Gluc proteins were still detected in *Rab8a*$^{-/-}$ MEF-conditioned media **(Fig.**

15B), suggesting that *Rab8a* deletion partially compromised Wnt secretion, observations consistent with data on Wnt5a/b secretion **(Fig. 15B)**.

So far our data showed that Rab8a regulates Wnt protein secretion. Next we examined if Rab8a is involved in secretion of other cargoes and determined if secretory activities of several non-Wnt ligands, including another important morphogen – Sonic hedgehog (Shh)-Renilla luciferase (Ma et al., 2002), a biosynthetic cargo – secreted Alkaline Phosphatase (Yu et al., 2014), and a constitutively secreted cargo – Metridia Luciferase (Markova et al., 2004) are affected in absence of Rab8a. None of the above showed significant secretory abnormalities in *Rab8a*$^{-/-}$ MEFs **(Fig. 15C)**, suggesting a degree of cargo selectivity by Rab8a.

Absence of Rab8a does not affect Wnt signal transduction

Rab8a knockout intestine show reduced canonical Wnt signaling in crypt compartment that potentially affects the Paneth cell morphology in vivo as well as organoid morphology and its survival ex vivo. This phenotype observed in *Rab8a*$^{-/-}$ intestines however can be a result of impaired Wnt signal transduction, for instance if Rab8a vesicular trafficking targets Wnt receptors and co-receptors to the plasma membrane. Thus, next we examined if Wnt signal transduction is affected in absence of Rab8a. Interestingly, the amount of surface localized Frizzled receptors and Lrp6 co-receptor did not change in *Rab8a* null Mouse Embryonic Fibroblasts (MEFs) **(Fig. 16A)**. Most importantly, addition of Wnt3a proteins to cultured *Rab8a*$^{-/-}$ MEFs markedly stimulated cell surface Lrp6 phosphorylation (Ser1490) to a level equivalent to *Rab8a*$^{+/+}$

cells **(Fig. 16A)**, suggesting that *Rab8a*$^{-/-}$ cells can properly respond to exogenous ligand stimulation by assembling Lrp6-containing surface protein complex (Bilic et al., 2007). In Topflash reporter assays, *Rab8a*$^{-/-}$ MEFs showed lower basal reporter activities in serum-deprived conditions **(compare white bars in Fig. 16B)**, and again responded strongly to exogenous Wnt3a **(compare black bars, Fig. 16B)**.

Discussion

Our data show that absence of Rab8a function causes reduction in Wnt ligand (Wnt3a and Wnt5a) secretion and canonical Wnt signaling (Axin2 reporter activity) in intestines. However, Rab8a does not seem to affect the anterograde transport of Wnt (co-) receptors (Lrp6 and Fzd 1-10), activation of Lrp6 or transduction of Wnt signaling pathway in cells. All these data together suggest that Rab8a regulates canonical Wnt activity at the intestinal stem cell niche by regulating Wnt ligand secretion and not Wnt signaling in ligand receiving cells.

In presence of Wnt ligands, Frizzled and Lrp6 are recruited to the plasma membrane where they bind to their ligand (Wnt proteins) and recruit several proteins to form multiprotein complex. These proteins include Dishevleled, GSK3β, CK1γ, Axin2 and APC. Subsequently the protein signalosome complex is internalized through Caveolin mediated endocytosis to mature into multivesicular bodies where activity of GSK3β activity is inhibited. This leads to availability of β-catenin to enter nucleus and transcribe several Wnt target genes. In complement to our results, an independent study discovered the association of RAB8B, another isoform of RAB8, with Wnt activity in Wnt receiving cells (Demir et al., 2013). In vivo and in vitro data suggest that RAB8B acts as a positive regulator of Wnt/β-catenin signaling by regulating receptor activity at plasma membrane particularly by facilitating internalization of Caveolin mediated endocytosis of Lrp6 and thus amplifying Wnt signal at receiving end. Interestingly, RAB8B depletion did not affect other major signaling pathways including BMP4, TNFα and FGF8. The

authors also showed that deletion of RAB8A did not have any impact on Wnt signaling in these cells. Similarly, in this study we show that *Rab8b*-KD MEF cells did not affect Wnt3a-Gluc secretion. Thus, combination of our study and observations from Demir K. et al we propose that both isoforms of Rab8 have mutually exclusive functions- Rab8a regulates Wnt secretion in ligand secreting cells and Rab8b regulates Wnt receptor activity in Wnt receiving cells. Additionally, both isoforms have selective preference towards and potentiate Wnt/β-catenin signaling.

Deleting Rab8a in vivo or in mammalian cell lines did not abolish Wnt secretion completely. For instance, as compared to *Gpr177* MEFs, *Rab8a* null MEFS showed residual Wnt secretory activity in their media (**Fig. 15B**). Additionally we observed few *Axin2*$^{LacZ/+}$ cells in *Rab8a*$^{-/-}$ crypts (**Fig. 12**). Since canonical Wnt signaling is essential for organoid growth and survival ex vivo (Farin et al., 2012), taken together, we show that absence of Rab8a compromised Wnt secretion only partially. That being said, residual Wnt protein activity was potentiated by R-Spondin1 in crypt culture media to support survival of at least 30% *Rab8a*$^{-/-}$ or *Rab8a*$^{L/L}$*; Villincre* organoids.

Rab8a did not affect Frizzled or Lrp6 expression and its activation in Wnt receiving cells, however interestingly enough, we observed that *Rab8a*$^{-/-}$ MEFs were hyper-sensitive to presence of exogenous Wnt3a. This indicates towards a plausible explanation for how *Rab8a*$^{-/-}$ crypts tolerate loss in Wnt activity in vivo (**Fig. 7**). We speculate that global loss of Rab8a reduces Wnt proteins in ISC niche that subsequently changes properties of *Rab8a* null Wnt receiving cells making them hyper-responsive to

presence of ligands. This allows amplification of canonical Wnt signaling in *Rab8a*$^{-/-}$ cells despite of reduced Wnt levels in the surrounding.

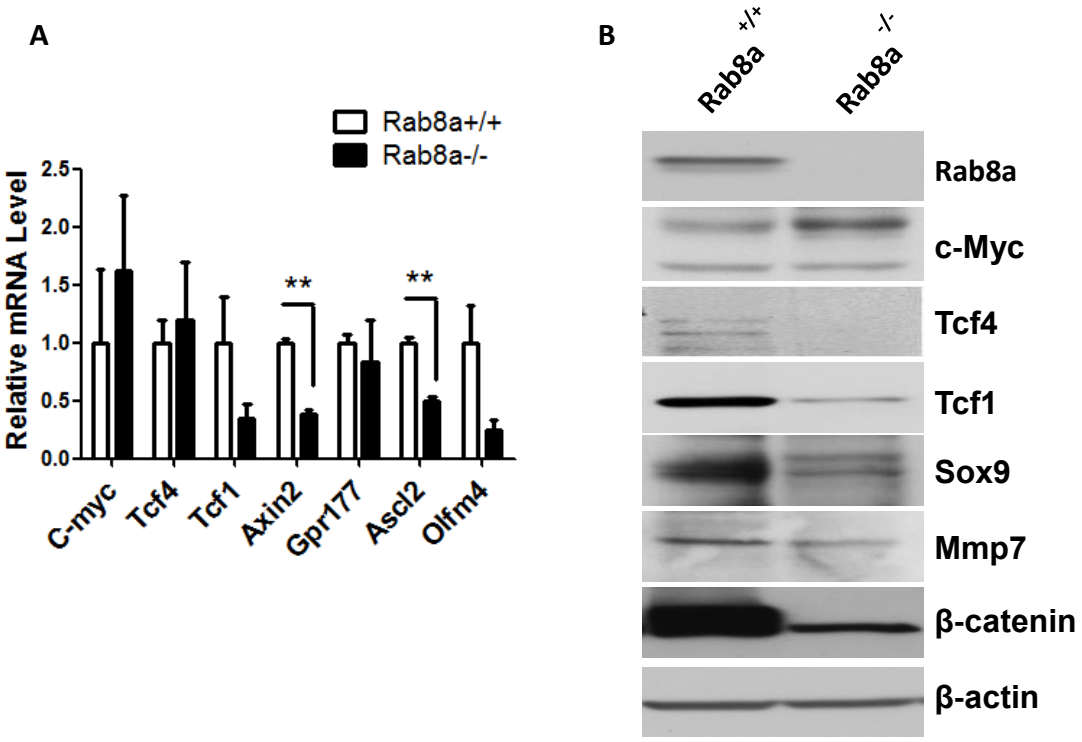
A
Rab8a+/+
Rab8a-/-
Relative mRNA Level
2.5
2.0
1.5
1.0
0.5
0.0
**
**
C-myc
Tcf4
Tcf1
Axin2
Gpr177
Ascl2
Olfm4
B
+/+
-/-
Rab8a
Rab8a
c-Myc
Tcf4
Tcf1
Sox9
Mmp7
β-catenin
β-actin

Figure 10: Analysis of canonical Wnt activity in intestinal tissue using quantitative RT-PCR and immunoblot

A. Quantitative RT-PCR showed reduced canonical Wnt target genes such as *Tcf1*, *Olfm4*, *Axin2* and *Ascl2* in *Rab8a*$^{-/-}$ intestines. Other canonical Wnt target genes such as *C-myc*, *Tcf-4* and *Gpr177* did not show statistically significant changes in their expression in absence of *Rab8a*.

B. Western blots using total intestinal lysates showed reduced levels of Tcf1, Tcf4, Sox9, Mmp7 and β-catenin levels in *Rab8a*$^{-/-}$ intestines. Western blotting did not detect any Rab8a in *Rab8a*$^{-/-}$ intestines. Protein levels of C-myc were increased in *Rab8a*$^{-/-}$ intestines.

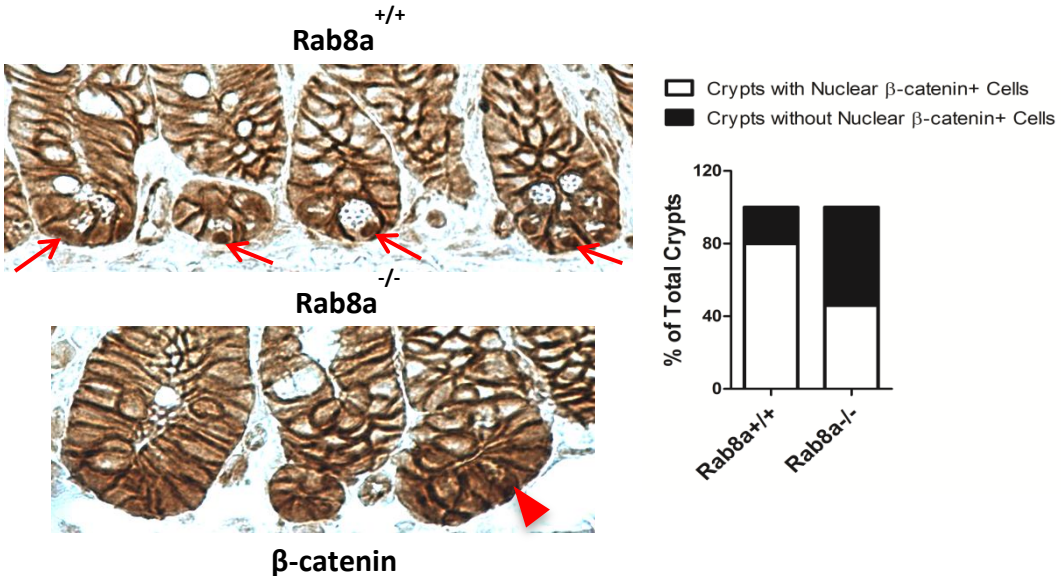
+/+
Rab8a
-/-
Rab8a
β-catenin
Crypts with Nuclear β-catenin+ Cells
Crypts without Nuclear β-catenin+ Cells
% of Total Crypts
120
80
40
0
Rab8a+/+
Rab8a-/-

Figure 11: Examination of nuclear β-catenin by immunohstochemistry

Immunohistochemistry for β-catenin (**brown**) showed reduced number of crypts with nuclear β-catenin^{+} Paneth cells in *Rab8a*$^{-/-}$ mice (**arrowhead**) that are frequently observed in wild-type intestines (**arrows**). Crypts with detectable Paneth cells were scored for their positive or negative inclusion for nuclear β-catenin (N=50 for each genotype). ~60% of *Rab8a*$^{-/-}$ and ~20% of wild-type crypts with Paneth cells did not show any nuclear β-catenin staining.

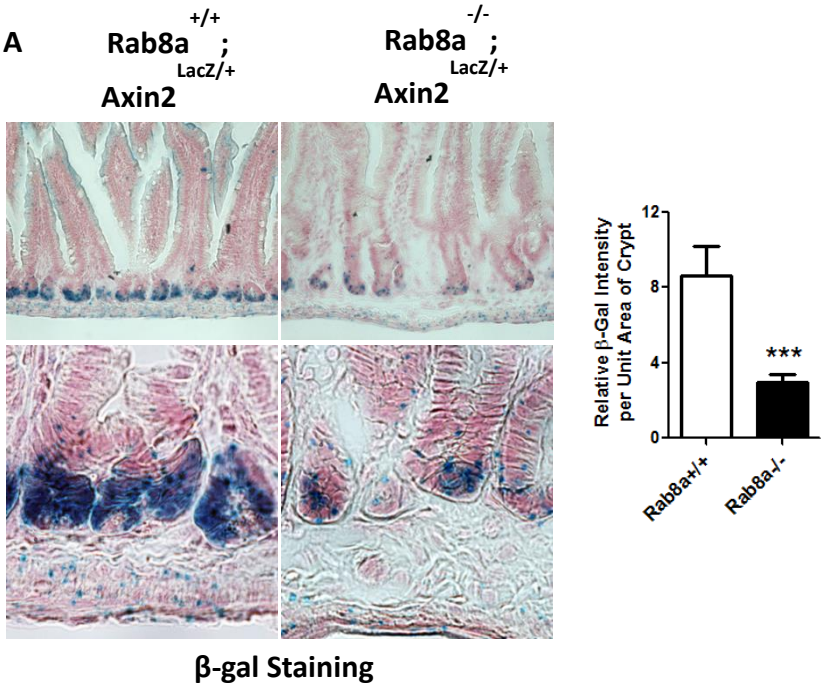
A
Rab8a +/+ ; Axin2 LacZ/+
Rab8a -/- ; Axin2 LacZ/+
Relative β-Gal Intensity per Unit Area of Crypt
12
8
4
0
***
Rab8a+/+
Rab8a-/-
β-gal Staining

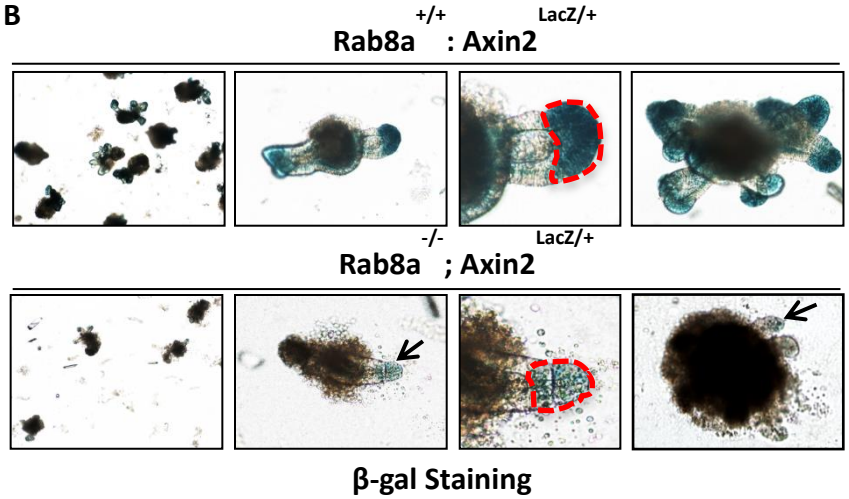
B
Rab8a +/+ : Axin2 LacZ/+
Rab8a -/- ; Axin2 LacZ/+
β-gal Staining

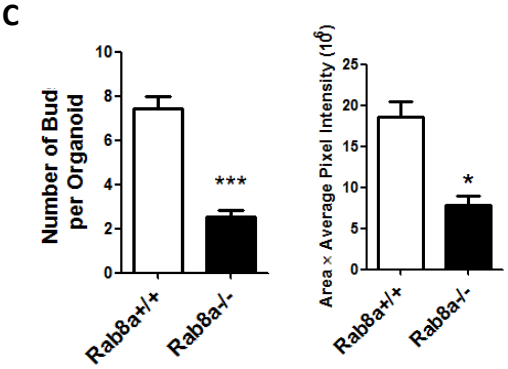
C
Number of Bud per Organoid
10
8
6
4
2
0
***
Rab8a+/+
Rab8a-/-
Area × Average Pixel Intensity (10⁶)
25
20
15
10
5
0
*
Rab8a+/+
Rab8a-/-

Figure 12: Analysis of canonical Wnt signaling in crypt compartment using immunohistochemical staining for β-gal

A. Brighfield images of β-Gal staining (**blue**) from mouse small intestines showed significant reduction of Axin2 reporter activity in crypts and underlying smooth muscle in *Axin2$^{lacZ/+}$; Rab8a$^{-/-}$* mice. The sections were counterstained with nuclear fast red (**pink**). The area covered by β-Gal staining and the intensity of β-Gal staining were quantified using Image J (Colour deconvolution) in each crypt. The graph was generated by plotting β-Gal staining per unit area in 30 continuous crypts from wild-type and *Axin2$^{lacZ/+}$; Rab8a$^{-/-}$* intestines. Quantifications showed significant reduction in Axin2 reporter activity in *Axin2$^{lacZ/+}$; Rab8a$^{-/-}$* crypts.

B. Brightfield images of β-Gal (**blue**) stained *Axin2$^{lacZ/+}$* and *Axin2$^{lacZ/+}$; Rab8a$^{-/-}$* intestinal organoids showed significantly reduced β-Gal staining in the crypt domains (enclosed bud areas in **red**), reduced bud number, reduced bud size and larger central lumen in *Rab8a$^{-/-}$* organoids. Images were taken at day 10 after crypt-seeding. **Arrows** point to small buds in *Rab8a$^{-/-}$* organoids.

C. Quantifications (N=50 for each genotype per experiment) showed reduced number of buds in individual *Rab8a$^{-/-}$* organoids. Organoids from each genotype were also analyzed (N=25 for each genotype per experiment) for β-galactosidase stained bud areas (**circled in red** in images shown in **Fig. 12B**) using Image J (Colour deconvolution). Graph

generated by multiplying intensity and area covered by β-Gal showed significant reduction in Axin2 reporter activity in *Axin2*$^{lacZ/+}$*; Rab8a*$^{-/-}$ intestinal organoid buds.

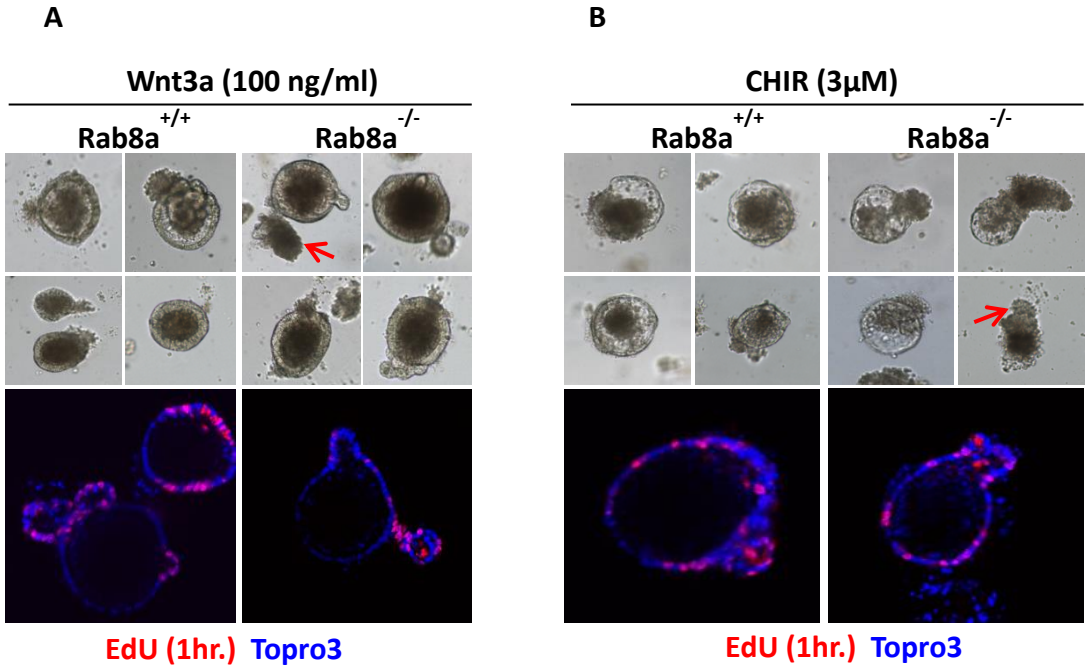
A
Wnt3a (100 ng/ml)
Rab8a +/+
Rab8a -/-
EdU (1hr.) Topro3
B
CHIR (3μM)
Rab8a +/+
Rab8a -/-
EdU (1hr.) Topro3

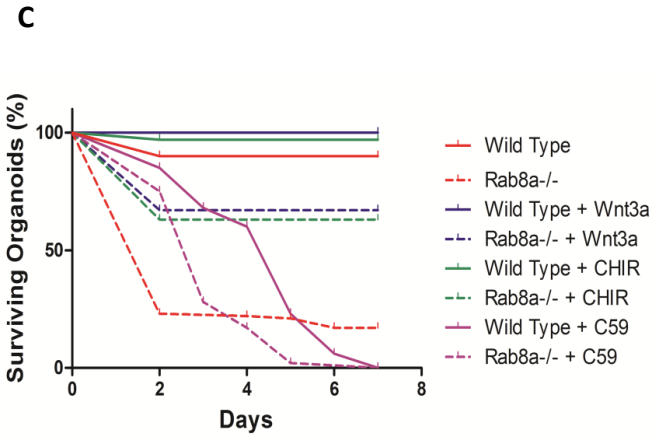
C
Surviving Organoids (%)
100
50
0
0
2
4
6
8
Days
Wild Type
Rab8a-/-
Wild Type + Wnt3a
Rab8a-/- + Wnt3a
Wild Type + CHIR
Rab8a-/- + CHIR
Wild Type + C59
Rab8a-/- + C59

Figure 13: Analysis of effect of exogenous activation of Wnt pathway in intestinal organoids

A-B. After seeding, *Rab8*$^{+/+}$ and *Rab8a*$^{-/-}$ intestinal organoids (N=100 for each genotype) were immediately supplemented with Wnt3a (100ng/ml) or GSK3β inhibitor (CHIR, 3μM). Brighfield images and immunofluorescent staining for proliferation (1Hr. EdU, **red**) and nucleus (Topro-3, **blue**) showed similar morphological and proliferative features of *Rab8a*$^{-/-}$ and *Rab8*$^{+/+}$ organoids with either Wnt3a or CHIR treatment. Wnt3a and CHIR supplements led to typical cyst like structures in both *Rab8a*$^{+/+}$ and *Rab8a*$^{-/-}$ organoids. **Arrows** point to *Rab8a*$^{-/-}$ organoids unresponsive to any treatment.

C. Crypts (n=100) of each genotype were seeded in triplicates, and the numbers of surviving organoids were counted daily afterwards until Day 7. Only ~30% of *Rab8a*$^{-/-}$ organoids survived through Day 7 in regular ENR media (**red dashed line**). Exogenous supplementation of Wnt3a or activation of Wnt downstream pathway by addition of CHIR restored the growth and morphology of *Rab8a*$^{-/-}$ organoids partially **(blue dashed line and green dashed line)** by ~50%.

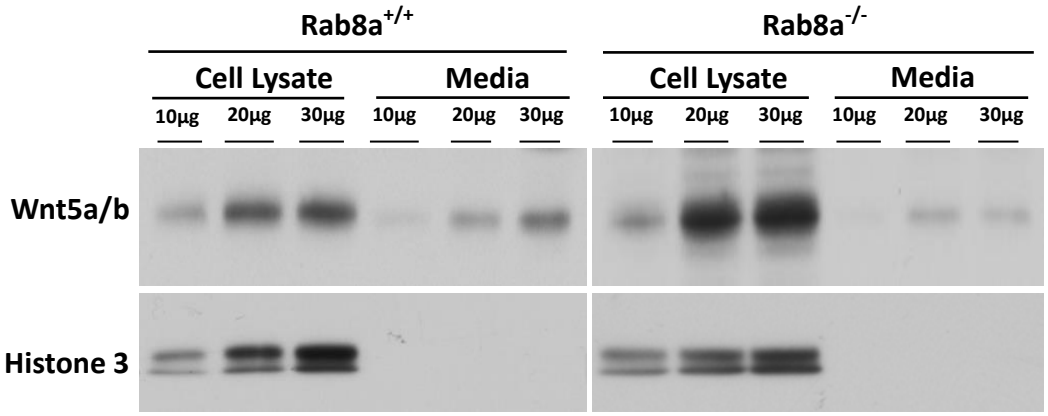
Rab8a+/+
Rab8a-/-
Cell Lysate
Media
Cell Lysate
Media
10µg
20µg
30µg
10µg
20µg
30µg
10µg
20µg
30µg
10µg
20µg
30µg
Wnt5a/b
Histone 3

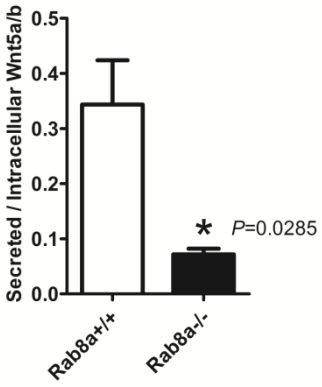
Secreted / Intracellular Wnt5a/b
0.5
0.4
0.3
0.2
0.1
0.0
*
P=0.0285
Rab8a+/+
Rab8a-/-

Figure 14: Analysis of Wnt5a/b secretion by MEFs

Wild-type and *Rab8a*$^{-/-}$ MEFs were cultured in Wnt free media until ~90% confluent. Concentrated conditioned media or cell lysates from wild-type and *Rab8a*$^{-/-}$ MEFs were analyzed by Western blots in increasing amounts. *Rab8a*$^{-/-}$ MEFs showed less secreted but more intracellular Wnt5a/b as compared to the wild-type MEFs. Histone-3 was used to detect any contamination from cells in conditioned media. Ratio of secreted/intracellular Wnt5a/b was deduced from corresponding samples (n=3, bar graph). Histone 3 was used to normalize corresponding Wnt5a/b protein bands. Quantifications showed reduced ratio of secreted to intracellular Wnt5a/b in *Rab8a*$^{-/-}$ MEFS.

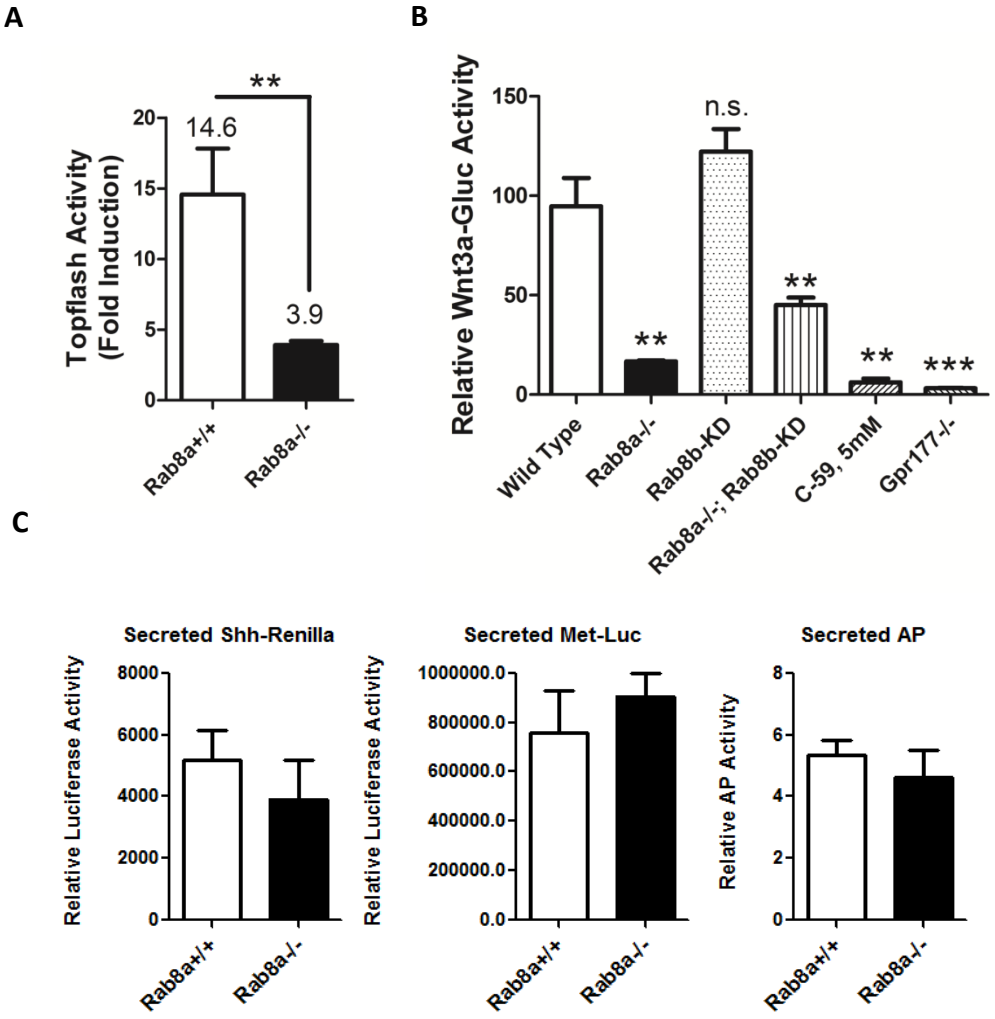
A
B
C
Topflash Activity (Fold Induction)
14.6
3.9
**
Rab8a+/+
Rab8a-/-
Relative Wnt3a-Gluc Activity
n.s.
**
***
Wild Type
Rab8a-/-
Rab8b-KD
Rab8a-/-; Rab8b-KD
C-59, 5mM
Gpr177-/-
Secreted Shh-Renilla
Relative Luciferase Activity
Secreted Met-Luc
Relative Luciferase Activity
Secreted AP
Relative AP Activity

Figure 15: Analysis of Wnt, Shh, Met-luc and SEAP secretion by MEFs

A. WNT5A or empty vectors were transiently transfected with Topflash reporter and Renilla plasmids into *Rab8a*$^{+/+}$ and *Rab8a*$^{-/-}$ MEFs, followed by dual luciferase assays. *Rab8a*$^{+/+}$ and *Rab8a*$^{-/-}$ MEFs showed 14.6 and 3.9 fold inductions of Topflash activities by transfected WNT5A compared to empty vector-transfected counterparts. Quantifications showed a significant (~10.7 fold) reduction in luciferase activity observed in *Rab8a*$^{-/-}$ cell lysates.

B. Wnt3a-Gluc was transiently transfected to wild-type, *Rab8a*$^{-/-}$, *Rab8b*-Knockdown, *Rab8a*$^{-/-}$; *Rab8b*-KD, and *Gpr177*$^{-/-}$ MEFs, with Firefly luciferase serving as control for transfection efficiency followed by dual luciferase assays. Secretion of Wnt3a-Gluc was inhibited by 5mM C59 in wild-type MEFs or achieved by *Gpr177* depletion. n.s stands for "not significant". *Rab8a*$^{-/-}$ MEFs showed ~80% reduction in Wnt3a-Gluc secretion as compared to wild-type counterparts.

C. Under similar experimental conditions as described in **Fig. 15B**, *Rab8a*$^{-/-}$ MEFs showed insignificant changes in Shh-Renilla, Met-Luc, and a bio-synthetic cargo Secreted Alkaline Phosphatase (SeAP) secretion.

A

MEFs	+/+	-/-	+/+	+/+	-/-	-/-
Wnt3a				+		+

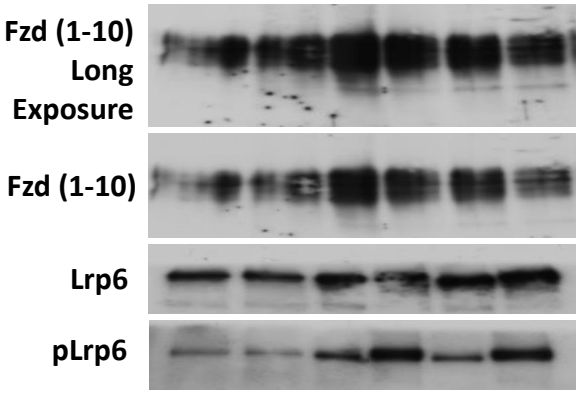

B

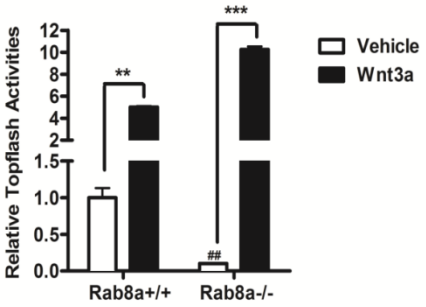

Figure 16: Analysis of Wnt receptor (Frizzleds (1-10)) and co-receptor (Lrp6) function in MEFs

A. Isolation of biotinylated surface proteins followed by immunoblot analysis showed similar levels of cell surface Fzd (1-10) and Lrp6 compared to *Rab8a*$^{+/+}$ MEFs. Note that exogenous Wnt3a stimulated surface Lrp6 phosphorylation (Ser1490) in *Rab8a*$^{+/+}$ and R*ab8a*$^{-/-}$ MEFs.

B. Wild-type and *Rab8a*$^{-/-}$ MEFs were transiently transfected with Renilla luciferase (transfection control) and Topflash reporter plasmids in Wnt-free media. 24 hours post-transfection, Topflash activity was read in cell-lysates and normalized to Renilla-luciferase activities. Quantifications showed significantly lower basal Topflash activity ("##, $p<0.01$ compared to vehicle-treated *Rab8a*$^{+/+}$ MEFs, white bars) in *Rab8a*$^{-/-}$ cell lysates. Both wild-type and *Rab8a*$^{-/-}$ responded strongly to Wnt3a stimulation (**black bars**) as compared to vehicle-treated cells (**white bars**).

CHAPTER 5

GPR177 TRAFFICS THROUGH RAB8A VESICLES

Information included in this chapter is taken from and are published in Das et al., Development (2015), 142(12):2147-62

Rab8a has been shown to interact with the C-terminus of some classic GPCRs such as glutamate receptors and α/β adrenergic receptors (Dong et al., 2010; Esseltine et al., 2012). As described above, G-Protein Coupled Receptor- 177 (Gpr177) is an evolutionarily conserved transmembrane protein with a unique function of binding to and transporting only Wnt ligands without which Wnt proteins get accumulated in the ER. Given that Gpr177 mediated Wnt secretion is highly dependent on vesicular trafficking which ultimately is regulated by Rab8a, we investigated whether Gpr177 mediated Wnt secretion pathway intersects with Rab8a vesicular traffic.

Results

RAB8A and GPR177 are in the same protein complex

We established a stable Henrietta Lacks (HeLa) cell line expressing 3×Flag-GPR177 to identify regulators for WNT-GPR177 trafficking. Using cell lysates extracted in the presence of 1% Triton X-100, we performed co-immunoprecipitation (Co-IP) analyses to identify potential interactions between GPR177 and key trafficking regulators. We detected association of GPR177 with RAB5, RAB8A, and RAB9 **(Fig. 17A)**. As GPR177 is internalized into endosomes (Belenkaya et al., 2008) during retrograde trafficking, association of GPR177 with RAB5 and RAB9 reflected endocytosis of GPR177 (Gasnereau et al., 2011). Association between GPR177 and RAB8A vesicular compartment has not been described. Given that RAB8 transports several G protein-coupled receptors (GPCRs) (Dong et al., 2010; Esseltine et al., 2012), we postulated that RAB8A vesicles might be involved in anterograde traffic of WNT-GPR177 complex. Of

note, under similar conditions, 3×Flag-GPR177 was not detected in association with RAB7, RAB11, or VPS35 **(Fig. 17A)**, suggesting that GPR177 and RAB8A might exist in a relatively stable detergent-resistant complex. The interaction between GPR177 and RAB8A was likely physiologically relevant as a truncated GPR177 lacking the carboxyl-terminal cytoplasmic tail (GPR177Δ44) failed to associate with RAB8A **(Fig. 17B)**. Using Glutathione S-transferase (GST)-RAB8A fusion proteins, we performed GST pull-down assays using 3×Flag-GPR177 cell lysates and consistently detected binding of GPR177 to GST-RAB8A but not to GST, GST-CDC42, or GST-JFC-D1 **(Fig. 17C, D)**, suggesting that RAB8A and GPR177 indeed associate in a complex. When GPR177-mCherry and EGFP-RAB8A were transiently expressed in HeLa **(Fig. 18A)** or colonic epithelial Caco2 cells **(Fig. 18B),** 3 populations of vesicles- mCherry positive, EGFP positive, and mCherry/EGFP double-positive were observed and confirmed by line scans, indicating that some GPR177 traffic through RAB8A vesicles **(Fig. 18A, B)**.

Rab8a regulates Gpr177 localization

To further explore whether Gpr177 traffic was affected in Wnt-producers *in vivo*, we performed immunogold labeling of endogenous Gpr177 in *Rab8a*$^{+/+}$ and *Rab8a*$^{-/-}$ mouse intestines. The specificity of Gpr177 antibody (Fu et al., 2009) was affirmed by a 90%, 91%, and 93% reduction of gold particles in ER, non-ER vesicular compartment, and plasma membrane of *Gpr177*-deficient cells **(Fig. 22A, B)**, compared to wild type cells. Using identical labeling conditions, we detected an 11% total reduction of Gpr177^{+} gold particles in *Rab8a*$^{-/-}$ Paneth cells. From TEM montage images

we performed quantitative analyses on gold particle distributions at ER, plasma membrane, and non-ER Golgi/secretory vesicular compartments (independent duodenal and jejunum segments from 3 *Rab8a*$^{+/+}$ and 2 *Rab8a*$^{-/-}$ mice, **Fig. 19 and Fig. 20A, B**). A large cytoplasmic portion of Paneth cell is occupied by ER, where the majority of Gpr177^{+} gold particles were detected **(Fig. 19A, B)**. Comparison of intracellular distribution of gold particles in *Rab8a*$^{+/+}$ and *Rab8a*$^{-/-}$ Paneth cells suggested statistically insignificant differences of Gpr177 distributions in ER or non-ER compartments **(Fig. 19A)**, suggesting that Gpr177 can be exported from ER without Rab8a. However, we identified significant reduction of Gpr177^{+} gold particles adjacent to apical or basolateral plasma membranes **(Fig. 19A and Fig. 20A, B)**. This reduced peripheral Gpr177 localization was reflected by fewer surface gold particles per Paneth cell as well as an approximately 88% reduction of particles per unit length of plasma membrane in Paneth cells **(Fig. 20A, B)**.

To test whether Rab8a is necessary for anterograde transport of Gpr177 to cell surface, we directly measured surface-localized Gpr177 by surface-protein biotinylation and isolation. We detected an approximately 46% reduction of surface Gpr177 in *Rab8a*$^{-/-}$ MEFs **(Fig. 20C)**.

Given that Gpr177 is able to exit ER, we postulated that *Rab8a* absence might mis-sort Gpr177 into endolysosmal compartments, an observation made for microvillus enzymes in *Rab8a*$^{-/-}$ enterocytes (Sato et al., 2007). We were able to examine lysosome and MVBs due to their distinct morphologies **(Fig. 19C)**. We detected frequent

localization of Gpr177^{+} gold particles to lysosomes and MVBs in *Rab8a*$^{-/-}$ but not *Rab8a*$^{+/+}$ cells **(Fig. 19C)**, suggesting that the absence of Rab8a might have caused endo-lysosomal targeting of Gpr177.

We next determined whether Rab8a loss may increase endo-lysosomal transport of Gpr177 by establishing a Caco2 cell line with stable *RAB8A* knockdown. Compared to control knockdown Caco2 cells, *RAB8A* depletion caused 3-fold increase in targeting GPR177-EGFP into LAMP1^{+} compartments **(Fig. 21A)**. Treatment of *RAB8A*-depleted Caco2 cells with Bafilomycin-A that blocks endo-lysosomal functions increased total GPR177 amount **(Fig. 21B)**. This suggests that in the absence of RAB8A-mediated exocytosis, there is an enhanced endo-lysosomal transport of Gpr177, yet *RAB8A*-depleted cells continued to make new GPR177.

Discussion

Our data show that Rab8a and Gpr177 are present in the same functional protein complex. Rab8a vesicles regulate anterograde transport of Gpr177 to plasma membrane, in absence of which Gpr177 is probably mis-directed to endo-lysosomal organelles. The reduction in Wnt secretion observed due to loss of *Rab8a* in MEFs is potentially due to unavailability of Gpr177 to support Wnt transport from golgi to plasma membrane.

Using immunogold labelling, we were able to determine the localization of endogenous Gpr177 in several sub-cellular compartments. We observed $Gpr177^{+}$ colloidal gold particles in endoplasmic reticulum, golgi and plasma membrane of Paneth cells, the major Wnt secreting intestinal epithelial cells. Additionally, Gpr177 was not only localized to the apical plasma membrane of the Paneth cells that faces the lumen but also was found in the basolateral plasma membrane suggesting Wnt secretion by Paneth cells not only maintain ISCs but also might have a role in maintaining the underlying fibroblasts as these fibroblasts are also known to express Wnt receptors (Frizzleds, see **Table 2**) and might respond to epithelial Wnts. Conversely, Gpr177 immunogold particles found on plasma membrane of fibroblasts support the notion that mucosal Wnt secretion help in ISC maintenance (Das et al., 2015; Farin et al., 2012; San Roman et al., 2014). Due to lack of direct evidence regarding polarity of Frizzled/Lrp6 location, it is not known whether Wnt signaling is transduced through apical or basolateral domain of ISCs. However the position of ISCs with respect to Wnt secreting

cells (lateral to Paneth cells and above fibroblasts) prompt us to speculate that Frizzleds and Lrp5/6 are present in both apical and basolateral plasma membranes of ISCs. Additionally immediate morphological changes in response to Wnt/CHIR supplements via basolateral domains in organoids indicate Wnt signal transduction through both apical and basolateral domains in vivo but restricting the pathway activation through basolateral domain ex vivo.

Our study identifies Rab8a as a major regulator of Gpr177 vesicular trafficking and hence Wnt secretion. However, there are some questions that need to be resolved to understand the molecular mechanism of this process completely. Using mammalian cell cultures we show that in absence of Rab8a, a major molecular regulator of anterograde transport, Gpr177 is probably mis-directed to lysosomes. Absence of Rab8a might shift the dynamics of vesicular trafficking towards lysosomes since the cargo (Gpr177) is no more able to be trafficked to the destination compartment (plasma membrane in this case). This has already been observed in global *Rab8a* knockout mouse intestines where absence of Rab8a protein function mis-targets apical peptidases and transporters (including dipeptidyl peptidase IV) to lysosomes (Sato et al., 2007). There are additional examples of lysosomal enzymes (lysosomal hydrolases) that once synthesized and post-translationally modified are targeted to lysosomes from golgi without having to go through the endocytic pathway. It is possible that in absence of Rab8a, cargoes directed to plasma membrane are hijacked by a different Rab protein(s)/ vesicular machinery and mis-directed to lysosomes.

Secondly, what is the molecular or environmental signal that triggers Rab8a dependent exocytosis of Wnt/Gpr177 complex? Given that Wnt is an important morphogen that needs to function at the right space, time and concentration, Wnt secretion is most likely a highly regulated process. We speculate that several molecular signals in developmental and homeostatic states converge in nucleus leading to synthesis of Wnts. Once Wnt is post-translationally modified and ready to be secreted, several vesicular trafficking components including Rabs, coat proteins, cytoskeletal elements are recruited to the Wnt/Gpr177 containing vesicles and help it exocytose. Given the selective expression of Wnt genes by cells during different stages of development in embryo, especially in gut, it is less likely that Wnt is constitutively produced by the cell (Kemp et al., 2005; Lickert et al., 2001; Roelink and Nusse, 1991). We hypothesize that Wnt production is regulated by molecular signals in embryonic stages and in adults. Thus, once produced, binding of Wnt proteins to Gpr177 alone might be sufficient to trigger Wnt secretion.

Thirdly, what is the ultimate effector that carries out the function of Wnt/Gpr177 transport? Rab8a is a small GTPase that requires and should recruit an effector protein that would facilitate the vesicular transport of its cargoes. A potential candidate in this case would be Myosin V that has been shown to directly bind Rab8a in mammalian cell culture system (Hume et al., 2001; Rodriguez and Cheney, 2002; Roland et al., 2009). We postulate that Myosin being a motor protein upon recruitment would then mediate "vesicle walking" on actin cables to transport Wnt/Gpr177^{+} vesicles to the destination

compartment. Several such questions remain to be resolved, answers to which might shed light on cellular and molecular mechanisms driving Wnt secretion.

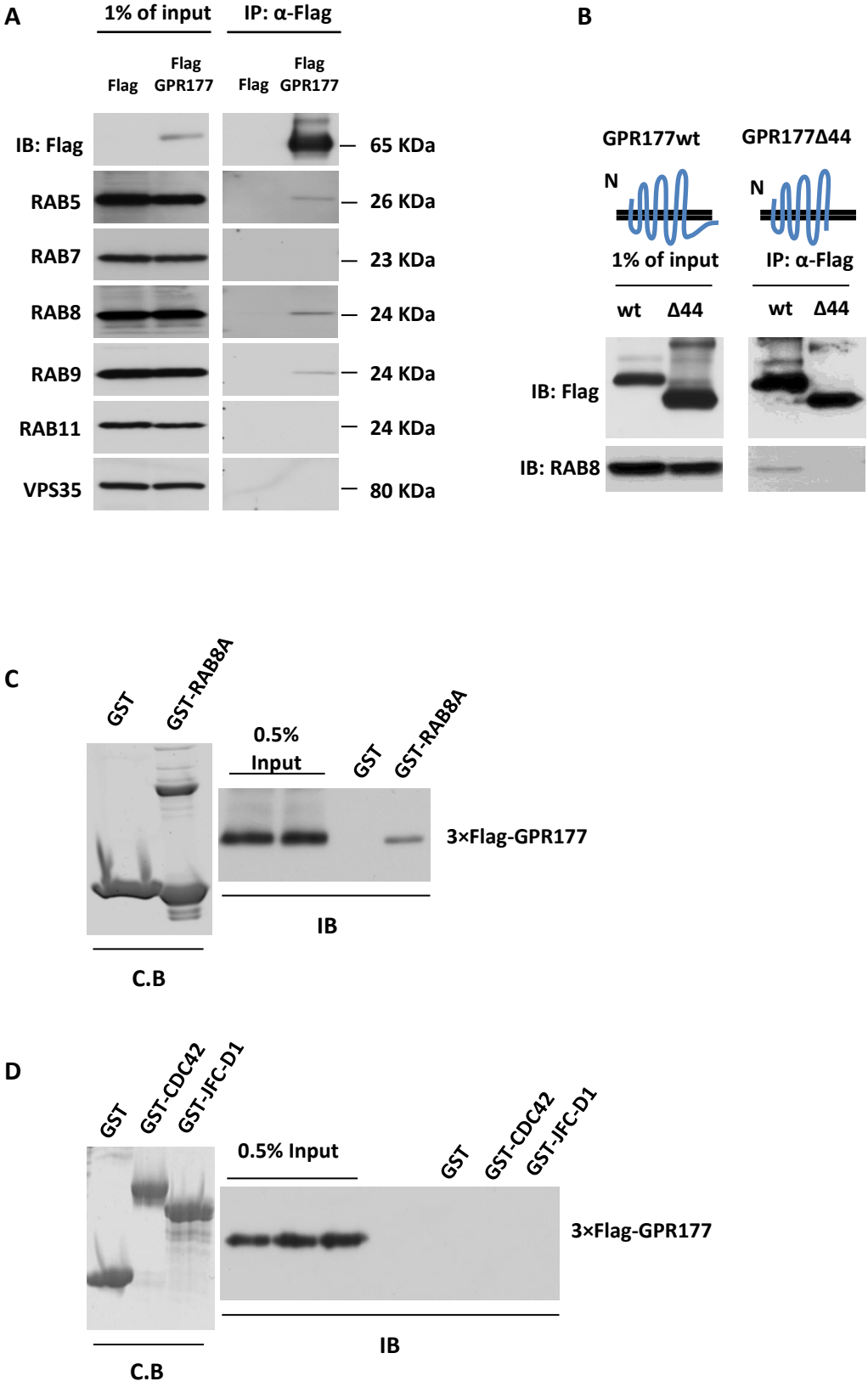
A
1% of input
IP: α-Flag
Flag
Flag GPR177
Flag
Flag GPR177
IB: Flag
RAB5
RAB7
RAB8
RAB9
RAB11
VPS35
65 KDa
26 KDa
23 KDa
24 KDa
24 KDa
24 KDa
80 KDa
B
GPR177wt
GPR177Δ44
N
N
1% of input
IP: α-Flag
wt
Δ44
wt
Δ44
IB: Flag
IB: RAB8
C
GST
GST-RAB8A
0.5% Input
GST
GST-RAB8A
3×Flag-GPR177
IB
C.B
D
GST
GST-CDC42
GST-JFC-D1
0.5% Input
GST
GST-CDC42
GST-JFC-D1
3×Flag-GPR177
IB
C.B

Figure 17: Examination of GPR177-RAB8A association using immunoprecipitation assays

A. Cell lysates from Hela cells stably expressing either Flag or Flag tagged GPR177 were subjected to immunoprecipitation in presence of 1% Triton X-100. Precipitates were blotted for various endogenous vesicular proteins including RAB5, RAB7, RAB8, RAB9, RAB11 and VPS35. RAB5, RAB8A and RAB9 co-immunoprecitated with Flag-GPR177 in Hela cells whereas RAB7, RAB11 and VPS35 were not detected in the precipitate under similar experimental conditions.

B. Under similar experimental conditions as described in **Fig. 17A**, Flag-GPR177Δ44 lacking C-terminal tail failed to co-immunoprecipitate with RAB8A in Hela cells

C-D. GST tagged RAB8A, CDC42 and JFC1 were expressed in BL21 and cell lysates from these bacterial cultures were immunoprecipitated using GSH beads. Precipitates were then incubated with cell lysates from Hela cells stably expressing Flag-GPR177 followed by immunoblot (IB) for Flag (GPR177). Commassie blue (C.B) staining was performed to check expression of GST tagged proteins by bacterial cells. Bacterial cell lysates from GST pull-down showed binding of Flag-GPR177 to GST-RAB8A, but not to GST alone, GST-CDC42, or GST-JFC-D1.

A

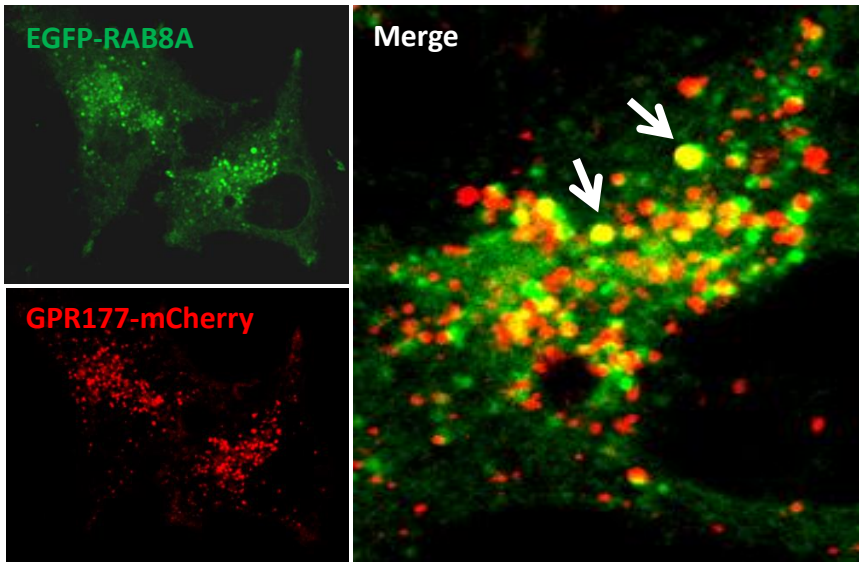
EGFP-RAB8A
Merge
GPR177-mCherry

B

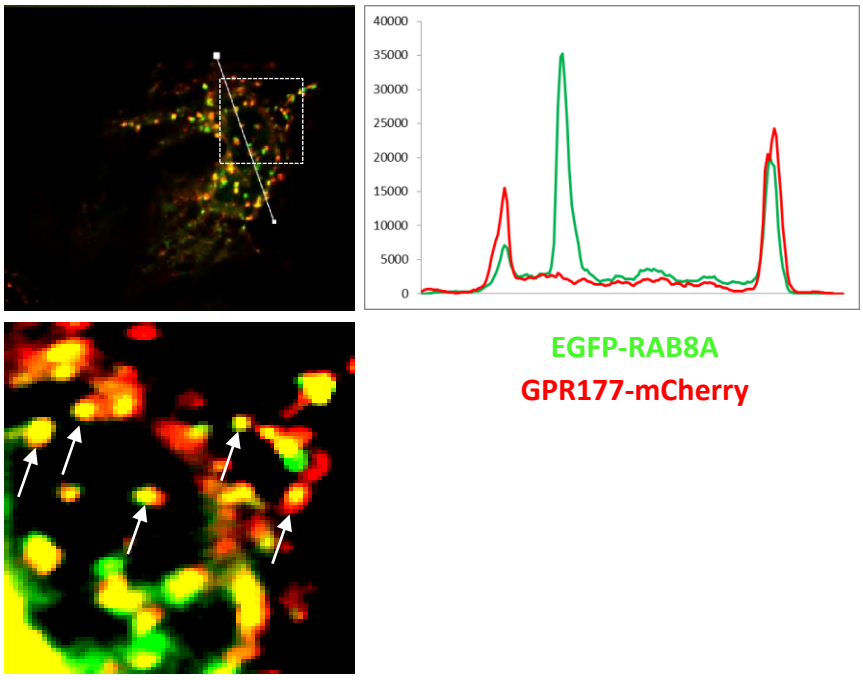
40000
35000
30000
25000
20000
15000
10000
5000
0
EGFP-RAB8A
GPR177-mCherry

Figure 18: Analysis of RAB8A and GPR177 localization using live cell images

A. Live cell imaging of Hela cells transiently co-transfected with GPR177-mcherry (**red**) and EGFP-RAB8A (**green**) detected colocalization of both fluorescent signals in some vesicular compartments (**arrows**).

B. Live cell imaging of Caco2 cells transiently co-transfected with GPR177-mcherry (**red**) and EGFP-RAB8A (**green**) detected colocalization of both fluorescent signals in some vesicular compartments (**arrows**). **Line scan** shows partial overlap of both fluorescent signals. **Arrows** point to vesicles positive for both fluorescent signals.

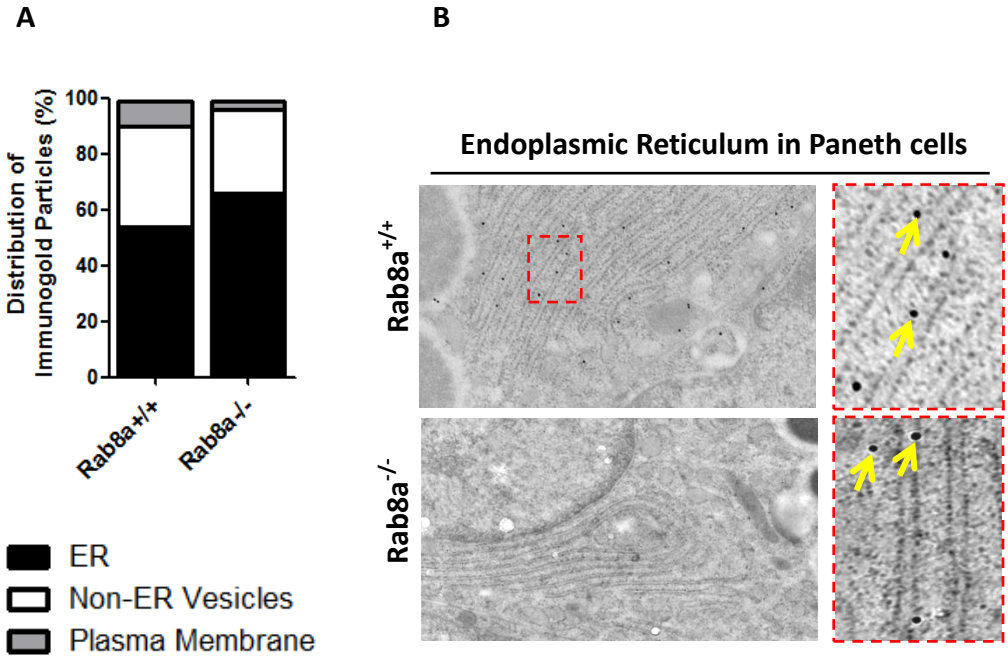
A
B
Distribution of Immunogold Particles (%)
100
80
60
40
20
0
Rab8a+/+
Rab8a-/-
ER
Non-ER Vesicles
Plasma Membrane
Endoplasmic Reticulum in Paneth cells
Rab8a+/+
Rab8a-/-

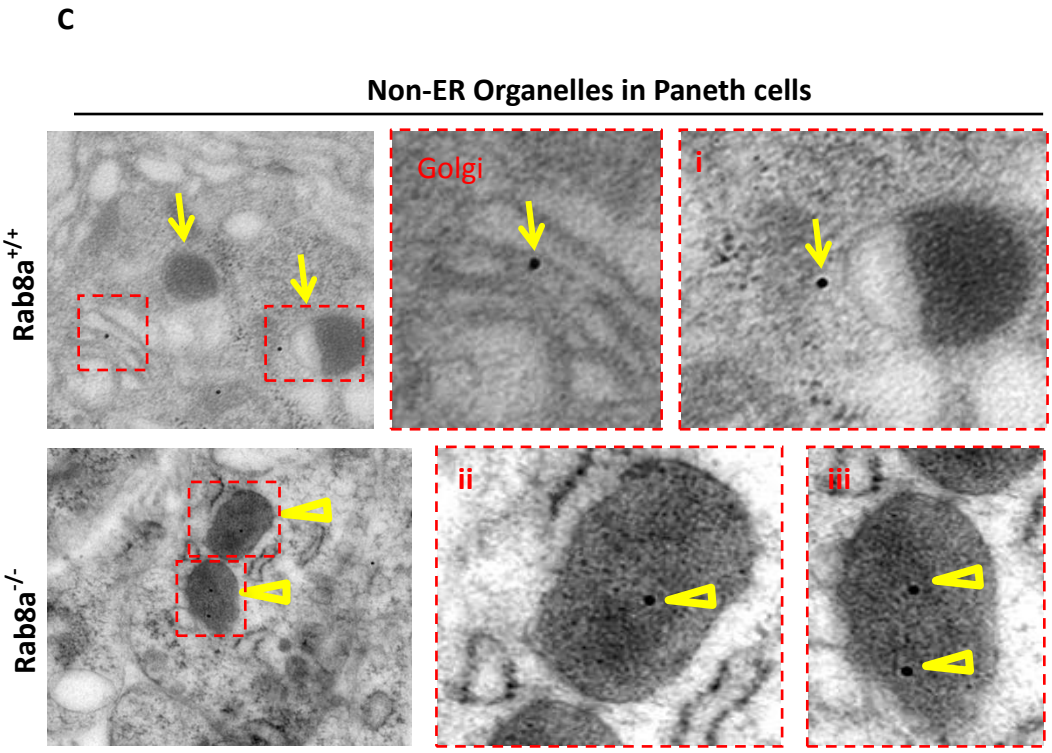
C
Non-ER Organelles in Paneth cells
Rab8a+/+
Rab8a-/-
Golgi
i
ii
iii

Figure 19: Analysis of Gpr177 localization in Paneth cells using immunoelectron microscopy

A. Quantifications using electron micrographs showed insignificant changes in distribution of $Gpr177^{+}$ immunogold particles in ER and non-ER compartments (golgi and vesicular compartments) of $Rab8a^{+/+}$ and $Rab8a^{-/-}$ Paneth cells. Reduction in number of $Gpr177^{+}$ immunogold particles was observed in plasma membrane of $Rab8a^{-/-}$ Paneth cells (also see **Figure 20A, B**).

B. Representative electron micrographs show significant number of $Gpr177^{+}$ gold particles in ER of $Rab8a^{+/+}$ and $Rab8a^{-/-}$ Paneth cells. **Arrows** point to individual gold particles.

C. Representative electron micrographs show localization of $Gpr177^{+}$ gold particles in Golgi and lysosomes (**boxed in red**). $Gpr177^{+}$ gold particles were observed frequently in lysosomes of $Rab8a^{-/-}$ Paneth cells (**empty arrowheads** shown in (**ii**) and (**iii**)) but not in lysosomes of $Rab8a^{+/+}$ Paneth cells (**arrows** shown in (**i**)).

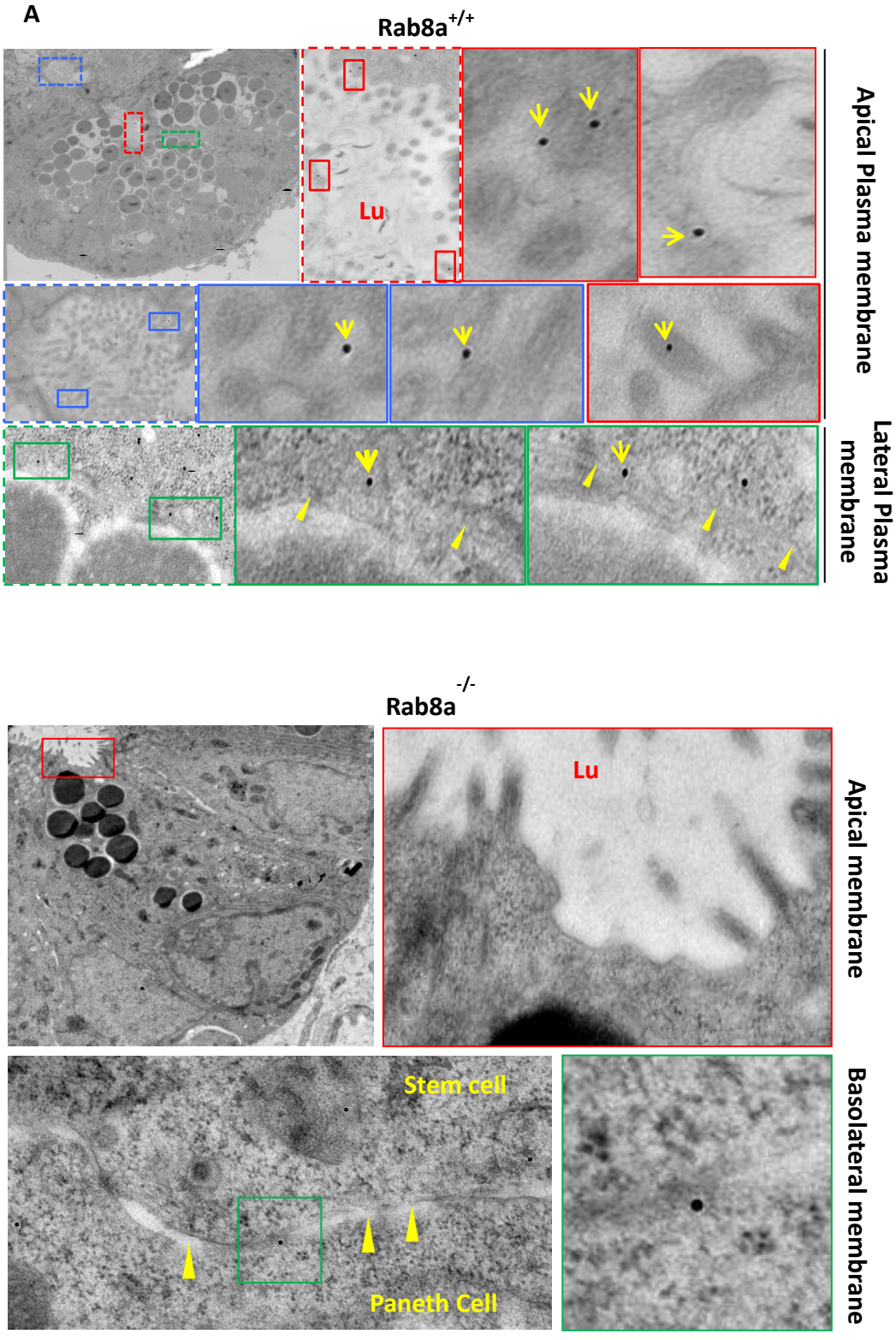
A
Rab8a+/+
Lu
Apical Plasma membrane
Lateral Plasma membrane
Rab8a-/-
Lu
Apical membrane
Stem cell
Paneth Cell
Basolateral membrane

B

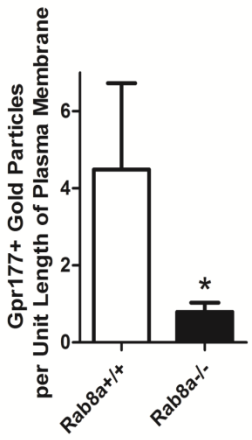
Gpr177+ Gold Particles
per Unit Length of Plasma Membrane
6
4
2
0
*
Rab8a+/+
Rab8a-/-

C

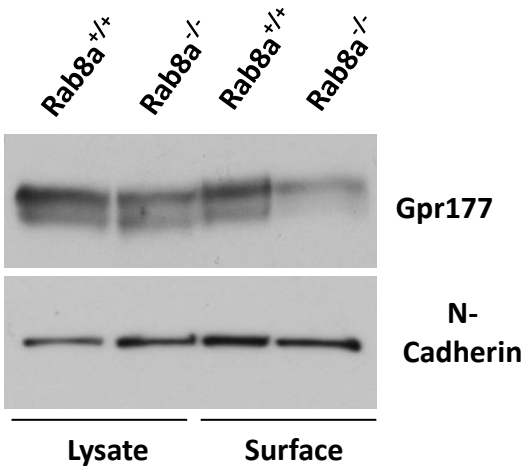
Rab8a+/+
Rab8a-/-
Rab8a+/+
Rab8a-/-
Gpr177
N-
Cadherin
Lysate
Surface

Figure 20: Analysis of surface localization of Gpr177 using immunoelectron microscopy and cell-surface biotinylation assay

A. Representative electron micrographs show Gpr177^{+} gold particles at apical (**blue** and **red** box) or basolateral (**green** box) plasma membranes in wild-type Paneth cells that are observed more frequently as compared to *Rab8a*$^{-/-}$ Paneth cells. Gpr177^{+} colloidal gold particles were rarely observed in apical membrane of *Rab8a*$^{-/-}$ Paneth cells. A residual gold particle at lateral membrane between a Paneth and stem cell in *Rab8a*$^{-/-}$ crypt is boxed in **green**. **Arrows** point to individual Gpr177 gold particle. **Arrowheads** point to plasma membranes between a stem cell and a Paneth cell. **Lu** stands for "lumen".

B. Gpr177^{+} colloidal gold particles observed on apical and basolateral plasma membrane were counted and the perimeter of each Paneth cell was measured using ImageJ. Quantifications showed reduced number of Gpr177^{+} gold particles per unit length of *Rab8a*$^{-/-}$ Paneth cell plasma membrane as compared to their control counterparts.

C. Cell-surface protein biotinylation and isolation detected decreased amount of surface Gpr177 in *Rab8a*$^{-/-}$ MEFs.

A

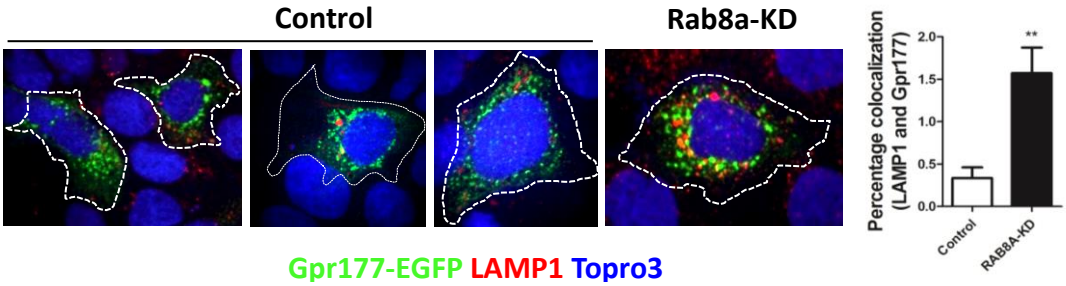
Control
Rab8a-KD
Gpr177-EGFP LAMP1 Topro3
Percentage colocalization (LAMP1 and Gpr177)
2.0
1.5
1.0
0.5
0.0
**
Control
RAB8A-KD

B

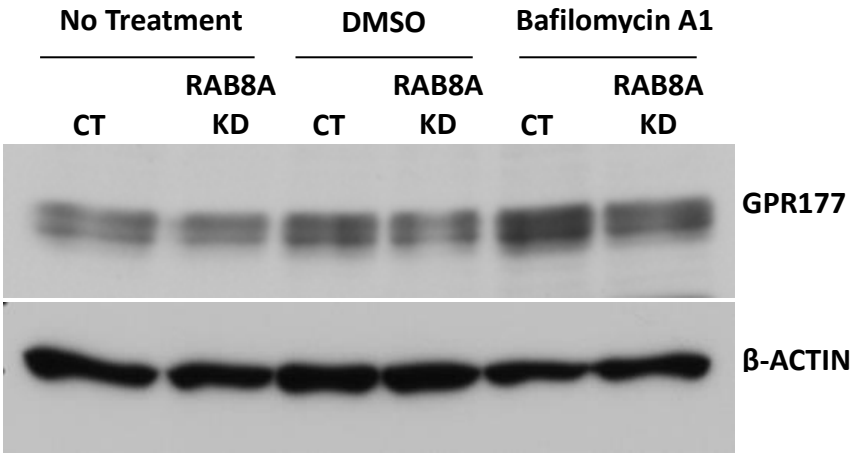
No Treatment
DMSO
Bafilomycin A1
CT
RAB8A KD
CT
RAB8A KD
CT
RAB8A KD
GPR177
β-ACTIN

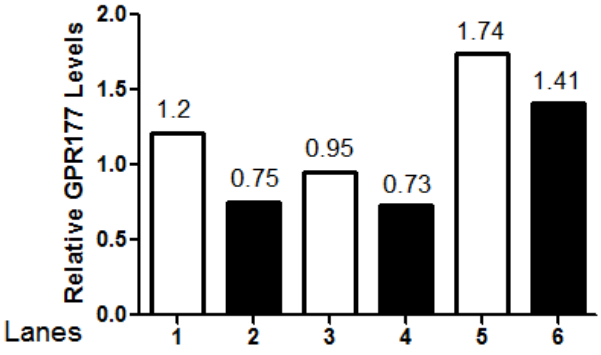
Relative GPR177 Levels
2.0
1.5
1.0
0.5
0.0
1.2
0.75
0.95
0.73
1.74
1.41
Lanes
1
2
3
4
5
6

Figure 21: Analysis of GPR177 localization in absence of RAB8A

A. Wild-type and *RAB8A*-KD Caco2 cells were transiently transfected with GPR177-GFP. Immunofluorescent staining for GFP (GPR177, **green**) and LAMP1 (**red**) showed increased co-localization of both proteins in *RAB8A*-KD Caco2 cells. Colocalization of both fluorescent signals was quantified using Volocity (n=20). A 2-fold increase of GPR177 (GFP, **green**) localization in the late endosome and lysosome (LAMP1, **red**) was observed in *RAB8A*-KD Caco2 cells. Nuclear staining with Topro-3 is shown in **blue**.

B. Wild type and *RAB8A*-KD Caco2 cells were treated with Bafilomycin A1, a lysosomal inhibitor. Cell lysates were collected after 18 hours and subjected to immunoblot analysis. Treatment with Bafilomycin A1 increased total GPR177 levels in control and *RAB8A*-KD Caco2 cells. Densitometric analysis of GPR177 protein bands relative to β-ACTIN bands were performed on immunoblots using Image J. Quantifications showed higher GPR177 protein levels upon Bafilomycin A1 treatment as compared to non-treated or DMSO treated conditions.

CHAPTER 6

GPR177 MAINTAINS INTESTINAL STEM CELLS EX VIVO

Some information included in this chapter is taken from and are published in Das et al., Development (2015), 142(12):2147-62

Wingless-type MMTV integration site family members (Wnts) is an essential morphogen that play an essential role in the growth and development of mammalian tissue (Clevers et al., 2014). Wnt at correct space, time and concentration forms a functional gradient in many mammalian tissues; absence of which may lead to several diseased conditions including congenital defects and cancer (Clevers, 2006).

Wnt is a highly lipidated protein that like most other proteins synthesized and post-translationally modified in the endoplasmic reticulum (ER). A unique acyl-O-transferase enzyme Porcupine glycosylates and lipidates Wnts enabling them to bind to G-protein coupled receptor- 177 (Gpr177), a conserved and specific Wnt transporter protein. Gpr177 then traffics Wnt ligands from ER to cell membrane through Rab8a mediated vesicular transport (Das et al., 2015). Once the Wnt/Gpr177 complex reaches the cell membrane, Wnt is released into the extra-cellular space allowing it to induce signaling in cell bearing its receptors (Frizzled) and co-receptors (Lrp5/6). On the other hand, after establishing Wnt exocytosis, Gpr177 returns to golgi and ER via endocytosis for yet another cycle of Wnt secretion. Several molecules including AP2, Dynamin, Rab5, SNX3 and most importantly the Retromer complex mediate this endocytic process (reviewed in (Das et al., 2012)).

At the ligand-receiving end, Wnt upon binding to (co-) receptors translocates the β-catenin destruction complex to the plasma membrane. The β-catenin destruction complex is composed of multiple proteins- Axis inhibitor (Axin), Adenomatous Polyposis Coli (Apc), Caesin Kinase 1 (CK1), Glycogen Synthase Kinase 3 (GSK3) and E3 ubiquitin

ligase β-Trcp. Unavailability of this complex in cytoplasm allows β-catenin to escape ubiquitination and its ultimate degradation in proteasomes. Instead now β-catenin translocates to nucleus and promotes gene expression of several Wnt dependent genes with the help of T-cell factor (Tcf) and Lymphoid enhancing factor (Lef) transcription factors.

Development and maintenance of intestinal tissue is heavily dependent on Wnt signaling pathway (Clarke, 2006; Krausova and Korinek, 2014). Wnt pathway not only maintains the stem cell renewal but also regulates the maturation of Paneth cells, a descendent daughter cell, the close association of which provides Wnt3 and maintains stem cell activity in culture (Sato et al., 2011). The role of canonical Wnt pathway in maintaining intestinal steady state has been well established in several mouse models. In adult intestinal tissue, loss of function mutations (in *Tcf4* or *β-catenin*) leading to functional reduction of canonical Wnt pathway causes loss of crypts and proliferative compartment. This ultimately leads to death in mice within a week (Fevr et al., 2007; Korinek et al., 1998; van Es et al., 2012a). On the other hand 90% of colonic cancer cases in humans are associated with mutations causing hyper-activation of Wnt pathway (Cancer Genome Atlas, 2012). Conventional knockout mouse models ($Apc^{min/+}$ or $\beta\text{-}catenin^{\Delta ex3/\Delta ex3}$) have confirmed the same by demonstrating hyper-proliferation, adenoma and tumor formation leading to mortality in mice upon hyper-activation of Wnt pathway genes in small intestine (Andreu et al., 2008; Korinek, 1997; Romagnolo et al., 1999).

In contrast to the unequivocal significance of molecules involved in Wnt signal transduction, the role of molecular regulators regulating (Wnt) ligand secretion in ISC maintenance is still under scrutiny. Wnt3 is a ligand expressed by Paneth cells and essential for maintenance of stem cells in absence of Paneth cells (Sato et al., 2011). However interestingly, no effects in number/distribution of Paneth or stem cells were observed when gene encoding Wnt3 was deleted from adult mouse intestine (Farin et al., 2012). Similarly, intestinal stem cell homeostasis was unperturbed when *Porcupine* or *Vps35*, a member of multi-protein Retromer complex with a function in retrograde transport of Gpr177, were deleted in adult intestinal tissue (de Groot et al., 2013; San Roman et al., 2014). The complex tissue micro-environment in intestine probably provides compensatory essential cues to maintain stem cells in vivo. When isolated from this complex microenvironment, stem cells seem to clearly rely on growth factors provided by Paneth cells. When cultured ex vivo, $Wnt3^{-/-}$ crypts demonstrated morphological defects but did not show mortality unless passaged. This overall suggests reduced clonogenicity of $Wnt3^{-/-}$ stem cells or reduced support from $Wnt3^{-/-}$ Paneth cells in $Wnt3^{L/L}$*; VillincreER* mice which makes Wnt3 indispensable for crypt growth and maintenance in absence of physiological conditions (Farin et al., 2012). Thus, there ought to be a separate population of source-cells that provides Wnt3 (or other functionally redundant (non-Wnt/)Wnt ligands) for stem cell maintenance in intestine.

To identify these non-Paneth Wnt sources and check if Wnt ligands are essential for intestinal homeostasis in mice, we deleted *Gpr177*, from both epithelium as well as extra-epithelial cells of intestine thus terminating Wnt ligand secretion in early

developmental stages and in adult mice. Our data show that acute absence of Gpr177 function in adult mice does not affect intestinal tissue homeostasis, however, when deleted in early developmental stages demonstrate absence of Paneth and *Olfm4*$^{+}$ stem cells. Interestingly enough, these knockout mice were healthy and fertile implicating compensation in absence of conventional Wnt secretion; either from non-Wnt pathways capable of inducing Wnt signal transduction or an additional Wnt-source cell. Additionally, we were unable to culture *Gpr177*$^{-/-}$ crypts in absence of intestinal mucosal cells confirming the requirement of Wnt ligand secretion by Paneth (or stem) cells in maintaining intestinal stem cells. We were unable to rescue the mortality demonstrated by *Gpr177* null crypts with Wnt3a or CHIR- a GSK3β inhibitor suggesting role of non-canonical Wnt ligands or an essential non-Wnt stem niche signal that potentially gets attenuated in absence of Wnt. Taken together, intestinal tissue demonstrates tremendous plasticity to cope with any alternation in stem cell niche composition.

Rab8a dependent Wnt ligand secretion maintains intestinal stem cells ex vivo (**Chapters 3, 4**) (Das et al., 2015). Rab8a potentially carries out this function with Gpr177 (**Chapter 3**) (Das et al., 2015), a well-conserved GPCR that has an established role in secretion of Wnts (Das et al., 2012). We reasoned that since Rab8a and Gpr177 act together to secrete Wnt, depletion of Gpr177 from the intestinal crypt compartment should demonstrate similar or even stronger (given that Gpr177 is indispensable for Wnt secretion) phenotype as compared to *Rab8a*$^{-/-}$ intestines. Gpr177 helps in secreting almost all Wnt ligands and generating multiple Wnt or multiple Frizzled knockouts is nearly impossible. Thus given the specificity demonstrated by Gpr177, we expected this

genetic model to represent efficient depletion of Wnt activity at an upstream ligand secretion level.

Results

Depletion of Gpr177 mRNA in several Gpr177 intestine specific knockouts

Global *Gpr177* knockouts are not viable past E8.5 (Carpenter et al., 2010; Fu et al., 2009). Thus we crossed *Gpr177*$^{loxp/loxp}$ (*Gpr177*$^{L/L}$) mouse line to several transgenic mouse lines expressing Cre recombinases which include Villincre, Smooth Muscle Actin creERT2 (SMACreERT2) and Transgelincre (Taglncre). Villincre is expressed in all intestinal epithelial cells. As mentioned earlier (**Chapter 3**), the deletion of *Gpr177* was confirmed by immunogold labelling for endogenous Gpr177 and a significant reduction in total number of Gpr177^{+} gold particles was observed in the *Gpr177*$^{L/L}$*; Villincre* knockout Paneth cells (**Fig. 22**). Additionally, quantitative real time PCR showed ~57% reduction in *Gpr177* mRNA in total intestinal tissue (**Fig. 24A**). Previous studies have shown evidences supporting the existence of non-epithelial Wnt sources that contribute to intestinal stem cell maintenance (Farin et al., 2012; Gregorieff et al., 2005; Kabiri et al., 2014; Miyoshi et al., 2012; San Roman et al., 2014). Thus, in addition to Villincre, we utilized two other Cre-recombinase transgenic mouse-lines to delete *Gpr177* from intestinal non-epithelial cells. These were tamoxifen inducible SMAcre and constitutively active Taglncre. Using these two Cre-lines (in presence of Villincre), we expected to evaluate the tissue specific chronic and acute effect of *Gpr177* deletion on total intestinal tissue respectively. These relatively novel Cre mouse lines (SMAcreERT2 and

Taglncre) were crossed to *Rosa26*$^{YFP/+}$ mouse line and the expression pattern was determined by immunostaining corresponding adult intestinal histological sections with anti- GFP/YFP antibody. Intestinal tissues were harvested from *SMAcreERT2; Rosa26*$^{YFP/+}$ mice two days after being injected with tamoxifen (*SMAcreERT2* (TAM+2days)). SMAcreERT2 was primarily expressed in smooth muscle underlying the intestinal epithelium (**Fig. 23A**) but was also occasionally observed in lamina propria (**Fig. 23Ai**). Taglncre was strongly expressed in both smooth muscles (**Fig. 23, arrow**) and lamina propria (**Fig. 23Bii**). Quantitative real time PCR showed a ~72% and ~67% reduction in *Gpr177* mRNA from *Gpr177*$^{L/L}$*; Villincre; SMAcreERT2* (TAM+2days) and *Gpr177*$^{L/L}$*; Villincre; Taglncre* intestines respectively (**Fig. 24A**). This was additionally confirmed by in-situ hybridization that also indicates that most of *Gpr177* is expressed by enterocytes (**Fig. 24B, C**). The contribution of smooth muscle and lamina propria towards *Gpr177* was minimal (**Fig. 24C**). Some discrepancies in *Gpr177* mRNA levels were seen in *Gpr177*$^{L/L}$*; Villincre; Taglncre* knockouts (compare age-matched littermates **Mouse 782 and 783 in Fig. 24B**) which might explain statistically insignificant differences in *Gpr177*mRNA levels in these knockouts as compared to wild-type (**Fig. 24A**).

Reduction of Lysozyme^{+} and Olfm4^{+} cells in Gpr177$^{L/L}$; Villincre; Taglncre mouse intestines

To investigate the role of Gpr177 in Wnt dependent intestinal homeostasis, we immunostained the intestinal tissue sections from *Gpr177* knockouts for Lysozyme. Interestingly, no significant reduction in Lysozyme^{+} Paneth cells was seen in *Gpr177*$^{L/L}$*;*

Villincre or *Gpr177$^{L/L}$; Villincre; SMAcreERT2* (TAM+2days) *knockouts* (**Fig. 25A, B**). However, crypts in *Gpr177$^{L/L}$; Villincre; Taglncre* knockout intestines frequently lacked Lysozyme^{+} Paneth cells (**Fig. 25A (arrows) B (quantification)**). In concurrence, in situ hybridization for *Olfm4^{+}* stem cells were frequently missing in *Gpr177$^{L/L}$; Villincre; Taglncre* knockout crypts (**Fig. 26A, arrows**) but no significant difference was observed in *Gpr177$^{L/L}$; Villincre; SMAcreERT2 (TAM+2days)* knockouts (**Fig. 26A**). Together, this suggests that absence of epithelial Wnt source (in *Gpr177$^{L/L}$; Villincre* intestines) and an absence of *Gpr177* for an acute time-span (in *Gpr177$^{L/L}$; Villincre; SMAcreERT2(TAM+2days)* intestines) are insufficient to affect intestinal stem cell niche. On the contrary, absence of *Gpr177* from epithelial (enterocytes) and non-epithelial (smooth muscle and lamina propria) Wnt secreting cells from an early embryonic developmental stage such as in *Gpr177$^{L/L}$; Villincre; Taglncre* knockout intestines perturbs Paneth and stem cells homeostasis. Additionally, no significant difference was observed in EdU^{+} (30 mins) proliferative compartment of either knockout (**Fig. 26B**). Given that Gpr177 function is indispensable for Wnt activity in vivo (reviewed in (Das et al., 2012)), we performed quantitative real time PCR to assess Wnt dependent Paneth cells (*Mmp7*, *Defensin-5* and *CD44*), stem cells (*Msi1*, *Ascl2* and *Olfm4*) and some Wnt downstream effectors (*Axin2* and *Tcf4*). Surprisingly, we observed insignificant differences in mRNA levels except *Defensin-5* in *Gpr177$^{L/L}$; Villincre; SMAcreERT2(TAM+2days)* and *Mmp7* in *Gpr177$^{L/L}$; Villincre; Taglncre* total intestines suggesting histologically undetectable defects in Paneth cell function in *Gpr177$^{L/L}$; Villincre; SMAcreERT2(TAM+2days)* (also see **Fig. 25**). Interestingly, though not

statistically significant, we noted a ~40% reductions in *Olfm4* expression in *Gpr177$^{L/L}$; Villincre; Taglncre* intestine consistent with our ISH results (**Fig. 26A**).

Gpr177 regulates stem cell activity of organoids

Multiple signaling pathways cross-talk and maintain intestinal tissue in vivo. Thus to determine and distinguish (from other pathways) the role of Gpr177 dependent Wnt pathway in maintaining intestinal stem cell activity, we cultured *Gpr177$^{L/-}$; Villincre* crypts in absence of extra-epithelial support. When seeded, *Gpr177$^{L/-}$; Villincre* knockout crypts possessed Paneth cells as evident from dense crypt bases (**Fig 27A, boxed images 1 and 2**). However, *Gpr177* deleted crypts were unable to survive through Day 4 in regular ENR media (**Fig. 27B, Ci, Cii**) suggesting compromised stem cell activity in *Gpr177* null organoids. This defect in stem cells could also be due to lack of sufficient signaling support by *Gpr177$^{-/-}$* Paneth cells within *Gpr177$^{L/L}$; Villincre* organoids. All *Gpr177$^{L/L}$; Villincre* organoids were growth arrested by Day 3 in (ENR) culture and dead by Day 4 (compare growth of wild-type organoids to *Gpr177$^{L/L}$; Villincre* organoids in **Fig. 27Cii**). This growth defect was however only partially rescued by addition of recombinant murine Wnt3a or CHIR99021 (GSK3β inhibitor) (**Fig. 27B and 27D-F**). Effect of Wnt3a treatment was assessed by typical cyst like crypt morphology seen in wild-type organoids as early as Day2 in culture. *Gpr177$^{-/-}$* organoids responded to canonical Wnt3a in a dose dependent manner rescuing their growth by 3% in 100ng/ml and 13% in 200ng/ml of recombinant Wnt3a (**Fig. 27B**). Interestingly, most surviving *Gpr177* deleted organoids at Day 5 responded to Wnt3a completely which was evident by their cyst like

structures (**Fig. 27Di, asterisks and Fig. 27Ei, asterisks and Fig. 27Eii**) In a similar experimental set-up, we also evaluated the effect of CHIR on *Gpr177* null organoids (**Fig. 27F**). Effect of CHIR treatment was affirmed by mostly cyst like morphology of wild-type crypts (**Fig 27Fi**, wild-type in **Fig. 27Fii**) except few which escaped complete GSK3β inhibition and managed to differentiate on Day 5 (wild-type organoids in **Fig. 27Fi, hashtag and Fig. 27Fii**). Treatment with CHIR rescued survivability of *Gpr177*$^{-/-}$ crypts by 30% (**Fig. 27B**). Despite of this improvement in survivability, unlike Wnt3a treatment (200ng/ml) (**Fig. 27Ei, Eii**), CHIR treated *Gpr177* null organoids did not show a typical cyst like morphology instead formed tubular buds (**Fig. 27Fi, asterisks**) which eventually regressed and the organoids were growth arrested (**Fig. 27Fii**). Taken together, activating canonical Wnt pathway exogenously (either by Wnt3a or CHIR treatment) was insufficient to rescue survivability of *Gpr177* null organoids completely.

Discussion

Previous studies show that Wnt ligands cannot be secreted in absence of Gpr177 (reviewed in (Das et al., 2012)). However in vivo, no significant differences were observed in number of Paneth cells in *Gpr177$^{L/-}$; Villincre* mice confirming the existence of extra-epithelial Wnt sources (Farin et al., 2012; San Roman et al., 2014). Most *Gpr177$^{L/-}$; Villincre; TagIncre* intestinal crypts were largely devoid of Lysozyme^{+} Paneth cells. However, these mice did not show dramatic differences in the transcriptional level of multiple Paneth cell-specific genes suggesting defects in post-natal maturation of Paneth cells rather than embryonic Paneth cell fate commitment. We next assessed the status of Paneth cells in a conditional knockout mouse model *Gpr177$^{L/-}$; Villincre; SMAcreERT2* (TAM+2days), which did not show any major differences in number and distribution of Paneth cells. Since, the SMAcre was induced only for an acute period of time (2 days); further studies with chronic deletion of *Gpr177* would give us deeper insights into the role of Wnt pathway on adult intestinal homeostasis.

In contrast to our in vivo data, a rather drastic phenotype was observed when *Gpr177$^{-/-}$* crypts were cultured without any mucosal support. All *Gpr177* null crypts die by Day 4 in culture which could not be rescued completely by exogenous activation of canonical Wnt pathway suggesting dependence of these crypts on non-canonical Wnt ligands (Wnt2b, Wnt4 and Wnt5a) usually provided by extra-epithelial fibroblasts intestine. An alternative explanation would be indirect attenuation of an essential non-Wnt stem cell signal (such as Notch or Hedgehog or EGF) upon reduction in Wnt activity

that affects the overall survivability of *Gpr177*$^{-/-}$ crypts ex vivo. Thus it will be interesting to see if the phenotype can be rescued by activating canonical and non-canonical signals together ex vivo. This could be achieved by supplementing organoids with recombinant Wnt2b protein and CHIR or co-culturing organoids with fibroblasts and CHIR.

As mentioned earlier, cascades of signaling events help in the development and maintenance of intestinal tissue- such as Wnt, Notch, EGF, BMP, HH (reviewed in (van der Flier and Clevers, 2009)). Out of these morphogens, Wnt is of particular importance as it constantly feeds the regenerative power of stem cells at crypt base. To gain deeper understanding of Wnt dependent-molecular events that drive embryogenesis and adulthood, tremendous amount of research have focused on conventional knockout mouse models with loss/gain of function for members of Wnt pathway (van der Flier and Clevers, 2009); especially in organogenesis and maintenance of intestine (Andreu et al., 2008; Fevr et al., 2007; Korinek, 1997; Korinek et al., 1998; Romagnolo et al., 1999; van Es et al., 2012a). Most of these studies investigate the function of molecules regulating Wnt signal transduction in Wnt receiving cells. Unfortunately the role of upstream events associated with Wnt secretion in ligand secreting cells is less explored causing several gaps in our understanding; some of which are discussed below.

Firstly, are Wnt ligands redundant in function? There are at least 6 Wnt ligands (Wnt3, 6, 9b, 2b, 4, 5a) expressed in the small intestine of mouse (Gregorieff et al., 2005), out of which canonical Wnt3 is expressed by Paneth cells, a cell type essential to maintain intestinal stem cells (Sato et al., 2011). However, in absence of *Wnt3* in adult

mouse intestinal epithelium, no significant change was observed in vivo (Farin et al., 2012). Interestingly, when cultured without mucosal support, *Wnt3* null organoids did not demonstrate mortality and survived with some morphological changes through even second passage. Observed growth deficit in *Wnt3* null organoids was rather subtle for their predicted importance in organogenesis and maintenance of intestine (Farin et al., 2012; Sato et al., 2011). This prompts the question if canonical Wnt 6/9 (predominant in intestine) could compensate for the loss of function of Wnt3.

There exist 19 Wnts in vertebrates, 6 in intestine. It is nearly impossible to generate a all- *Wnt* knockout mouse. In addition to overcoming this set back, our study circumvents the problems that may arise due to functional redundancy within Wnt ligands. By deleting *Gpr177*, a unique transporter for all-Wnts, we expected to abrogate all-Wnt secretion and hence determine the contribution of Wnt activity on intestinal homeostasis. *Gpr177* null stem cells clearly depict reduced regenerative abilities which lead to growth arrest and death of *Gpr177*$^{-/-}$ organoids. We suspect profound in vivo tissue adaptation (absent ex vivo) in these knockouts; thus it will be interesting to see whether these knockout animals regenerate their intestinal epithelium when challenged by a chemical insult such as with Dextran sodium sulfate (DSS) or radiation.

Another intriguing question yet to be resolved concerns the source cell-type of Wnt ligands. Clearly, epithelial and extra-epithelial cells are a constant source of Wnt ligands in intestine (Farin et al., 2012; Sato et al., 2011), however they don't seem to be the only ones (San Roman et al., 2014). Porcupine, an acyl-O-transferase post-

translationally modifies specifically all Wnts which allows them to bind to Gpr177 and further to Frizzled receptors at the receiving end (Chen et al., 2009; Najdi et al., 2012). Despite of Porcupine's significance in Wnt ligand transport and function, intestinal epithelium and mucosa when deprived of the gene do not demonstrate any phenotype; suggesting existence of an additional source of Wnt ligands in intestine. We documented a similar observation in *Gpr177* knockouts. Some of the proposed Wnt sources are immune cells, endothelial cells and neurons which may come into action when needed.

Interestingly, transgenic mice with gain/loss of function of Wnt components at the signal receiving end demonstrate a rather severe consequence than mouse models with genes deleted for molecules critical in Wnt ligand secreting cells. For instance, in intestine, mutations either deactivating *Apc* or activating *β-catenin* constitutively lead to uncontrolled growth of crypt cells leading to adenoma, formation of tumors and eventual death of mice within a week (Andreu et al., 2008; Korinek, 1997; Romagnolo et al., 1999). Similarly, mutations inactivating *β-catenin* or *Tcf4* causes reduced proliferation and lack of crypts ultimately leading to death of mice (Fevr et al., 2007; Korinek et al., 1998; van Es et al., 2012a). Note that these loss/gain-of-function studies were performed using conditional intestine-specific knockouts. On the other hand, deletion of essential molecules in Wnt secreting cells, *Porcupine* or *Gpr177*, cause only subtle changes in vivo ((Kabiri et al., 2014; San Roman et al., 2014) and this study). The impact (in this study characterized as reduced regenerative ability of stem cells) of these deletions is demonstrated only when knockout crypts are isolated from the

complex environment in intestine and cultured ex vivo. More interestingly, the impact of gene deletion is higher, only when these regulatory molecules (Porcupine, Gpr177 or Retromer component Vps35) are depleted globally at an early embryonic stage, causing embryonic lethality in mice (Barrott et al., 2011; Carpenter et al., 2010; Fu et al., 2009; Radice et al., 1991). Our data show tolerance to *Rab8a* and *Gpr177* deletion by intestinal tissue, implicating presence of compensatory signals in intestinal tissue contributed by either Wnt or non-Wnt secreting extra-epithelial cells which seem to be capable of activating the β-catenin/Tcf4/Lef-regulated Wnt pathway in intestine. Thus, in context of above cited studies and data from this study, it is tempting to propose that global loss of function of Wnt proteins are essential for embryonic development of mammalian embryos however are most likely dispensable for adult intestinal crypt homeostasis. In contrary, Wnt signal transduction is essential for both embryonic development and maintenance adult intestinal tissue.

A

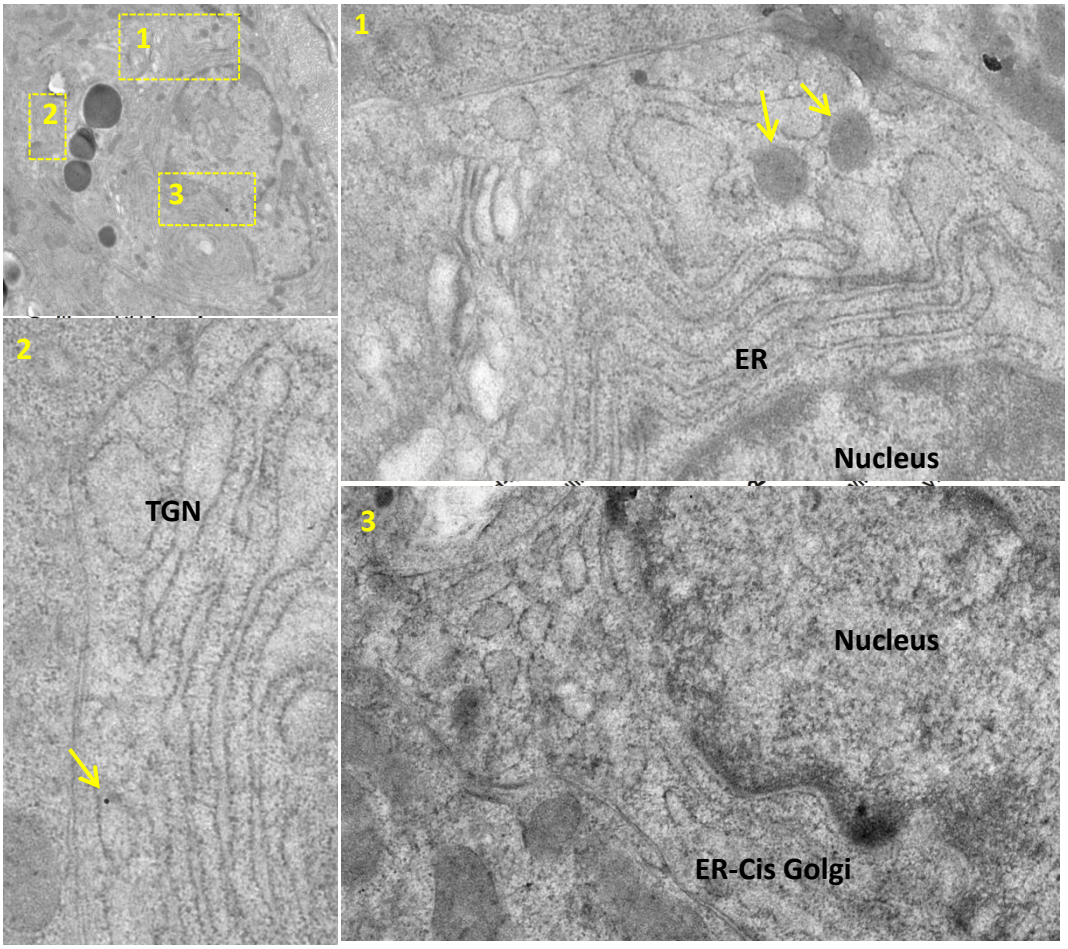
1
2
3
1
ER
Nucleus
2
TGN
3
Nucleus
ER-Cis Golgi

B

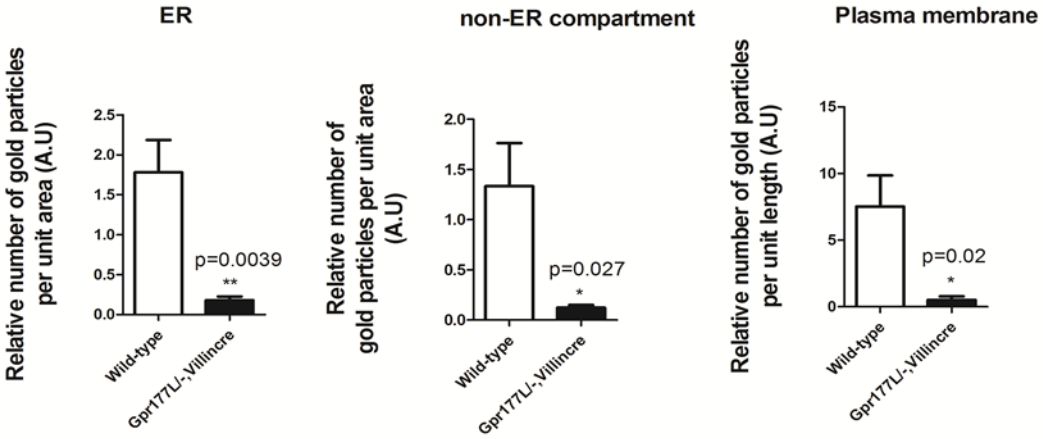
ER
Relative number of gold particles per unit area (A.U)
2.5
2.0
1.5
1.0
0.5
0.0
p=0.0039
**
Wild-type
Gpr177L/-;Villincre
non-ER compartment
Relative number of gold particles per unit area (A.U)
2.0
1.5
1.0
0.5
0.0
p=0.027
*
Wild-type
Gpr177L/-;Villincre
Plasma membrane
Relative number of gold particles per unit length (A.U)
15
10
5
0
p=0.02
*
Wild-type
Gpr177L/-;Villincre

Figure 22: Verification of *Gpr177* deletion in Paneth cells by immunoelectron microscopy

A. Immunoelectron micrographs showed an overall lack of gold particles in *Gpr177*-deficient Paneth cells from *Gpr177$^{L/-}$; Villincre* mice including their absence in ER and endo-lysosome (image **1**), Trans-golgi (image **2**) and ER-cis golgi (image **3**). **Arrows** show rarely observed residual Gpr177^{+} gold-particles. **Images 1-3** are magnified from yellow-boxed areas in a *Gpr177* deficient Paneth cell.

B. To quantify the distribution of Gpr177 in Paneth cells, number of Gpr177^{+} colloidal gold particles were counted in several sub-cellular compartments such as ER, non-ER (Golgi/vesicle) and plasma membrane along with the area (ER and non-ER) or perimeter (plasma membrane) covered by each compartment in wild-type and *Gpr177$^{L/-}$; Villincre* Paneth cells. Quantifications showed 90%, 91% and 93% reduction in number of Gpr177^{+} gold particles per unit area (or length) of ER, non-ER and plasma membrane (respectively) of *Gpr177$^{L/-}$;Villincre* Paneth cells.

A

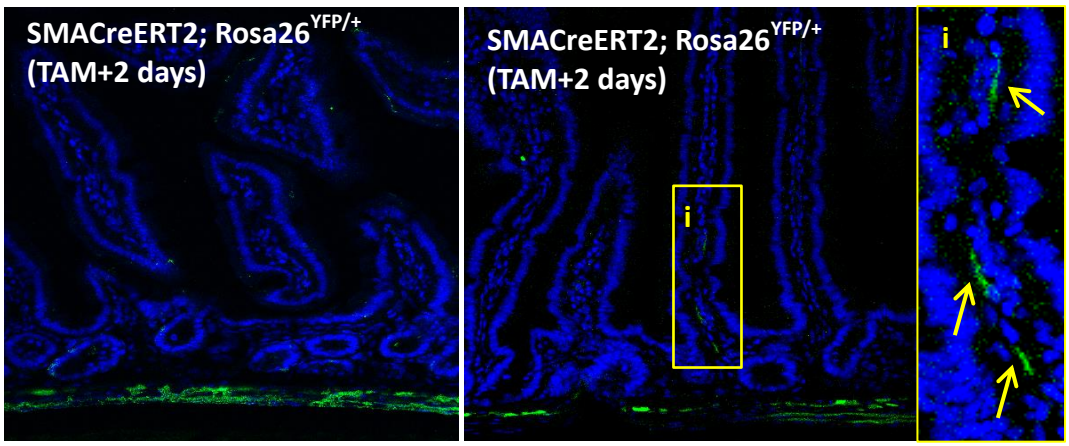
SMACreERT2; Rosa26YFP/+
(TAM+2 days)
SMACreERT2; Rosa26YFP/+
(TAM+2 days)
i
i

YFP

B

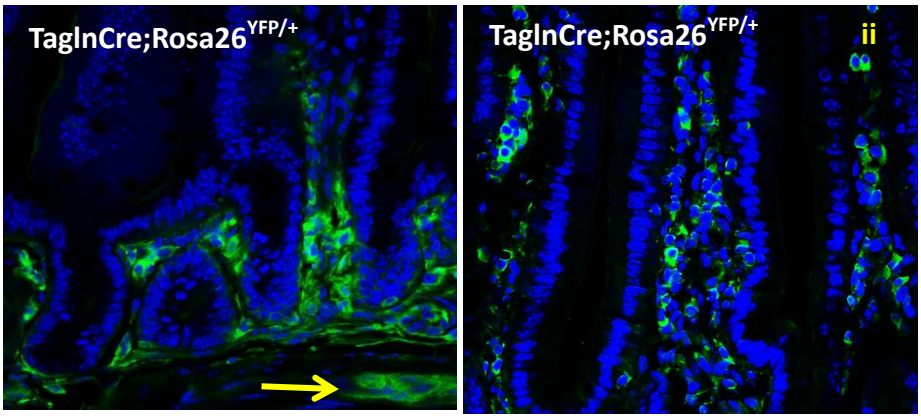
TagInCre;Rosa26YFP/+
TagInCre;Rosa26YFP/+
ii

YFP

Figure 23: Characterization of SMAcre- and Taglncre- recombinases expression using *Rosa26*$^{YFP/+}$ reporter mouse line

A. Immunofluorescent staining for YFP showed strong expression of SMAcre recombinase in smooth muscle and milder expression in lamina propria (**boxed in yellow** and shown in (**i**)). **Arrows** point to lamina propria cells expressing YFP (SMAcre).

B. Immunofluorescent staining for YFP staining showed strong expression of Taglncre recombinase by smooth muscle (**arrow**) and lamina propria (as shown in (**ii**)) cells.

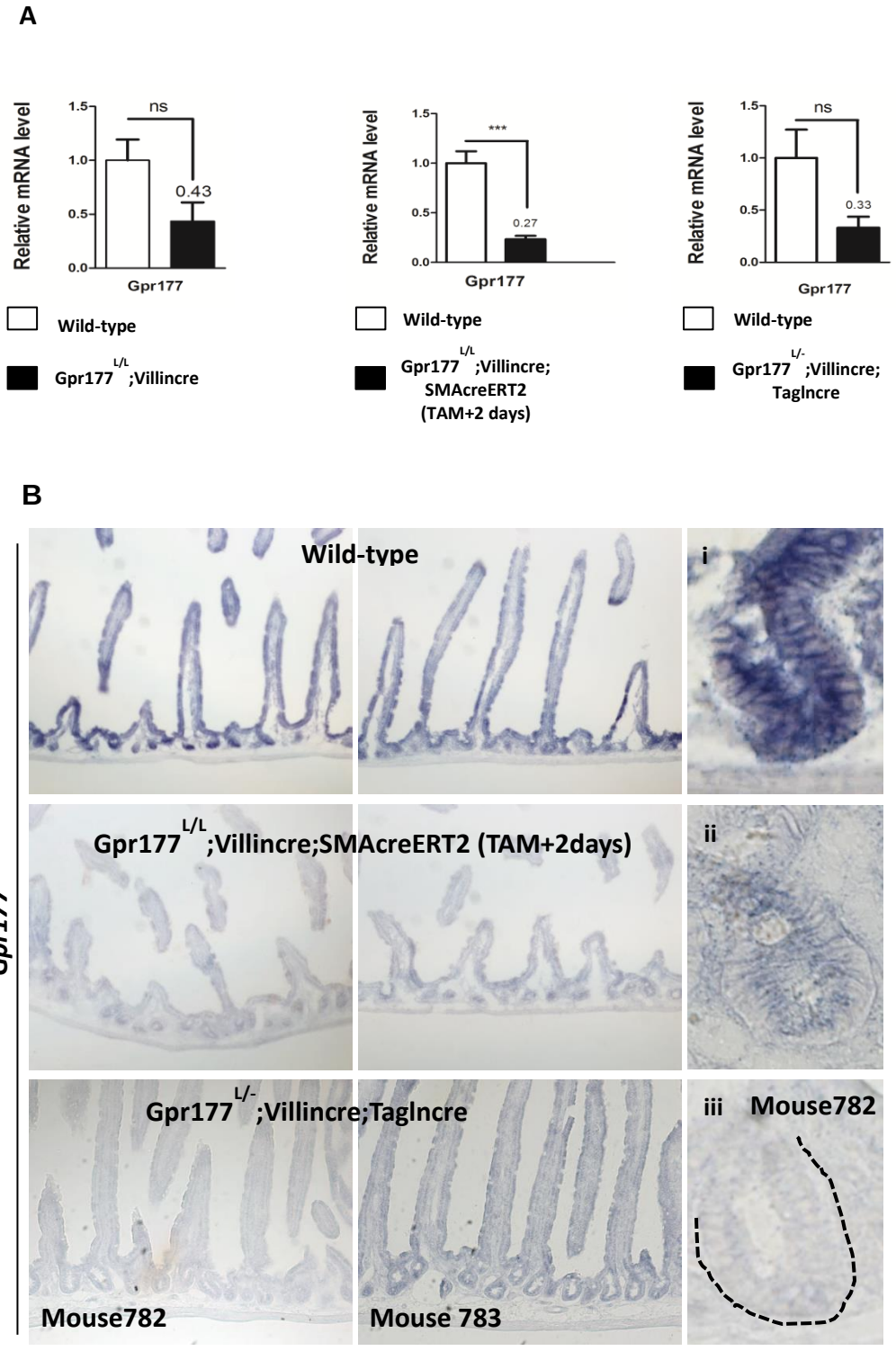
A
Relative mRNA level
1.5
1.0
0.5
0.0
ns
0.43
Gpr177
Wild-type
Gpr177 L/L ;Villincre
***
0.27
Gpr177
Wild-type
Gpr177 L/L ;Villincre; SMAcreERT2 (TAM+2 days)
ns
0.33
Gpr177
Wild-type
Gpr177 L/- ;Villincre; Taglncre
B
Gpr177
Wild-type
i
Gpr177 L/L ;Villincre;SMAcreERT2 (TAM+2days)
ii
Gpr177 L/- ;Villincre;Taglncre
iii
Mouse782
Mouse782
Mouse 783

C

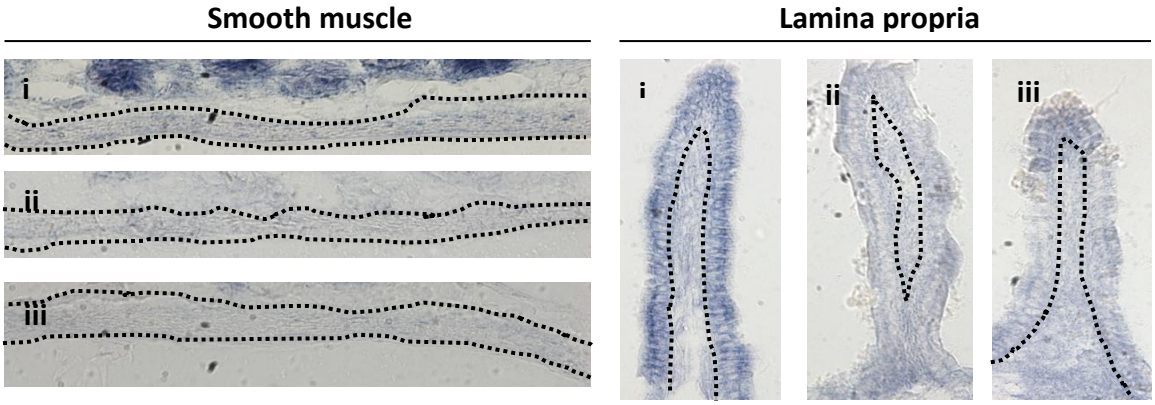

Figure 24: Verification of *Gpr177* deletion in several *Gpr177*-knockout mice using quantitative PCR and in-situ hybridization

A. Quantitative RT-PCR showed reduction of *Gpr177* mRNA levels in *Gpr177$^{L/L}$;Villincre* (n=4), *Gpr177$^{L/L}$;Villincre;SMAcreERT2*(TAM+2days) (n=5) and *Gpr177$^{L/-}$;Villincre;Taglncre* (n=3) knockouts. Most significant difference was observed in *Gpr177$^{L/L}$;Villincre;SMAcreERT2* (TAM+2days) knockouts when compared to the control counterparts.

B. In situ hybridization showed reduction of *Gpr177* mRNA levels in *Gpr177$^{L/L}$;Villincre;SMAcreERT2*(TAM+2days) and *Gpr177$^{L/-}$;Villincre;Taglncre* knockouts. Levels of *Gpr177* deletion varied between *Gpr177$^{L/-}$;Villincre;Taglncre* knockouts (compare images from littermates **Mouse 782** and **Mouse 783**). Mouse 783 showed higher *Gpr177* expression.

C. In situ hybridization showed no significant differences in *Gpr177* levels in extra-epithelial cells (smooth muscle and lamina propria) of intestine of wild-type **(i)**, *Gpr177$^{L/L}$; Villincre; SMAcreERT2* (TAM+2 days) **(ii)** and *Gpr177$^{L/L}$; Villincre; Taglncre* knockouts **(iii)**.

A

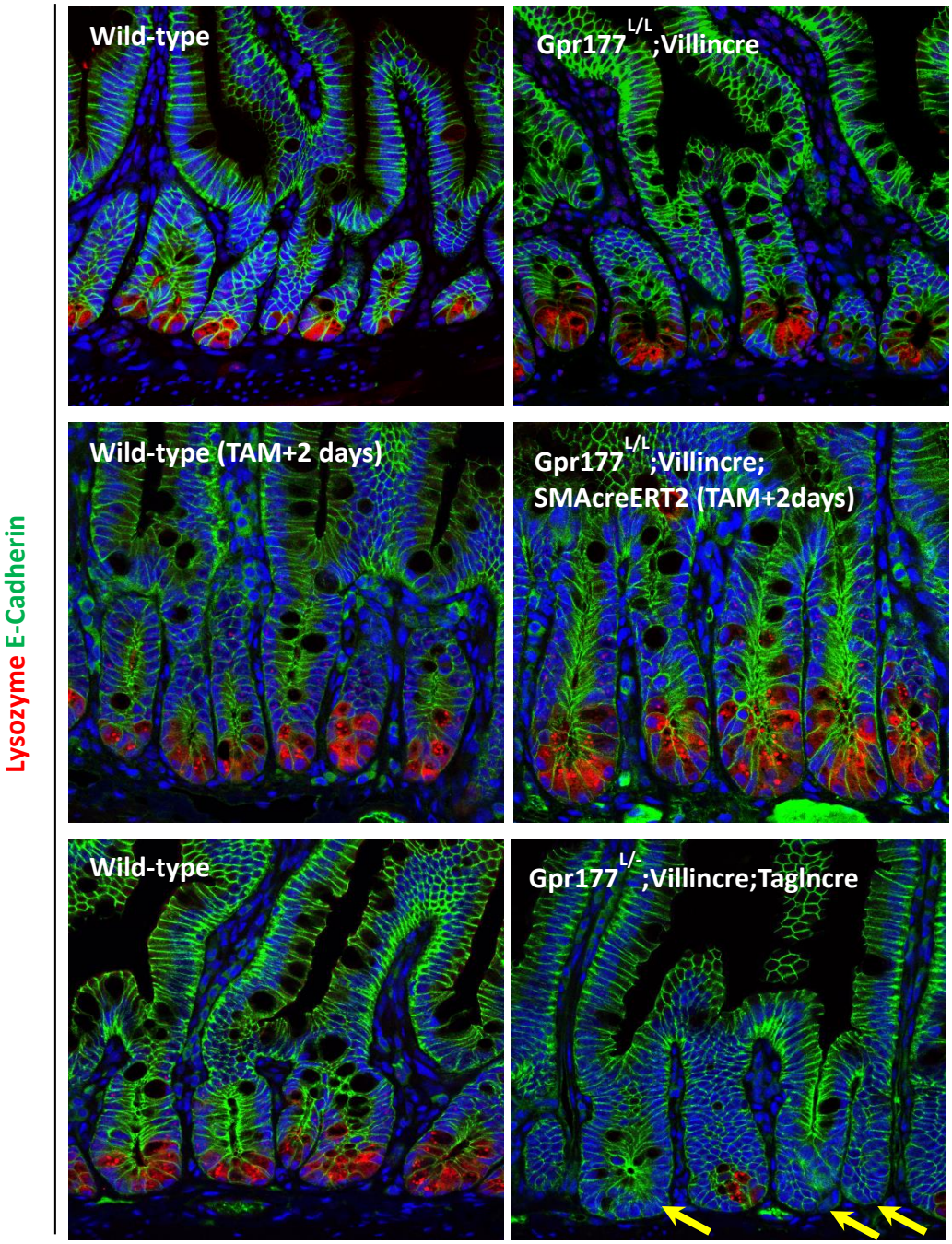
Wild-type
Gpr177 L/L ;Villincre
Wild-type (TAM+2 days)
Gpr177 L/L ;Villincre;
SMAcreERT2 (TAM+2days)
Wild-type
Gpr177 L/- ;Villincre;TagIncre
Lysozyme E-Cadherin

B

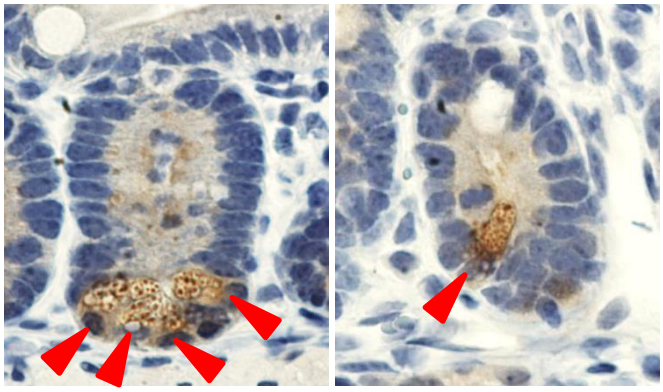

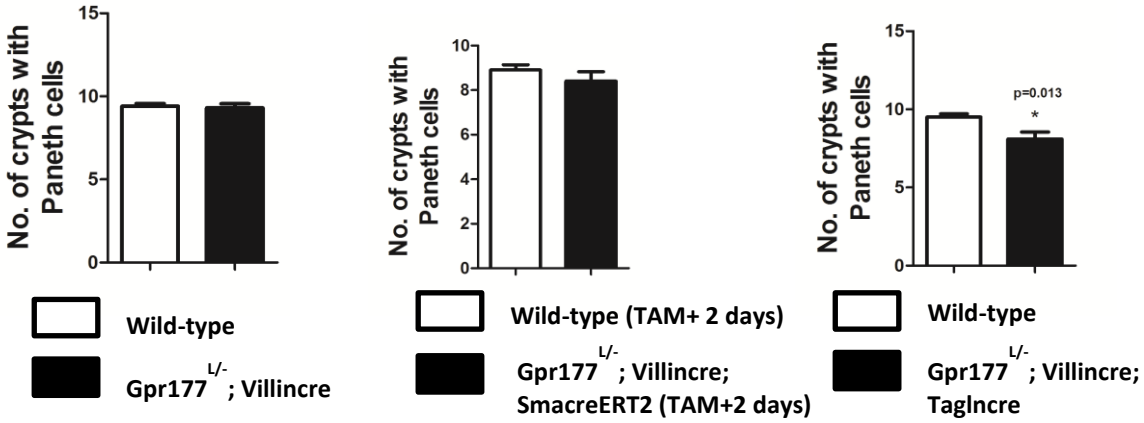
No. of crypts with Paneth cells
15
10
5
0
Wild-type
Gpr177 L/- ; Villincre
No. of crypts with Paneth cells
10
8
6
4
2
0
Wild-type (TAM+ 2 days)
Gpr177 L/- ; Villincre; SmacreERT2 (TAM+2 days)
No. of crypts with Paneth cells
15
10
5
0
p=0.013
*
Wild-type
Gpr177 L/- ; Villincre; Taglncre

Figure 25: Analysis of Lysozyme^{+} Paneth cells using histological staining procedures

A. Immunofluorescent staining for Lysozyme (**red**) and E-Cadherin (**green**) showed reduction in number of Paneth cells in *Gpr177$^{L/-}$; Villincre; Taglncre* mouse intestines (**arrows**). Nulcear staining with Topro-3 is shown in **blue**.

B. Immunohistochemical staining for lysozyme (**brown**) was used to quantify the number of Paneth cells in 50 continuous crypts. Crypts counted as Paneth cell^{+} crypts are shown in representative bright field images. Arrowheads point to Lysozyme^{+} Paneth cells considered for quantification. Quantifications showed a significant reduction in number of Paneth cells was observed *in Gpr177$^{L/-}$; Villincre; Taglncre* mice.

A

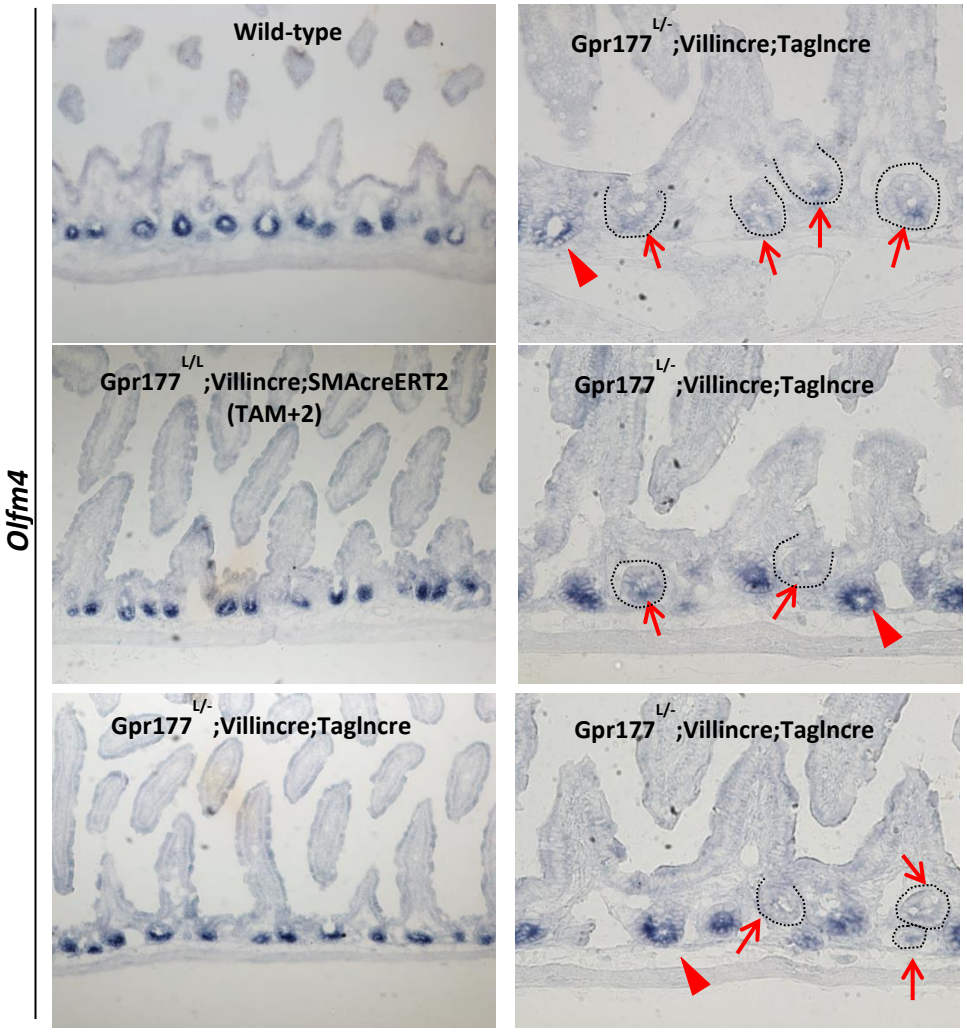
Olfm4
Wild-type
Gpr177 L/- ;Villincre;Taglncre
Gpr177 L/L ;Villincre;SMAcreERT2 (TAM+2)
Gpr177 L/- ;Villincre;Taglncre
Gpr177 L/- ;Villincre;Taglncre
Gpr177 L/- ;Villincre;Taglncre

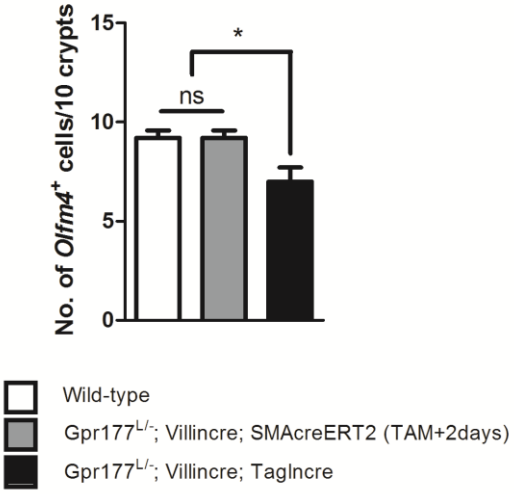
No. of Olfm4+ cells/10 crypts
15
10
5
0
ns
*
Wild-type
Gpr177L/-; Villincre; SMAcreERT2 (TAM+2days)
Gpr177L/-; Villincre; Taglncre

B

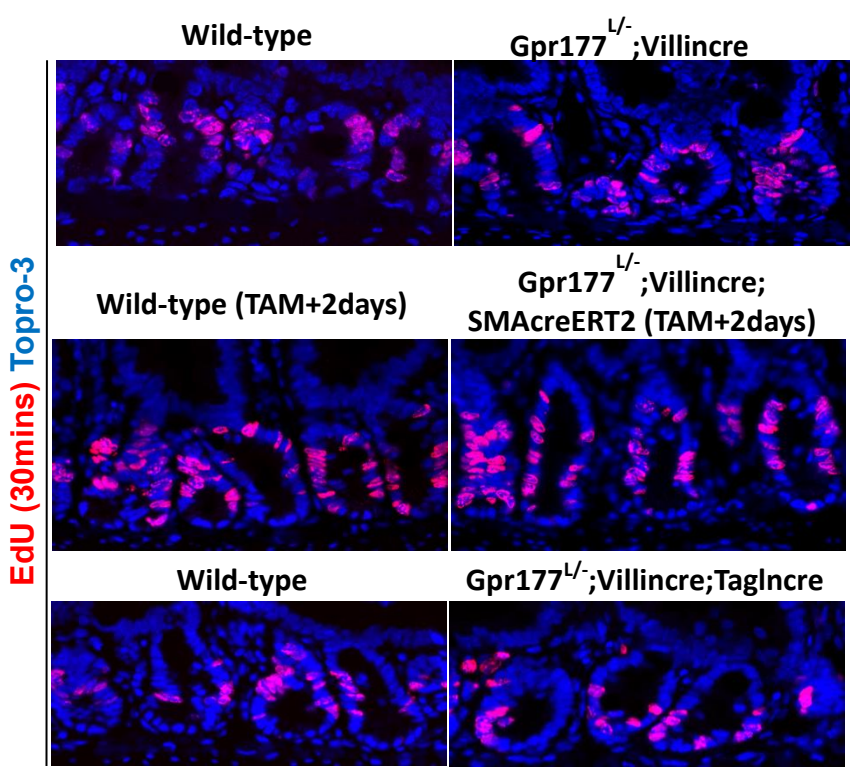
Wild-type
Gpr177L/-;Villincre
EdU (30mins) Topro-3
Wild-type (TAM+2days)
Gpr177L/-;Villincre;
SMAcreERT2 (TAM+2days)
Wild-type
Gpr177L/-;Villincre;Taglncre

C

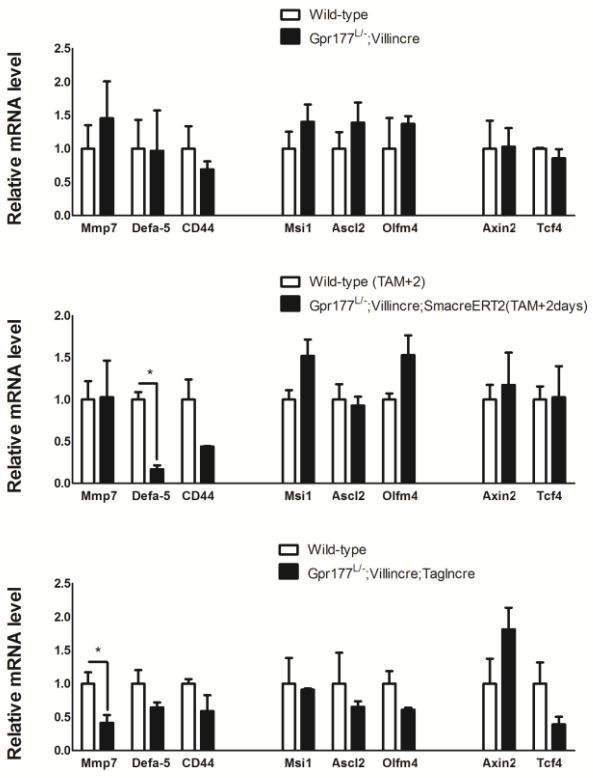
Wild-type
Gpr177L/-;Villincre
Relative mRNA level
Mmp7
Defa-5
CD44
Msi1
Ascl2
Olfm4
Axin2
Tcf4
Wild-type (TAM+2)
Gpr177L/-;Villincre;SmacreERT2(TAM+2days)
Wild-type
Gpr177L/-;Villincre;Taglncre

Figure 26: Analysis of stem and proliferative cells in several *Gpr177*-knockout intestines

A. In situ hybridization for *Olfm4* mRNA showed no significant difference in distribution, number or expression of *Olfm4*$^{+}$ stem cells in *Gpr177*$^{L/L}$*;Villincre; SMAcreERT* (TAM+2days) knockouts. *Olfm4*$^{+}$ stem cells were absent frequently only in *Gpr177*$^{L/-}$*;Villincre;TagIncre* knockouts (**arrows, bar graph**). **Arrowheads** point to adjacent crypts with *Olfm4*$^{+}$ cells.

B. Immunofluorescent staining for EdU (30 minutes, **red**) showed no significant difference in EdU^{+} proliferative cell zone in various *Gpr177* knockouts. Nuclear staining with Topro-3 is shown in **blue**.

C. Quantitative real time PCR using total intestinal lysates showed no statistically significant reduction in several Paneth cell (Mmp7, Defa-5 and CD44), stem cell (Msi1, Ascl2 and Olfm4) and Wnt target (Axin2 and Tcf4) signature gene expression. A significant reduction however was observed in *Defa-5* mRNA levels in *Gpr177*$^{L/L}$*;Villincre;SMAcreERT2* (TAM+2days) knockouts and *Mmp7* mRNA levels in *Gpr177*$^{L/-}$*;Villincre;TagIncre* knockouts indicating possible defects in Paneth cell maturation (also see **Figure 25**).

A

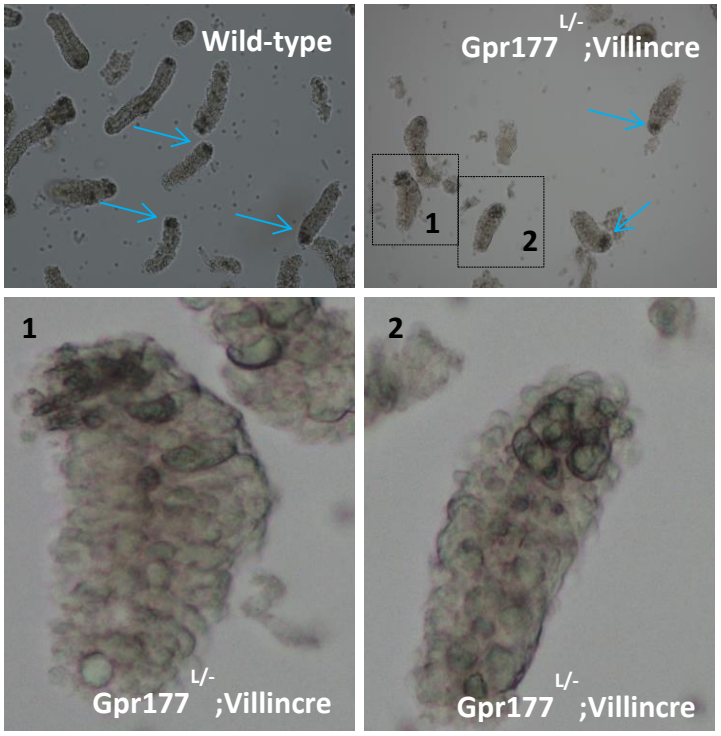
Wild-type
Gpr177 L/- ;Villincre
1
2
1
2
Gpr177 L/- ;Villincre
Gpr177 L/- ;Villincre

B

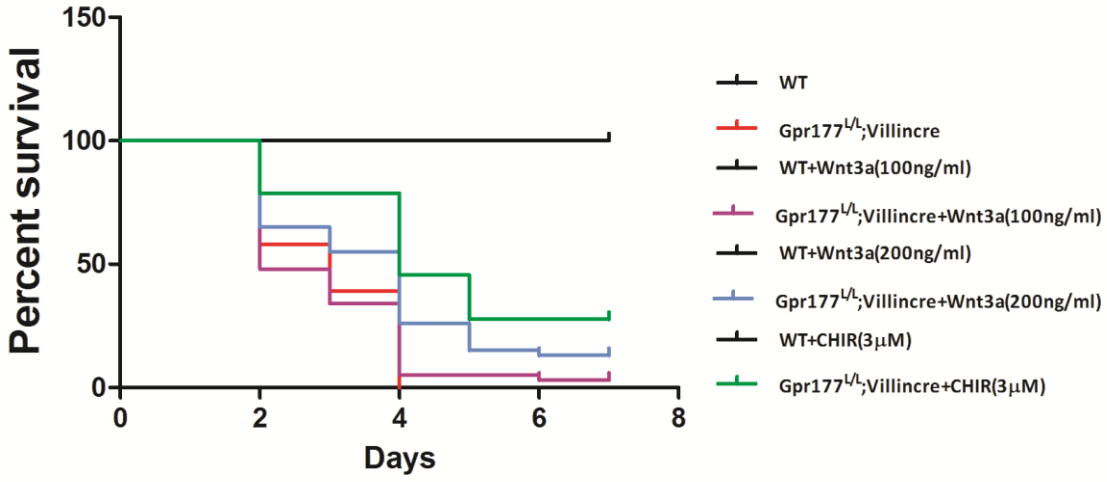
Percent survival
150
100
50
0
0
2
4
6
8
Days
WT
Gpr177L/L;Villincre
WT+Wnt3a(100ng/ml)
Gpr177L/L;Villincre+Wnt3a(100ng/ml)
WT+Wnt3a(200ng/ml)
Gpr177L/L;Villincre+Wnt3a(200ng/ml)
WT+CHIR(3μM)
Gpr177L/L;Villincre+CHIR(3μM)

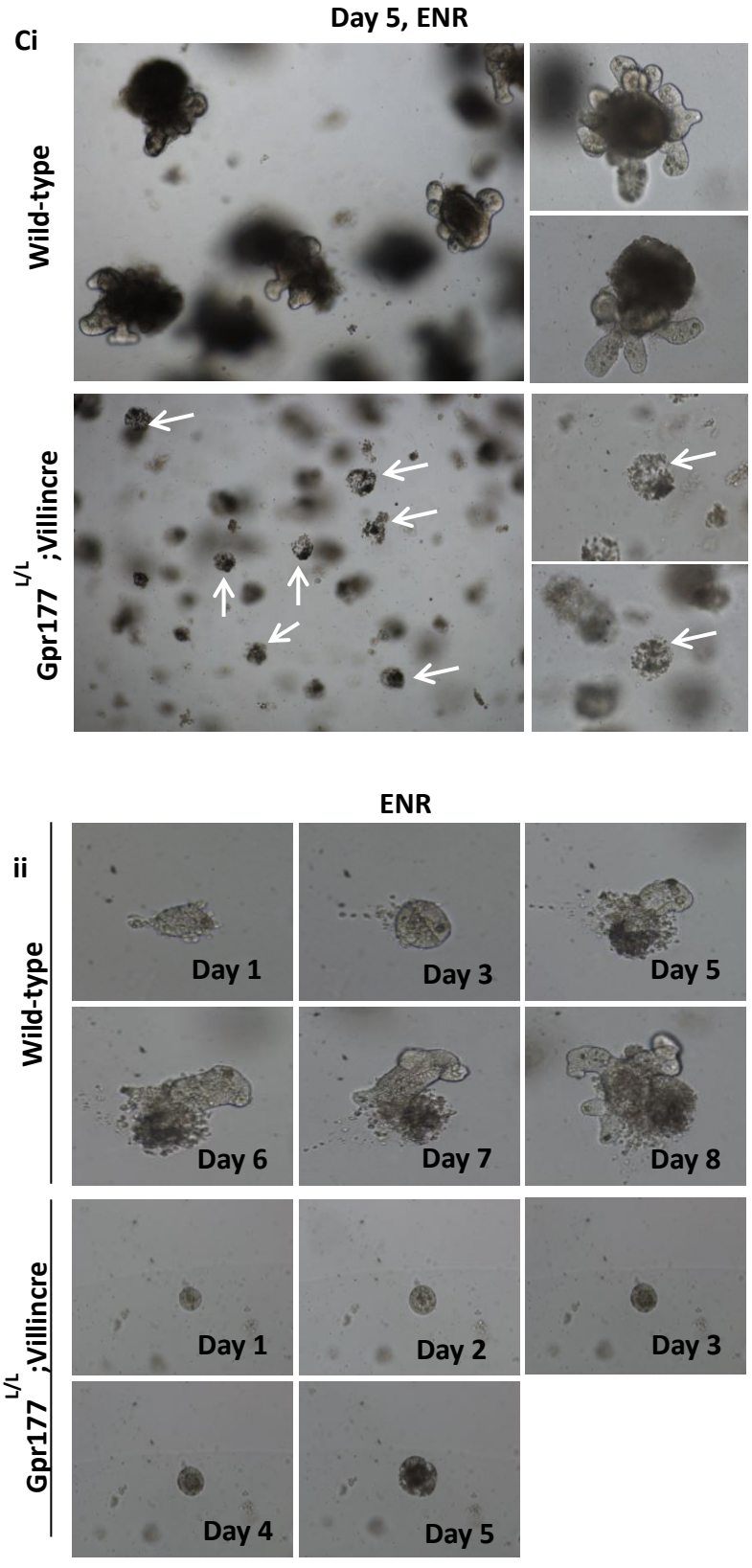
Ci
Day 5, ENR
Wild-type
Gpr177L/L;Villincre
ii
ENR
Wild-type
Day 1
Day 3
Day 5
Day 6
Day 7
Day 8
Gpr177L/L;Villincre
Day 1
Day 2
Day 3
Day 4
Day 5

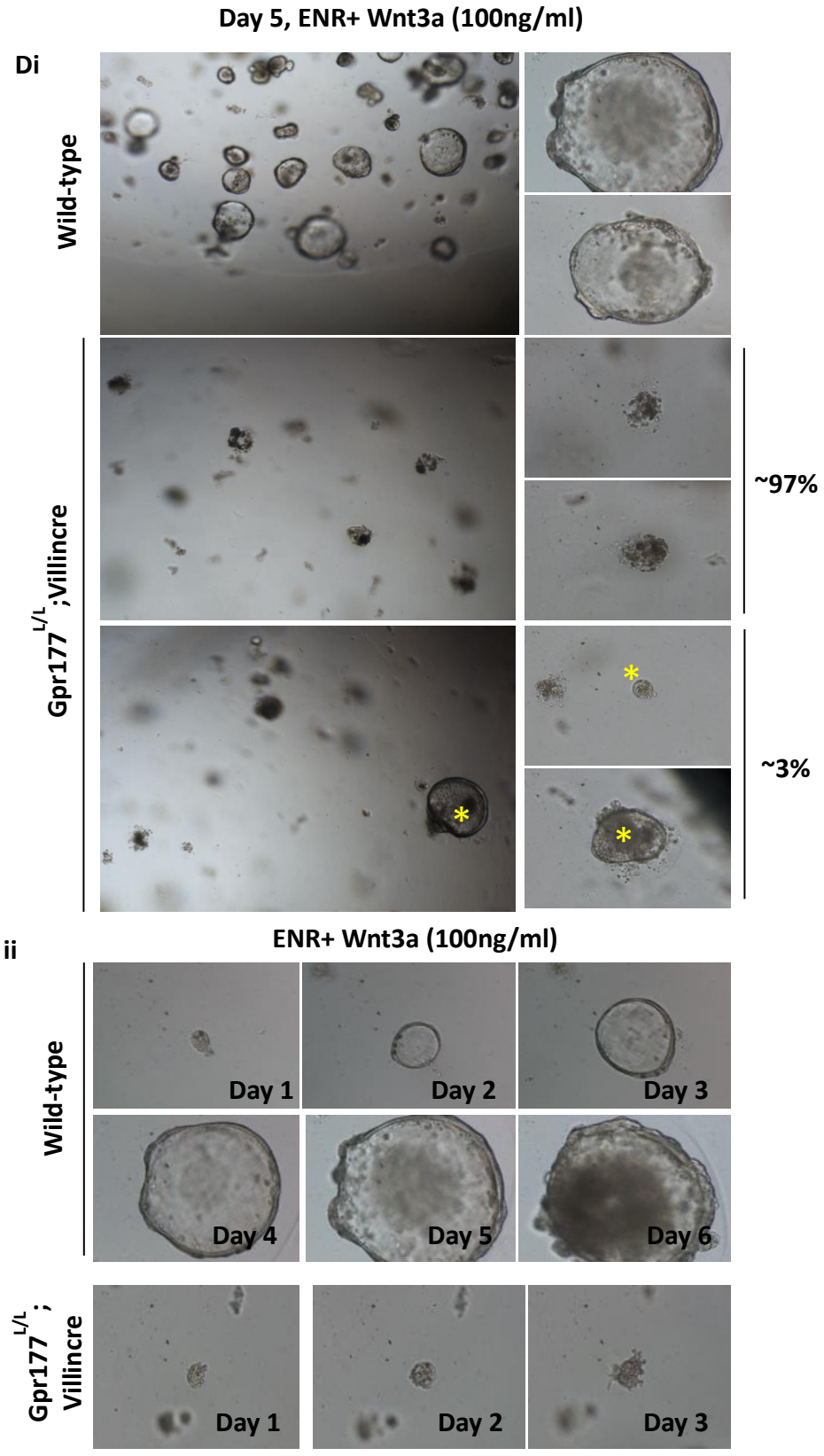
Day 5, ENR+ Wnt3a (100ng/ml)
Di
Wild-type
Gpr177L/L;Villincre
~97%
~3%
ii
ENR+ Wnt3a (100ng/ml)
Wild-type
Day 1
Day 2
Day 3
Day 4
Day 5
Day 6
Gpr177L/L; Villincre
Day 1
Day 2
Day 3

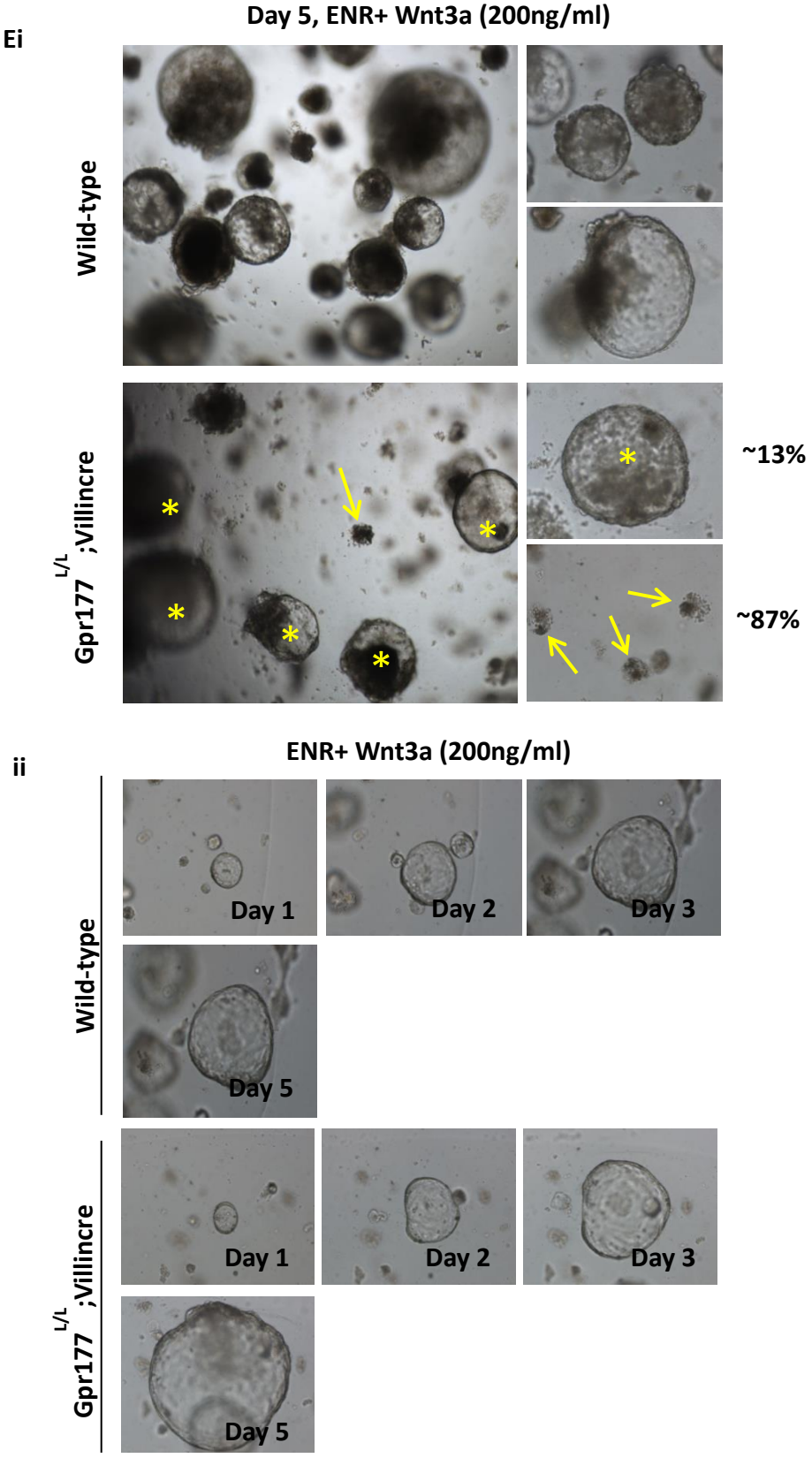
Ei
Day 5, ENR+ Wnt3a (200ng/ml)
Wild-type
Gpr177 L/L ;Villincre
~13%
~87%
ii
ENR+ Wnt3a (200ng/ml)
Wild-type
Day 1
Day 2
Day 3
Day 5
Gpr177 L/L ;Villincre
Day 1
Day 2
Day 3
Day 5

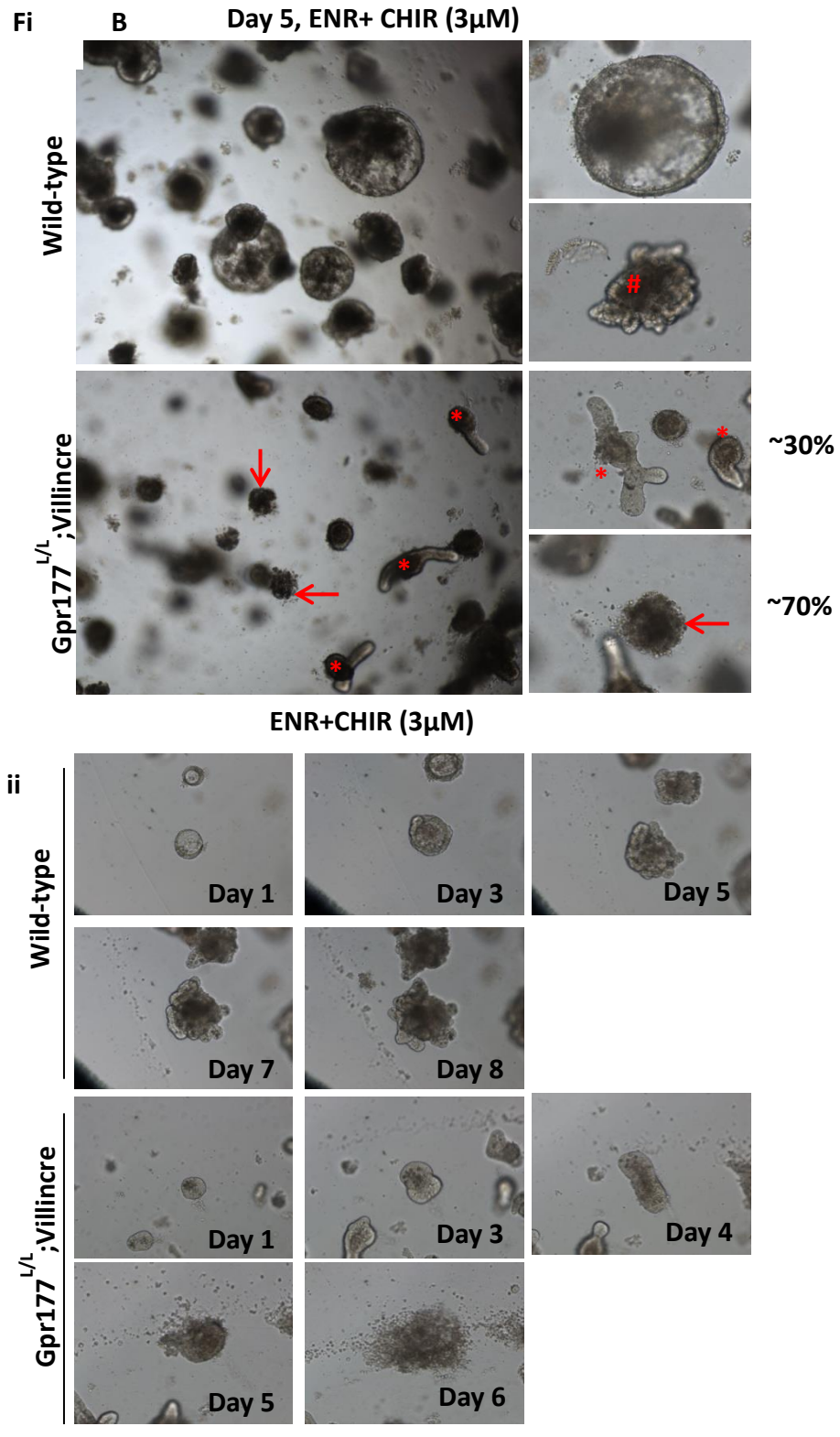
Fi
B
Day 5, ENR+ CHIR (3µM)
Wild-type
Gpr177L/L;Villincre
~30%
~70%
ENR+CHIR (3µM)
ii
Wild-type
Day 1
Day 3
Day 5
Day 7
Day 8
Gpr177L/L;Villincre
Day 1
Day 3
Day 4
Day 5
Day 6

Figure 27: Analysis of morphology and growth of *Gpr177* null organoids

A. Bright-field images of Wild-type and *Gpr177* deleted crypts cultured ex vivo showed presence of Paneth cells in *Gpr177* null crypts on day of seeding (**arrows** point to Paneth cell^{+} crypt bases).

B. Quantification of number of surviving wild-type and *Gpr177* null crypts (n=500 per genotype and treatment) cultured ex vivo showed 3% survival with Wnt3a (100ng/ml, **purple line**), 13% survival with Wnt3a (200ng/ml, **blue line**) or 30% survival with CHIR, a GSK3β inhibitor, (3μM, **green line**). All *Gpr177* null crypts died by day 4 in culture ex vivo (**red line**).

C. i) Representative bright-field images of crypt cultures show wild-type and *Gpr177* null crypts in ENR medium. All knockout crypts died by Day 4 (**arrows**).

ii) Bright-field images show the growth of individual representative wild-type or *Gpr177* null crypt cultured in ENR medium. The knockout crypt was growth arrested by Day 3 and dead by Day 5.

D. i) Representative bright-field images of crypt culture show wild-type and *Gpr177* null crypts in ENR medium supplemented with 100ng/ml of recombinant murine Wnt3a protein. Insignificant (~3%, also see **Figure 27 (B)**) improvement was observed in the survival of *Gpr177* null crypts in presence of 100ng/ml of Wnt3a (**asterisks**).

ii) Bright-field images show the growth of individual representative wild-type or *Gpr177* null crypt cultured in ENR medium supplemented with 100ng/ml Wnt3a.

E.i) Representative bright-field images of crypt cultures show wild-type and *Gpr177* null crypts in ENR medium supplemented with 200ng/ml of recombinant murine Wnt3a protein. ~13% of *Gpr177* deleted crypts survived in presence of 200ng/ml of Wnt3a as observed by the end of Day 7 in culture. Note that only cyst-structured knockout organoids were observed on Day 5 (**asterisks**). **Arrow** points to dead organoids.

ii) Bright-field images show the growth of individual representative wild-type or *Gpr177* null crypt cultured in ENR medium supplemented with 200ng/ml Wnt3a.

F.i) Representative bright-field images of crypt cultures show wild-type and *Gpr177* null crypts in ENR medium supplemented with 3µM of CHIR99021. ~30% of *Gpr177* deleted crypts survived in presence of 3µM of CHIR as observed by the end of Day 7. Note that surviving knockout organoids begin with cyst like structures but mostly differentiate to form tubular buds at the end of Day 5 in culture (**asterisks**) after which they start regressing (**arrows**) and eventually die (also see 27**F(ii)**). Some wild-type crypts started differentiating even in presence of CHIR at Day 5 (**hashtag**).

ii) Bright-field images show the growth of individual representative wild-type or *Gpr177* null crypt cultured in ENR medium supplemented with 3µM of CHIR.

CHAPTER 7

DISCUSSION AND FUTURE STUDIES

Some information included in this chapter is taken from and are published in Das et al., Development (2015), 142(12):2147-62

In this study *Rab8a* knockout mice serve as a genetic model for loss of Paneth cells to primarily study maintenance and regeneration of intestinal crypts. Our study of Rab8a function in mouse intestinal crypt compartment extended previous analysis performed in differentiated enterocytes (Sato et al., 2007). The observed crypt defects in *Rab8a* knockout mice likely precede the apical transport abnormalities in enterocytes that are derived from the crypt progenitors. Our finding that Rab8a affects Gpr177 mediated Wnt secretion and Paneth cell maturation impinges on a growing body of studies linking vesicular traffic to niche signal transduction and maintenance (Feng and Gao, 2014; Goldenring, 2013).

Rab8a regulates Wnt secretion in intestine

Rab8a deletion clearly impacted Wnt signaling in intestinal crypts. This was strongly supported by *Axin2* reporter analysis *in vivo* and in organoid culture, as well as by the defective Paneth cell maturation in *Rab8a*$^{-/-}$ crypts. Mechanistically, these phenotypes could be caused by defective traffic of Wnt (co-) receptors–Lrp6 and Frizzled. This possibility was ruled out on the basis of several evidences. Firstly, *Rab8a*$^{-/-}$ MEFs still responded to exogenous Wnt ligands by phosphorylating Lrp6 cytosolic tail and activating Top-flash Wnt reporter. Second, exogenous Wnt3a and GSK3β inhibitor partially restored growth and survival as well as changed the morphology of *Rab8a*$^{-/-}$ organoids. Third, an independent screening assay by Demir et al. showed that RAB8A did not affect the process of Wnt-receiving (Demir et al 2013). These data corroborated the view that unlike RAB8B that regulates Wnt-receiving and LRP6 endocytosis, RAB8A

plays a distinct role in Wnt producing cells. Likewise, we did not observe an impact of RAB8B on Wnt secretion.

In *Rab8a*$^{-/-}$ Paneth cells or sub-epithelial fibroblasts, immunogold labeling of Gpr177 and surface protein isolation demonstrated reduced localization of Gpr177 adjacent to cell surface. It appears that disruption of Rab8a-dependent transport weakens Gpr177-mediated Wnt secretion by re-routing Gpr177 into endolysosomal compartments. Similar observation was also made following a defective retromer-dependent Gpr177 retrieving (Eaton 2008). After synthesis in ER, lysosomal hydrolases and membrane proteins are transported directly from Golgi apparatus and TGN to late endosomes, via vesicles that exclude other proteins of distinct destinations. It is still not entirely clear how loss of Rab8a might cause mis-packaging of Gpr177 into lysosome-targeting vesicles. In absence of Rab8a, post-Golgi Gpr177 vesicles may be hijacked by distinct Rab GTPases (e.g., Rab9) facilitating endolysosomal fusion. Instead of beind destined to the plasma membrane, some brush border enzymes are also mis-targeted into lysosome in *Rab8a*$^{-/-}$ enterocytes (Sato et al., 2007), hinting similarities in defective cargo transport in absence of Rab8a. Of note, Sec4, the Rab8a homolog in yeast, predominantly mediates post-Golgi vesicle secretion (Das and Guo, 2011; Hutagalung and Novick, 2011; Seabra et al., 2002).

The view that Rab8a vesicles promote export of Gpr177-Wnt also provided additional support for the physiological involvement of RAB8 in GPCR anterograde trafficking (Takeda et al., 2011). RAB8 was shown to modulate exocytosis of

metabotrophic glutamate receptor (Esseltine et al., 2012), α2B and β2 adrenergic receptors (Dong et al., 2010) in human embryonic kidney cells and primary neurons with an interaction with C-terminus of β2 adrenergic receptors (Dong et al., 2010).

In *Rab8a*$^{-/-}$ MEFs, we observed a rather selective impact on Wnt secretion. Rabs and other membrane trafficking regulators are often considered to be generic modulators of protein transport. However, accumulating evidences suggest that perturbing these trafficking processes impact a rather specific pathway (Knowles et al., 2015; Okamoto et al., 2014). For instance, depletion of RAB8B impacted Wnt signalosome activity and no other signaling pathways (Demir et al., 2013). Disrupting retromer function by ablating Vps35 or sorting nexin 3 (SNX3) impaired primarily Wnt secretion (Eaton, 2008; Harterink et al., 2011). Furthermore, partial loss of Rab1 and Rab11 preferentially affected Notch signaling in *Drosophilla* (Charng et al., 2014; Emery et al., 2005), whereas genetic mutation of Rab23 specifically perturbed Hedgehog signaling pathway (Eggenschwiler et al., 2001; Evans et al., 2003), with its potential targets being Suppressor of fused (Chi et al., 2012), or/and Smoothened– another GPCR (Boehlke et al., 2010). Certain cargos are destined to their target compartment through multiple sequential intracellular routes; each route controlled by a different set of specific molecular regulators. Some of these intracellular pathways might limit the cargo-flux through a particular compartment making the molecules involved in that pathway (and not any other pathway) essential for cargo destination and ultimately its function. This might be a plausible explanation for an obvious impact of Rab8 dependent exocytic pathway on specifically Wnt secretion or similar such examples cited above.

Additionally, as individual Rab8a^{+} vesicles may contain heterogeneous cargos, it is unlikely that Rab8a traffics only Gpr177. This also suggests that the classification of molecular regulators (such as Rabs) should not be simply based on the compartment they occupy but also include specificity towards cargo.

Rab8a mediated Wnt secretion regulates Paneth cells

The organoid-forming capacity of Lgr5^{+} stem cells in culture was enhanced by association with Paneth cells (Sato et al., 2011). We found that *Rab8a*$^{-/-}$ organoids resembled *Wnt3*$^{-/-}$ or *Atoh1*$^{-/-}$ organoids (Durand et al., 2012; Farin et al., 2012), showing poor clonogenic activities. Vast majority of surviving Rab8a organoids contained tiny Paneth cell-containing buds, suggesting that the few remaining Paneth cells may have facilitated residual colonogenic activities of the knockout organoids. These data favored the notion that Paneth cells were perhaps the major stem cell supporters in cultured enteroids after growth support from non-epithelial compartments was eliminated. Additionally survival of some (~30%) organoids in absence of *Rab8a* implies that function of Rab8a in Paneth or stem cells ex vivo is not indispensable.

A subset of Lgr5^{+} label retaining cells (LRCs) were identified to express both CBC and Paneth cell gene signatures (Buczacki et al., 2013), and proposed to be precursors of Paneth cells capable of regeneration following injury. Our data suggested that the lack of extracellular Wnts in *Rab8a*$^{-/-}$ crypts might resemble injury-like stress that blocked Paneth cell maturation from their precursors. Importantly, despite the lack of mature Paneth cells, *Wnt3*-expressing crypt cells remained in knockout crypts, in addition to

some crypt cells ectopically expressing *Wnt3a*, suggesting that aberrant transdifferentiation might be triggered by stress induced by *Rab8a* deletion.

Intestinal stem cells adapt to Wnt perturbations

Actively cycling stem cells give rise to different populations of daughter cells that contribute to tissue function in steady state conditions. Upon tissue injury or stress these stem cells are capable of self-renewing and undergo differentiation to regenerate the entire tissue. Regenerative medicine takes advantage of this property of stem cells to use them as therapeutic targets and rescue deteriorated organ function due to aging, disease or birth defects. This could be achieved by majorly two ways that are reviewed in (Lane et al., 2014). Firstly, transplanting healthy adult stem/differentiated cells to diseased organ. For instance, surgical transplantation of epidermal or corneal cells to burnt areas helps repair burn injuries. Hematopoietic stem cell transplantation has several applications in therapy including treatment of Thalassemia or restoration of immune/hematopoietic system of cancer patients after chemotherapy. An alternate approach is to manipulate the stem cell niche components. For instance, bone marrow failure could be treated by thrombopoietin mimetics, a secreted growth factor.

Preclinical studies are trying to explore the potential of adult stem cells by mimicking tissue injury and investigating the response of adult stem cells in injured areas. Fast replenishment by resident adult stem cells makes intestine a fine model to study tissue regeneration. Studies have shown, for instance, $Dll1^{+}$ secretory progenitor cells are capable of de-differentiating and giving rise to entire hierarchy of daughter

cells in intestine (van Es et al., 2012b). Similarly, quantitative loss of $Lgr5^+$ actively cycling stem cells leads to activation of "reserve pool" of stem cells that regenerates the intestinal tissue epithelia (Tian et al., 2011). We also see an expansion of $Hopx^+$ cells when Rab8a is deleted from intestinal tissue. These mechanisms to cope-up loss of intestinal stem cells must have arisen to support function of vital organs/tissue and ultimately the survivability of animals. Our study portrays an excellent example of how stem cell activity drives organ function that ultimately helps animals survive natural selection.

This study provided us an opportunity to examine intestinal stem cell response to perturbed niche Wnt signal. Firstly, Rab8a deficiency reduced roughly 80% of Wnt secretion. Cells might respond to this by increasing their sensitivity to the ligand. This was indeed observed in *Rab8a*$^{-/-}$ MEFs. Second, LRC secretory precursors express both Lgr5 and Paneth cell gene signatures, and contribute to epithelial regeneration upon tissue injury (Buczacki et al., 2013). We found a clear blockage of Paneth cell maturation and an increased $Lgr5^+$ cell number in *Rab8a*$^{-/-}$ crypts. These increased *Rab8a*$^{-/-}$ $Lgr5^+$ cells are certainly different from typical CBCs in healthy animals, and might reflect Paneth cell precursors, as they could express Paneth cell genes as shown in previous studies. Third, the debatable quiescent crypt cells, in particular the $Bmi1^+$ ones, have been shown resistant to Wnt perturbation and capable of converting into $Lgr5^+$ cells (Tian et al., 2011; Yan et al., 2012). *Rab8a*$^{-/-}$ crypts also contained more $Hopx^+$ cells in addition to increased $Lgr5^+$ cells, collectively suggesting a certain degree of crypt cell repopulation in response to Wnt depletion in ISC niche.

Although intestinal crypt-villus damages were induced in extreme Wnt-perturbation models exemplified by Dickkopf homolog 1 (Dkk1) overexpression (Kuhnert et al., 2004; Pinto et al., 2003) and *Tcf4*$^{-/-}$ mice (van de Wetering et al., 2002), removal of Wnt production from a number of Wnt-producing sources has so far been insufficient to perturb crypt stem cells (Farin et al., 2012; Kabiri et al., 2014; San Roman et al., 2014) which is also consistently observed in several *Gpr177* knockout mice included in this study. Factors contributing to intestinal regenerative abilities may arise from multiple reasons. Injury-induced apoptotic cells have been shown to be a source of Wnt3 to support regeneration (Galliot, 2013). Autocrine Wnts by adult stem cells may constitute their self-niche for renewal (Lim et al., 2013). Finally, crypt cells insensitive to either R-Spondin or Dkk1 may exist to replenish the epithelia (Yan et al., 2012), presumably in Wnt-independent fashion. Given the fact that vast majority of colon cancer cells contain constitutively active Wnt pathway thereby do not rely on external Wnts, it is not entirely surprising to observe strong cell resilience to Wnt ligand perturbation. Cell lineage analysis may help better understand the exact molecular features of *Rab8a* deficient crypt cells. Whether Gpr177 regulates Wnt secretion in intestinal stem cells in addition to Paneth cells, as it does in other organs (Jiang et al., 2013; Stefater et al., 2011), requires further studies. Thus, *Rab8a* deletion induced epithelial stress that provokes crypt cell alteration. We conclude that Rab8a affects Wnt secretion and Paneth cell maturation at the intestinal stem cell niche.

Synergistic effect of Rab8a and Gpr177 functions maintain organoid growth

Since *Rab8a* and *Gpr177* were deleted in the entire intestinal epithelium (including Paneth and stem cells), we cannot distinguish whether the growth defects observed in *Rab8a*$^{-/-}$ and *Gpr177*$^{-/-}$ organoids were due to non-functional Paneth cells or stem cells. To determine if Rab8a/Gpr177 dependent Wnt secretion has a direct effect on organoid survivability via stem cells (not via Paneth cells), it is necessary to isolate and culture single Lgr5^{+} stem cells from each knockout. If *Rab8a*$^{-/-}$ or *Gpr177*$^{-/-}$ single Lgr5^{+} stem cells are able to grow into organoids in presence of exogenous Wnt support, the growth defects demonstrated by *Rab8a*$^{-/-}$ or *Gpr177*$^{-/-}$ organoid cultures could be accounted to nonfunctional stem cells in these knockout intestines.

Loss of *Rab8a* and *Gpr177* led to reduced Wnt secretion but demonstrate very different consequences in vivo. *Rab8a* deletion in intestine elicits an obvious negative effect on Paneth cell number but results in increase in proliferative Lgr5^{+} compartment of intestine. *Gpr177* deletion in intestine however demonstrates a less severe Paneth cell phenotype and mild reduction in number of *Olfm4*$^{+}$ cells. Despite of tolerance to intestinal loss of *Rab8a* and *Gpr177* in vivo, *Rab8a*$^{-/-}$ and *Gpr177*$^{-/-}$ organoids showed reduced growth and survivability in culture. Interestingly, unlike *Rab8a* null organoids that showed ~50% rescue in survivability in response to Wnt3a supplement, *Gpr177* null organoids responded minimally to Wnt3a supplement of same concentration by showing only 3% survival. This indicates a clear difference in contribution of Rab8a and Gpr177 in maintenance of organoids ex vivo. This difference can be explained by the fact that *Rab8a*$^{-/-}$ Paneth cells still express Gpr177 protein. We postulate that this residual Gpr177 maintains 30% of *Rab8a*$^{-/-}$ organoids in vitro. In addition to the Gpr177

mediated Wnt secretion by *Rab8a*$^{-/-}$ Paneth cells, exogenous treatment of Wnt3a helps *Rab8a*$^{-/-}$ stem and its niche cells reach a "threshold" Wnt signaling sufficient to recover their function- as reflected by improved growth and survival. In contrast to Rab8a, Gpr177 function is absolutely necessary for all-Wnt secretion without which the stem and niche cells are unable to induce Wnt pathway to a minimal threshold even upon addition of Wnt3a. Secondly, given the hypersensitivity towards Wnt3a protein, lower concentrations of Wnt3a in media might be sufficient to activate Wnt pathway in *Rab8a*$^{-/-}$ cells. Thus it will also be interesting to analyze receptor/co-receptor activity in *Gpr177*$^{-/-}$ cells. Normal or reduced receptor activity may lead to non-responsiveness of *Gpr177*$^{-/-}$ organoids to exogenous Wnt3a.

Unlike Rab8a, Gpr177 is a unique transporter for all Wnt ligands. Hence, as expected we observed a greater impact of loss of *Gpr177* on crypt survivability as compared to loss of *Rab8a* only. Our data show that Rab8a and Gpr177 are present in the same protein complex and potentially work together to secrete Wnt proteins. However based on our results from Wnt3a-Gluc secretion assay and organoid survival assay, there exists a clear difference in contribution of each protein towards this function- a higher contribution of Gpr177 compared to Rab8a. We thus speculate that function of each of these proteins probably composes a separate tier of regulation that Wnt proteins go through, to be successfully secreted by a cell- Gpr177 responding to upstream signaling trigger(s) and Rab8a directing mechanics of vesicular trafficking.

Conclusion

Under homeostatic conditions, such as observed in vivo, crypt number changes insignificantly. However, crypt culture occurs under non-homeostatic conditions where constant budding process involves exponential amplification of stem and its niche cells. Under ex vivo conditions, when isolated from intestines, *Rab8a*$^{-/-}$ or *Gpr177*$^{-/-}$ crypts are unable to support establishment and maintenance of three dimensional organoid structures. Thus our data suggest that both *Rab8a* and *Gpr177* are essential for clonogenic activity of stem cells ex vivo. Additionally live mice, under steady-state conditions, are tolerant to intestinal loss of function of Rab8a and Gpr177.

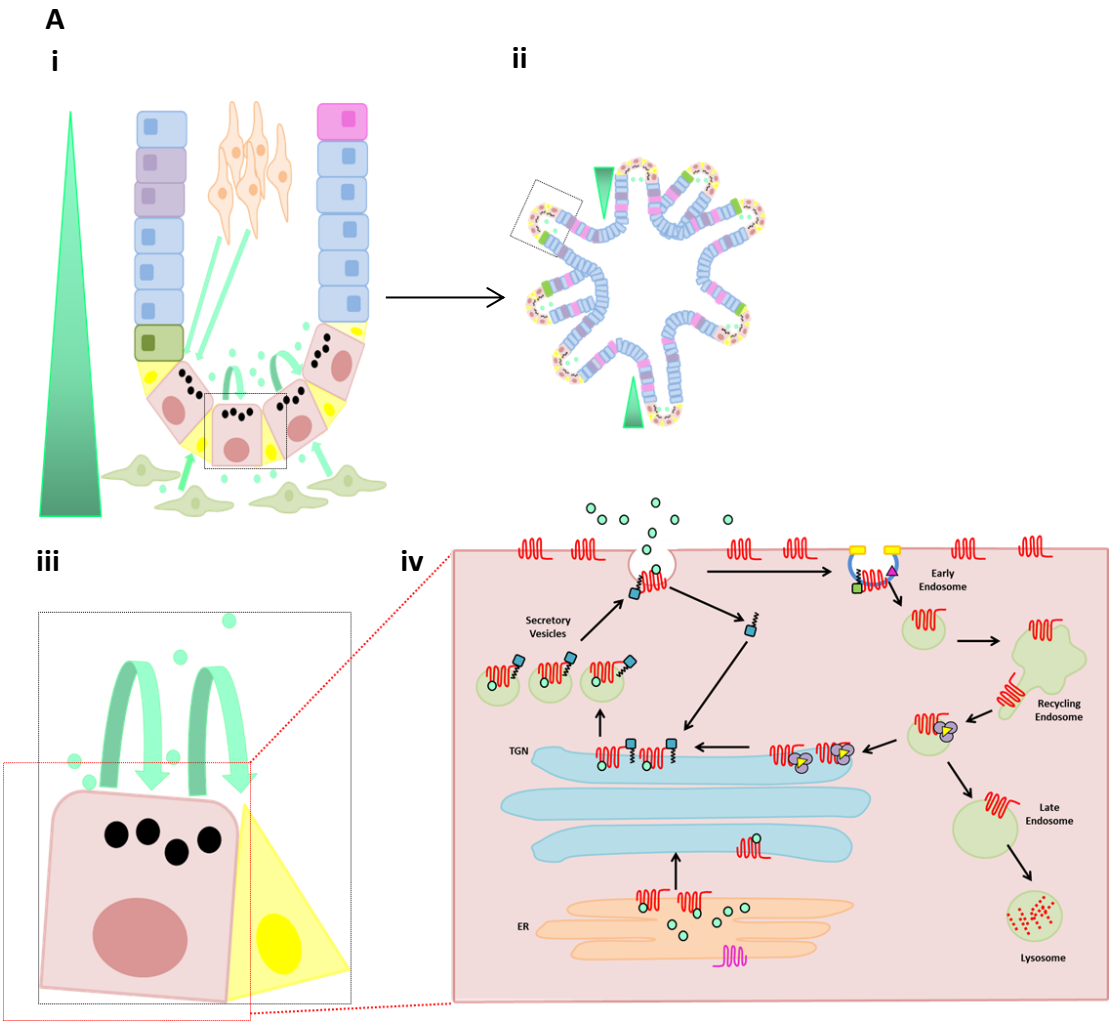
A
i
ii
iii
iv
Secretory Vesicles
Early Endosome
Recycling Endosome
TGN
Late Endosome
ER
Lysosome

B

i **ii**

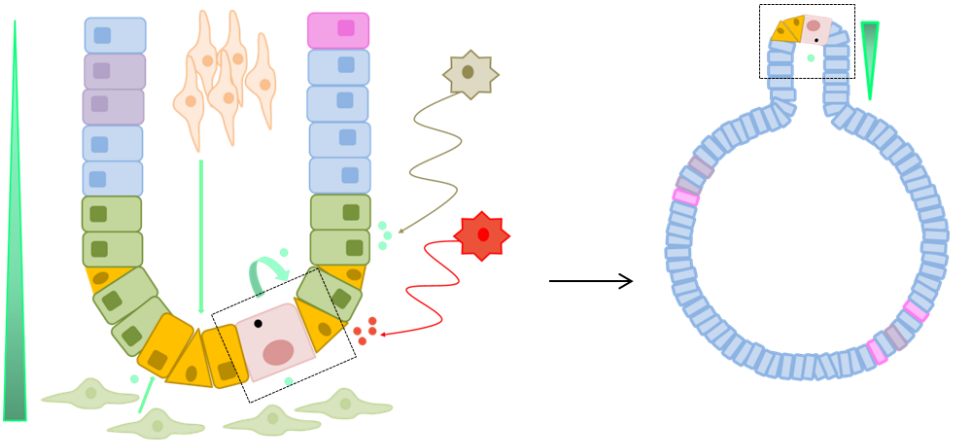

iii **iv**

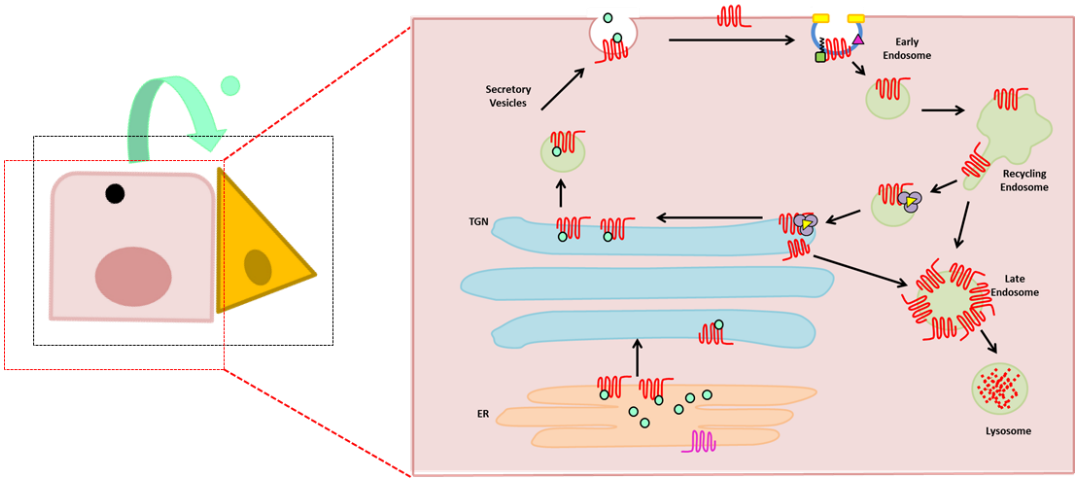
Early
Endosome
Secretory
Vesicles
Recycling
Endosome
TGN
Late
Endosome
ER
Lysosome

C

i

ii

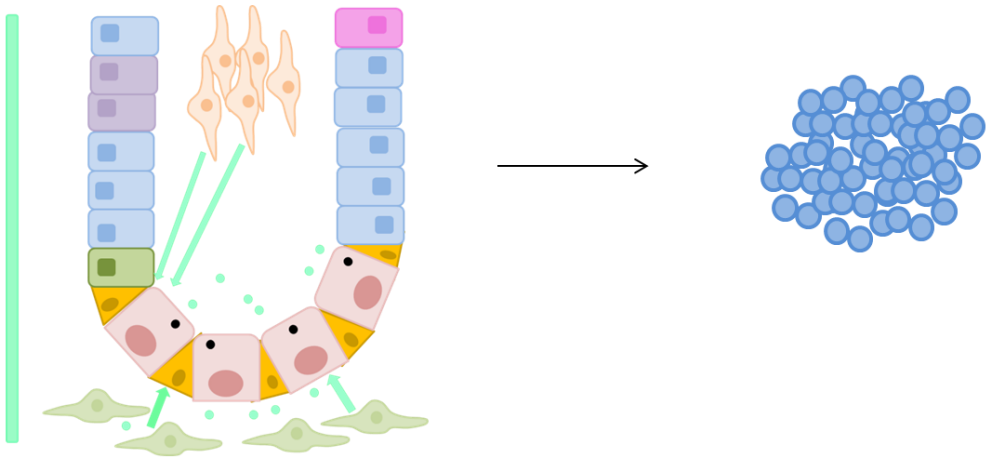

iii

iv

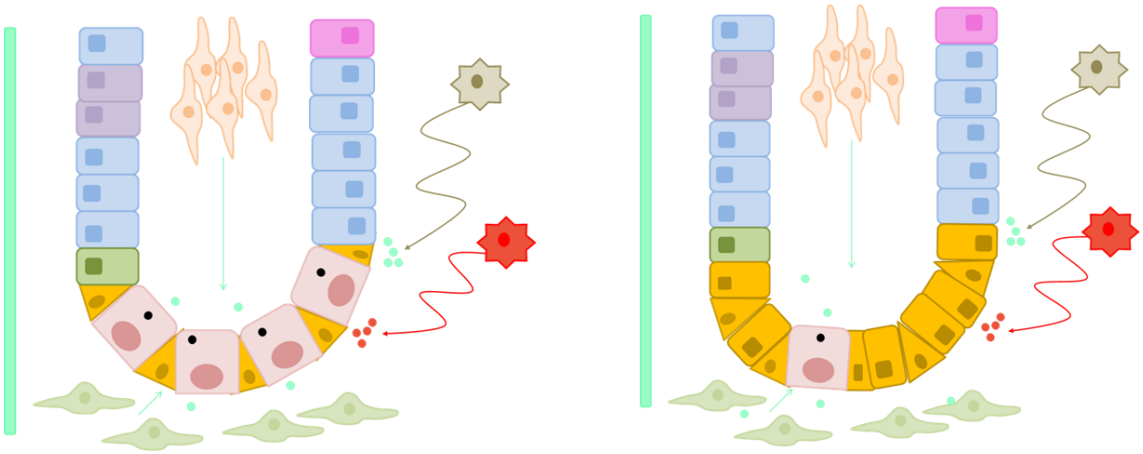


Sub-epithelial fibroblasts
Fibroblasts in lamina propria
Paneth cell
Stem cell
+4 cell
and
Stem cells with reduced clonogenicity
Dead cell
Wnt pathway inducing (Wnt or non-Wnt) ligands
Enteroendocrine cells
Goblet cell
Eneterocyte
Paneth cell with reduced Wnt secreting ablities
and
Growth factors secreting cells (of unknown origin)
Gpr177
Wnt
Rab8a
Rab5
Porcupine
Dynamin
AP2
Retromer complex
Degraded Gpr177
Clathrin

Figure 28: (Summary and proposed working model) Rab8a and Gpr177 are important for anterograde transport of Wnt ligands in intestinal stem cell niche

A. In vivo, Wnt (**green**) exists as a gradient, the major sources being Paneth cells and extra-epithelial fibroblasts closest to the crypt bottom (**i, iii**). Ex vivo, Wnt from Paneth cells are the major contributor to stem cell niche (**ii, iii**). Wnts secreted by Paneth cells are utilized by themselves and the stem cells (Black boxed area from **i** and **ii** are shown in **iii**). **(iv)** Wnt ligands and Gpr177 are synthesized and post-translationally modified by Porcupine in the ER, facilitating binding of Wnt to Gpr177. Gpr177 then transports Wnt ligands from ER to Golgi from where with help of Rab8a, Wnt ligands reach plasma membrane. Upon release of Wnt ligands into extra-cellular space, Gpr177 is retrieved from the plasma membrane by endocytosis mediated by Dynamin, AP2, Clathrin and Rab5. Later, Gpr177 is directed to Golgi in a retromer dependent manner for yet another cycle of Wnt secretion. During this process, a small fraction of Gpr177 pool is degraded in lysosome.

B. In global absence of Rab8a, in vivo, Paneth cell number and ultra-structure is significantly affected (**i**). Additionally we observe reduced Wnt gradient (**green, i, ii, iii**). Despite of this, an expansion of $Lgr5^{+}$, $Bmi1^{+}$ and $Hopx^{+}$ epithelial cell compartment is observed which might not represent typical stem cell population(s) as they were unable to support the crypt growth and survival ex vivo (**i, ii**). We propose that the composition of ISC niche might have been altered in these mice (**i**). In live animals epithelial or non-

epithelial intestinal cells of unknown origin may provide typical Wnt/non-Wnt ligands to support tissue homeostasis which is lost in culture conditions. At cellular level, absence of Rab8a reduces Gpr177 mediated Wnt secretion to the plasma membrane, instead, Gpr177 is somehow mis-targeted to lysosomal compartments (**iv**).

C. i and **ii** represent *Gpr177$^{L/-}$; Villincre* mouse intestines. **iii** and **iv** *represent Gpr177$^{L/-}$; Villincre; SMAcreERT2* (TAM+2 days) and *Gpr177$^{L/-}$; Villincre; Taglncre* mouse intestines respectively. In absence of Gpr177 in intestinal epithelium, other potential non-Paneth cell sources of Wnt maintain the stem cells (**green, i**) and the gradient of Wnt is most likely affected. Gpr177 mediated Wnt secretion by Paneth cell is essential for maintenance of ISCs in absence of mucosal Wnts (**ii**). Acute loss of Gpr177 has no effect on number of Paneth or stem cells in adult mice probably because of other unknown sources of Wnt or compensatory stem cell niche signals (**iii**). Interestingly, absence of Gpr177 from both intestinal epithelium and mucosa at an early embryonic state affected number of Lysozyme^{+} Paneth cells and *Olfm4*$^{+}$ epithelial cells in vivo, a phenotype that resembles *Rab8a* global knockout mouse intestine (**iv**) and most likely follows similar adaptation strategies in live animals. Both *Gpr177$^{L/-}$; Villincre; SMAcreERT2* (TAM+2 days) and *Gpr177$^{L/-}$; Villincre; Taglncre* mouse intestines most likely demonstrate reduced Wnt gradient (**green**).

Bibliography

Andreu, P., Peignon, G., Slomianny, C., Taketo, M.M., Colnot, S., Robine, S., Lamarque, D., Laurent-Puig, P., Perret, C., and Romagnolo, B. (2008). A genetic study of the role of the Wnt/beta-catenin signalling in Paneth cell differentiation. Dev Biol *324*, 288-296.

Ang, A.L., Folsch, H., Koivisto, U.M., Pypaert, M., and Mellman, I. (2003). The Rab8 GTPase selectively regulates AP-1B-dependent basolateral transport in polarized Madin-Darby canine kidney cells. The Journal of cell biology *163*, 339-350.

Angers, S., and Moon, R.T. (2009). Proximal events in Wnt signal transduction. Nature reviews Molecular cell biology *10*, 468-477.

Attar, N., and Cullen, P.J. (2010). The retromer complex. Adv Enzyme Regul *50*, 216-236.

Banziger, C., Soldini, D., Schutt, C., Zipperlen, P., Hausmann, G., and Basler, K. (2006). Wntless, a conserved membrane protein dedicated to the secretion of Wnt proteins from signaling cells. Cell *125*, 509-522.

Barker, N., van Es, J.H., Kuipers, J., Kujala, P., van den Born, M., Cozijnsen, M., Haegebarth, A., Korving, J., Begthel, H., Peters, P.J.*, et al.* (2007). Identification of stem cells in small intestine and colon by marker gene Lgr5. Nature *449*, 1003-1007.

Barrott, J.J., Cash, G.M., Smith, A.P., Barrow, J.R., and Murtaugh, L.C. (2011). Deletion of mouse Porcn blocks Wnt ligand secretion and reveals an ectodermal etiology of human focal dermal hypoplasia/Goltz syndrome. Proc Natl Acad Sci U S A *108*, 12752-12757.

Bartscherer, K., Pelte, N., Ingelfinger, D., and Boutros, M. (2006). Secretion of Wnt ligands requires Evi, a conserved transmembrane protein. Cell *125*, 523-533.

Belenkaya, T.Y., Wu, Y., Tang, X., Zhou, B., Cheng, L., Sharma, Y.V., Yan, D., Selva, E.M., and Lin, X. (2008). The retromer complex influences Wnt secretion by recycling wntless from endosomes to the trans-Golgi network. Dev Cell *14*, 120-131.

Bilic, J., Huang, Y.L., Davidson, G., Zimmermann, T., Cruciat, C.M., Bienz, M., and Niehrs, C. (2007). Wnt induces LRP6 signalosomes and promotes dishevelled-dependent LRP6 phosphorylation. Science *316*, 1619-1622.

Boehlke, C., Bashkurov, M., Buescher, A., Krick, T., John, A.K., Nitschke, R., Walz, G., and Kuehn, E.W. (2010). Differential role of Rab proteins in ciliary trafficking: Rab23 regulates smoothened levels. J Cell Sci *123*, 1460-1467.

Brault, V., Moore, R., Kutsch, S., Ishibashi, M., Rowitch, D.H., McMahon, A.P., Sommer, L., Boussadia, O., and Kemler, R. (2001). Inactivation of the beta-catenin gene by Wnt1-Cre-mediated deletion results in dramatic brain malformation and failure of craniofacial development. Development *128*, 1253-1264.

Bryant, D.M., Datta, A., Rodriguez-Fraticelli, A.E., Peranen, J., Martin-Belmonte, F., and Mostov, K.E. (2010). A molecular network for de novo generation of the apical surface and lumen. Nat Cell Biol *12*, 1035-1045.

Buczacki, S.J., Zecchini, H.I., Nicholson, A.M., Russell, R., Vermeulen, L., Kemp, R., and Winton, D.J. (2013). Intestinal label-retaining cells are secretory precursors expressing Lgr5. Nature *495*, 65-69.

Burton, J.L., Burns, M.E., Gatti, E., Augustine, G.J., and De Camilli, P. (1994). Specific interactions of Mss4 with members of the Rab GTPase subfamily. Embo J *13*, 5547-5558.

Cadigan, K.M., and Peifer, M. (2009). Wnt signaling from development to disease: insights from model systems. Cold Spring Harb Perspect Biol *1*, a002881.

Cancer Genome Atlas, N. (2012). Comprehensive molecular characterization of human colon and rectal cancer. Nature *487*, 330-337.

Carlton, J., Bujny, M., Peter, B.J., Oorschot, V.M., Rutherford, A., Mellor, H., Klumperman, J., McMahon, H.T., and Cullen, P.J. (2004). Sorting nexin-1 mediates tubular endosome-to-TGN transport through coincidence sensing of high- curvature membranes and 3-phosphoinositides. Current biology : CB *14*, 1791-1800.

Carlton, J.G., Bujny, M.V., Peter, B.J., Oorschot, V.M., Rutherford, A., Arkell, R.S., Klumperman, J., McMahon, H.T., and Cullen, P.J. (2005). Sorting nexin-2 is associated with tubular elements of the early endosome, but is not essential for retromer-mediated endosome-to-TGN transport. J Cell Sci *118*, 4527-4539.

Carpenter, A.C., Rao, S., Wells, J.M., Campbell, K., and Lang, R.A. (2010). Generation of mice with a conditional null allele for Wntless. Genesis *48*, 554-558.

Chabrillat, M.L., Wilhelm, C., Wasmeier, C., Sviderskaya, E.V., Louvard, D., and Coudrier, E. (2005). Rab8 regulates the actin-based movement of melanosomes. Molecular biology of the cell *16*, 1640-1650.

Chakraborty, A.K., Funasaka, Y., Araki, K., Horikawa, T., and Ichihashi, M. (2003). Evidence that the small GTPase Rab8 is involved in melanosome traffic and dendrite extension in B16 melanoma cells. Cell and tissue research *314*, 381-388.

Charng, W.L., Yamamoto, S., Jaiswal, M., Bayat, V., Xiong, B., Zhang, K., Sandoval, H., David, G., Gibbs, S., Lu, H.C.*, et al.* (2014). Drosophila Tempura, a novel protein prenyltransferase alpha subunit, regulates notch signaling via Rab1 and Rab11. PLoS biology *12*, e1001777.

Chen, B., Dodge, M.E., Tang, W., Lu, J., Ma, Z., Fan, C.W., Wei, S., Hao, W., Kilgore, J., Williams, N.S.*, et al.* (2009). Small molecule-mediated disruption of Wnt-dependent signaling in tissue regeneration and cancer. Nature chemical biology *5*, 100-107.

Chi, S., Xie, G., Liu, H., Chen, K., Zhang, X., Li, C., and Xie, J. (2012). Rab23 negatively regulates Gli1 transcriptional factor in a Su(Fu)-dependent manner. Cellular signalling *24*, 1222-1228.

Clarke, A.R. (2006). Wnt signalling in the mouse intestine. Oncogene *25*, 7512-7521.

Clevers, H. (2006). Wnt/beta-catenin signaling in development and disease. Cell *127*, 469-480.

Clevers, H., Loh, K.M., and Nusse, R. (2014). Stem cell signaling. An integral program for tissue renewal and regeneration: Wnt signaling and stem cell control. Science *346*, 1248012.

Clevers, H., and Nusse, R. (2012). Wnt/β-catenin signaling and disease. Cell *149*, 1192-1205.

Coombs, G.S., Yu, J., Canning, C.A., Veltri, C.A., Covey, T.M., Cheong, J.K., Utomo, V., Banerjee, N., Zhang, Z.H., Jadulco, R.C.*, et al.* (2010). WLS-dependent secretion of WNT3A requires Ser209 acylation and vacuolar acidification. J Cell Sci *123*, 3357-3367.

Crosnier, C., Stamataki, D., and Lewis, J. (2006). Organizing cell renewal in the intestine: stem cells, signals and combinatorial control. Nature reviews Genetics *7*, 349-359.

Das, A., and Guo, W. (2011). Rabs and the exocyst in ciliogenesis, tubulogenesis and beyond. Trends in cell biology *21*, 383-386.

Das, S., Yu, S., Sakamori, R., Stypulkowski, E., and Gao, N. (2012). Wntless in Wnt secretion: molecular, cellular and genetic aspects. Front Biol (Beijing) *7*, 587-593.

Das, S., Yu, S., Sakamori, R., Vedula, P., Feng, Q., Flores, J., Hoffman, A., Fu, J., Stypulkowski, E., Rodriguez, A.*, et al.* (2015). Rab8a vesicles regulate Wnt ligand delivery and Paneth cell maturation at the intestinal stem cell niche. Development *142*, 2147-2162.

de Groot, R.E., Farin, H.F., Macurkova, M., van Es, J.H., Clevers, H.C., and Korswagen, H.C. (2013). Retromer dependent recycling of the Wnt secretion factor Wls is dispensable for stem cell maintenance in the mammalian intestinal epithelium. PLoS One *8*, e76971.

de Lau, W., Barker, N., and Clevers, H. (2007). WNT signaling in the normal intestine and colorectal cancer. Front Biosci *12*, 471-491.

del Toro, D., Alberch, J., Lazaro-Dieguez, F., Martin-Ibanez, R., Xifro, X., Egea, G., and Canals, J.M. (2009). Mutant huntingtin impairs post-Golgi trafficking to lysosomes by delocalizing optineurin/Rab8 complex from the Golgi apparatus. Molecular biology of the cell *20*, 1478-1492.

Demir, K., Kirsch, N., Beretta, C.A., Erdmann, G., Ingelfinger, D., Moro, E., Argenton, F., Carl, M., Niehrs, C., and Boutros, M. (2013). RAB8B is required for activity and caveolar endocytosis of LRP6. Cell reports *4*, 1224-1234.

Deretic, D., Huber, L.A., Ransom, N., Mancini, M., Simons, K., and Papermaster, D.S. (1995). rab8 in retinal photoreceptors may participate in rhodopsin transport and in rod outer segment disk morphogenesis. J Cell Sci *108 (Pt 1)*, 215-224.

Dong, C., Yang, L., Zhang, X., Gu, H., Lam, M.L., Claycomb, W.C., Xia, H., and Wu, G. (2010). Rab8 interacts with distinct motifs in alpha2B- and beta2-adrenergic receptors and differentially modulates their transport. J Biol Chem *285*, 20369-20380.

Durand, A., Donahue, B., Peignon, G., Letourneur, F., Cagnard, N., Slomianny, C., Perret, C., Shroyer, N.F., and Romagnolo, B. (2012). Functional intestinal stem cells after Paneth cell ablation induced by the loss of transcription factor Math1 (Atoh1). Proc Natl Acad Sci U S A *109*, 8965-8970.

Eaton, S. (2008). Retromer retrieves wntless. Dev Cell *14*, 4-6.

Eggenschwiler, J.T., Espinoza, E., and Anderson, K.V. (2001). Rab23 is an essential negative regulator of the mouse Sonic hedgehog signalling pathway. Nature *412*, 194-198.

Emery, G., Hutterer, A., Berdnik, D., Mayer, B., Wirtz-Peitz, F., Gaitan, M.G., and Knoblich, J.A. (2005). Asymmetric Rab 11 endosomes regulate delta recycling and specify cell fate in the Drosophila nervous system. Cell *122*, 763-773.

Esseltine, J.L., Ribeiro, F.M., and Ferguson, S.S. (2012). Rab8 modulates metabotropic glutamate receptor subtype 1 intracellular trafficking and signaling in a protein kinase C-dependent manner. J Neurosci *32*, 16933-16942a.

Evans, T.M., Ferguson, C., Wainwright, B.J., Parton, R.G., and Wicking, C. (2003). Rab23, a negative regulator of hedgehog signaling, localizes to the plasma membrane and the endocytic pathway. Traffic *4*, 869-884.

Farin, H.F., Van Es, J.H., and Clevers, H. (2012). Redundant sources of Wnt regulate intestinal stem cells and promote formation of Paneth cells. Gastroenterology *143*, 1518-1529 e1517.

Feng, Q., and Gao, N. (2014). Keeping Wnt Signalosome in Check by Vesicular Traffic. J Cell Physiol.

Feng, S., Knodler, A., Ren, J., Zhang, J., Zhang, X., Hong, Y., Huang, S., Peranen, J., and Guo, W. (2012). A Rab8 guanine nucleotide exchange factor-effector interaction network regulates primary ciliogenesis. J Biol Chem *287*, 15602-15609.

Fevr, T., Robine, S., Louvard, D., and Huelsken, J. (2007). Wnt/beta-catenin is essential for intestinal homeostasis and maintenance of intestinal stem cells. Molecular and cellular biology *27*, 7551-7559.

Franch-Marro, X., Wendler, F., Griffith, J., Maurice, M.M., and Vincent, J.P. (2008). In vivo role of lipid adducts on Wingless. J Cell Sci *121*, 1587-1592.

Fre, S., Huyghe, M., Mourikis, P., Robine, S., Louvard, D., and Artavanis-Tsakonas, S. (2005). Notch signals control the fate of immature progenitor cells in the intestine. Nature *435*, 964-968.

Fu, J., Ivy Yu, H.M., Maruyama, T., Mirando, A.J., and Hsu, W. (2011). Gpr177/mouse Wntless is essential for Wnt-mediated craniofacial and brain development. Developmental dynamics : an official publication of the American Association of Anatomists *240*, 365-371.

Fu, J., Jiang, M., Mirando, A.J., Yu, H.M., and Hsu, W. (2009). Reciprocal regulation of Wnt and Gpr177/mouse Wntless is required for embryonic axis formation. Proc Natl Acad Sci U S A *106*, 18598-18603.

Galli, L.M., Barnes, T.L., Secrest, S.S., Kadowaki, T., and Burrus, L.W. (2007). Porcupine-mediated lipid-modification regulates the activity and distribution of Wnt proteins in the chick neural tube. Development *134*, 3339-3348.

Galliot, B. (2013). Injury-induced asymmetric cell death as a driving force for head regeneration in Hydra. Dev Genes Evol *223*, 39-52.

Gao, N., and Kaestner, K.H. (2010). Cdx2 regulates endo-lysosomal function and epithelial cell polarity. Genes Dev *24*, 1295-1305.

Gao, N., White, P., and Kaestner, K.H. (2009). Establishment of intestinal identity and epithelial-mesenchymal signaling by Cdx2. Dev Cell *16*, 588-599.

Gao, N., Zhang, J., Rao, M.A., Case, T.C., Mirosevich, J., Wang, Y., Jin, R., Gupta, A., Rennie, P.S., and Matusik, R.J. (2003). The role of hepatocyte nuclear factor-3 alpha (Forkhead Box A1) and androgen receptor in transcriptional regulation of prostatic genes. Mol Endocrinol *17*, 1484-1507.

Gasnereau, I., Herr, P., Chia, P.Z., Basler, K., and Gleeson, P.A. (2011). Identification of an endocytosis motif in an intracellular loop of Wntless protein, essential for its recycling and the control of Wnt protein signaling. J Biol Chem *286*, 43324-43333.

Gerges, N.Z., Backos, D.S., and Esteban, J.A. (2004). Local control of AMPA receptor trafficking at the postsynaptic terminal by a small GTPase of the Rab family. J Biol Chem *279*, 43870-43878.

Goel, S., Chin, E.N., Fakhraldeen, S.A., Berry, S.M., Beebe, D.J., and Alexander, C.M. (2012). Both LRP5 and LRP6 receptors are required to respond to physiological Wnt ligands in mammary epithelial cells and fibroblasts. J Biol Chem *287*, 16454-16466.

Goldenring, J.R. (2013). A central role for vesicle trafficking in epithelial neoplasia: intracellular highways to carcinogenesis. Nat Rev Cancer *13*, 813-820.

Goodman, R.M., Thombre, S., Firtina, Z., Gray, D., Betts, D., Roebuck, J., Spana, E.P., and Selva, E.M. (2006). Sprinter: a novel transmembrane protein required for Wg secretion and signaling. Development *133*, 4901-4911.

Gregorieff, A., and Clevers, H. (2005). Wnt signaling in the intestinal epithelium: from endoderm to cancer. Genes Dev *19*, 877-890.

Gregorieff, A., and Clevers, H. (2010). In situ hybridization to identify gut stem cells. Current protocols in stem cell biology *Chapter 2*, Unit 2F 1.

Gregorieff, A., Pinto, D., Begthel, H., Destree, O., Kielman, M., and Clevers, H. (2005). Expression pattern of Wnt signaling components in the adult intestine. Gastroenterology *129*, 626-638.

Haegebarth, A., and Clevers, H. (2009). Wnt signaling, lgr5, and stem cells in the intestine and skin. The American journal of pathology *174*, 715-721.

Haramis, A.P., Begthel, H., van den Born, M., van Es, J., Jonkheer, S., Offerhaus, G.J., and Clevers, H. (2004). De novo crypt formation and juvenile polyposis on BMP inhibition in mouse intestine. Science *303*, 1684-1686.

Harterink, M., Port, F., Lorenowicz, M.J., McGough, I.J., Silhankova, M., Betist, M.C., van Weering, J.R., van Heesbeen, R.G., Middelkoop, T.C., Basler, K.*, et al.* (2011). A SNX3-dependent retromer pathway mediates retrograde transport of the Wnt sorting receptor Wntless and is required for Wnt secretion. Nat Cell Biol *13*, 914-923.

Hattula, K., Furuhjelm, J., Arffman, A., and Peranen, J. (2002). A Rab8-specific GDP/GTP exchange factor is involved in actin remodeling and polarized membrane transport. Molecular biology of the cell *13*, 3268-3280.

Hattula, K., Furuhjelm, J., Tikkanen, J., Tanhuanpaa, K., Laakkonen, P., and Peranen, J. (2006). Characterization of the Rab8-specific membrane traffic route linked to protrusion formation. J Cell Sci *119*, 4866-4877.

Hattula, K., and Peranen, J. (2000). FIP-2, a coiled-coil protein, links Huntingtin to Rab8 and modulates cellular morphogenesis. Current biology : CB *10*, 1603-1606.

Haubruck, H., Engelke, U., Mertins, P., and Gallwitz, D. (1990). Structural and functional analysis of ypt2, an essential ras-related gene in the fission yeast Schizosaccharomyces pombe encoding a Sec4 protein homologue. Embo J *9*, 1957-1962.

He, X., Saint-Jeannet, J.P., Wang, Y., Nathans, J., Dawid, I., and Varmus, H. (1997). A member of the Frizzled protein family mediating axis induction by Wnt-5A. Science *275*, 1652-1654.

He, X.C., Zhang, J., Tong, W.G., Tawfik, O., Ross, J., Scoville, D.H., Tian, Q., Zeng, X., He, X., Wiedemann, L.M.*, et al.* (2004). BMP signaling inhibits intestinal stem cell self-renewal through suppression of Wnt-beta-catenin signaling. Nat Genet *36*, 1117-1121.

Henry, L., and Sheff, D.R. (2008). Rab8 regulates basolateral secretory, but not recycling, traffic at the recycling endosome. Molecular biology of the cell *19*, 2059-2068.

Hsiao, Y.C., Tong, Z.J., Westfall, J.E., Ault, J.G., Page-McCaw, P.S., and Ferland, R.J. (2009). Ahi1, whose human ortholog is mutated in Joubert syndrome, is required for Rab8a localization, ciliogenesis and vesicle trafficking. Human molecular genetics *18*, 3926-3941.

Huang, H., and He, X. (2008). Wnt/beta-catenin signaling: new (and old) players and new insights. Curr Opin Cell Biol *20*, 119-125.

Huber, L.A., de Hoop, M.J., Dupree, P., Zerial, M., Simons, K., and Dotti, C. (1993a). Protein transport to the dendritic plasma membrane of cultured neurons is regulated by rab8p. The Journal of cell biology *123*, 47-55.

Huber, L.A., Dupree, P., and Dotti, C.G. (1995). A deficiency of the small GTPase rab8 inhibits membrane traffic in developing neurons. Molecular and cellular biology *15*, 918-924.

Huber, L.A., Pimplikar, S., Parton, R.G., Virta, H., Zerial, M., and Simons, K. (1993b). Rab8, a small GTPase involved in vesicular traffic between the TGN and the basolateral plasma membrane. The Journal of cell biology *123*, 35-45.

Hume, A.N., Collinson, L.M., Rapak, A., Gomes, A.Q., Hopkins, C.R., and Seabra, M.C. (2001). Rab27a regulates the peripheral distribution of melanosomes in melanocytes. The Journal of cell biology *152*, 795-808.

Hutagalung, A.H., and Novick, P.J. (2011). Role of Rab GTPases in membrane traffic and cell physiology. Physiological reviews *91*, 119-149.

Ikeya, M., Lee, S.M., Johnson, J.E., McMahon, A.P., and Takada, S. (1997). Wnt signalling required for expansion of neural crest and CNS progenitors. Nature *389*, 966-970.

Jiang, M., Ku, W.Y., Fu, J., Offermanns, S., Hsu, W., and Que, J. (2013). Gpr177 regulates pulmonary vasculature development. Development *140*, 3589-3594.

Jin, Y., Sultana, A., Gandhi, P., Franklin, E., Hamamoto, S., Khan, A.R., Munson, M., Schekman, R., and Weisman, L.S. (2011). Myosin V transports secretory vesicles via a Rab GTPase cascade and interaction with the exocyst complex. Dev Cell *21*, 1156-1170.

Kabiri, Z., Greicius, G., Madan, B., Biechele, S., Zhong, Z., Zaribafzadeh, H., Edison, Aliyev, J., Wu, Y., Bunte, R.*, et al.* (2014). Stroma provides an intestinal stem cell niche in the absence of epithelial Wnts. Development *141*, 2206-2215.

Karlsson, L., Lindahl, P., Heath, J.K., and Betsholtz, C. (2000). Abnormal gastrointestinal development in PDGF-A and PDGFR-(alpha) deficient mice implicates a novel mesenchymal structure with putative instructive properties in villus morphogenesis. Development *127*, 3457-3466.

Kemp, C., Willems, E., Abdo, S., Lambiv, L., and Leyns, L. (2005). Expression of all Wnt genes and their secreted antagonists during mouse blastocyst and postimplantation development. Developmental dynamics : an official publication of the American Association of Anatomists *233*, 1064-1075.

Kim, J., Krishnaswami, S.R., and Gleeson, J.G. (2008). CEP290 interacts with the centriolar satellite component PCM-1 and is required for Rab8 localization to the primary cilium. Human molecular genetics *17*, 3796-3805.

Kim, T.H., Escudero, S., and Shivdasani, R.A. (2012). Intact function of Lgr5 receptor-expressing intestinal stem cells in the absence of Paneth cells. Proc Natl Acad Sci U S A *109*, 3932-3937.

Knodler, A., Feng, S., Zhang, J., Zhang, X., Das, A., Peranen, J., and Guo, W. (2010). Coordination of Rab8 and Rab11 in primary ciliogenesis. Proc Natl Acad Sci U S A *107*, 6346-6351.

Knowles, B.C., Weis, V.G., Yu, S., Roland, J.T., Williams, J.A., Alvarado, G.S., Lapierre, L.A., Shub, M.D., Gao, N., and Goldenring, J.R. (2015). Rab11a regulates Syntaxin 3 localization and microvillus assembly in enterocytes. J Cell Sci.

Kobayashi, T., Tsang, W.Y., Li, J., Lane, W., and Dynlacht, B.D. (2011). Centriolar kinesin Kif24 interacts with CP110 to remodel microtubules and regulate ciliogenesis. Cell *145*, 914-925.

Komekado, H., Yamamoto, H., Chiba, T., and Kikuchi, A. (2007). Glycosylation and palmitoylation of Wnt-3a are coupled to produce an active form of Wnt-3a. Genes to cells : devoted to molecular & cellular mechanisms *12*, 521-534.

Korinek, V. (1997). Constitutive Transcriptional Activation by a beta -Catenin-Tcf Complex in APC-/- Colon Carcinoma. Science *275*, 1784-1787.

Korinek, V., Barker, N., Moerer, P., van Donselaar, E., Huls, G., Peters, P.J., and Clevers, H. (1998). Depletion of epithelial stem-cell compartments in the small intestine of mice lacking Tcf-4. Nat Genet *19*, 379-383.

Korkut, C., Ataman, B., Ramachandran, P., Ashley, J., Barria, R., Gherbesi, N., and Budnik, V. (2009). Trans-synaptic transmission of vesicular Wnt signals through Evi/Wntless. Cell *139*, 393-404.

Krausova, M., and Korinek, V. (2014). Wnt signaling in adult intestinal stem cells and cancer. Cellular signalling *26*, 570-579.

Kremer, J.R., Mastronarde, D.N., and McIntosh, J.R. (1996). Computer visualization of three-dimensional image data using IMOD. J Struct Biol *116*, 71-76.

Kuhnert, F., Davis, C.R., Wang, H.T., Chu, P., Lee, M., Yuan, J., Nusse, R., and Kuo, C.J. (2004). Essential requirement for Wnt signaling in proliferation of adult small

intestine and colon revealed by adenoviral expression of Dickkopf-1. Proc Natl Acad Sci U S A *101*, 266-271.

Kurayoshi, M., Yamamoto, H., Izumi, S., and Kikuchi, A. (2007). Post-translational palmitoylation and glycosylation of Wnt-5a are necessary for its signalling. Biochem J *402*, 515-523.

Lane, S.W., Williams, D.A., and Watt, F.M. (2014). Modulating the stem cell niche for tissue regeneration. Nat Biotechnol *32*, 795-803.

Lickert, H., Kispert, A., Kutsch, S., and Kemler, R. (2001). Expression patterns of Wnt genes in mouse gut development. Mechanisms of development *105*, 181-184.

Lim, X., Tan, S.H., Koh, W.L., Chau, R.M., Yan, K.S., Kuo, C.J., van Amerongen, R., Klein, A.M., and Nusse, R. (2013). Interfollicular epidermal stem cells self-renew via autocrine Wnt signaling. Science *342*, 1226-1230.

Liu, P., Wakamiya, M., Shea, M.J., Albrecht, U., Behringer, R.R., and Bradley, A. (1999). Requirement for Wnt3 in vertebrate axis formation. Nat Genet *22*, 361-365.

Logan, C.Y., and Nusse, R. (2004). The Wnt signaling pathway in development and disease. Annu Rev Cell Dev Biol *20*, 781-810.

Lustig, B., Jerchow, B., Sachs, M., Weiler, S., Pietsch, T., Karsten, U., van de Wetering, M., Clevers, H., Schlag, P.M., Birchmeier, W.*, et al.* (2002). Negative feedback loop of Wnt signaling through upregulation of conductin/axin2 in colorectal and liver tumors. Molecular and cellular biology *22*, 1184-1193.

Ma, Y., Erkner, A., Gong, R., Yao, S., Taipale, J., Basler, K., and Beachy, P.A. (2002). Hedgehog-mediated patterning of the mammalian embryo requires transporter-like function of dispatched. Cell *111*, 63-75.

MacDonald, B.T., and He, X. (2012). Frizzled and LRP5/6 receptors for Wnt/β-catenin signaling. Cold Spring Harb Perspect Biol *4*.

MacDonald, B.T., Tamai, K., and He, X. (2009). Wnt/beta-catenin signaling: components, mechanisms, and diseases. Dev Cell *17*, 9-26.

Madison, B.B., Braunstein, K., Kuizon, E., Portman, K., Qiao, X.T., and Gumucio, D.L. (2005). Epithelial hedgehog signals pattern the intestinal crypt-villus axis. Development *132*, 279-289.

Markova, S.V., Golz, S., Frank, L.A., Kalthof, B., and Vysotski, E.S. (2004). Cloning and expression of cDNA for a luciferase from the marine copepod Metridia longa. A novel secreted bioluminescent reporter enzyme. J Biol Chem *279*, 3212-3217.

Mastronarde, D.N. (2005). Automated electron microscope tomography using robust prediction of specimen movements. J Struct Biol *152*, 36-51.

McConlogue, L., Castellano, F., deWit, C., Schenk, D., and Maltese, W.A. (1996). Differential effects of a Rab6 mutant on secretory versus amyloidogenic processing of Alzheimer's beta-amyloid precursor protein. J Biol Chem *271*, 1343-1348.

McMahon, A.P., and Bradley, A. (1990). The Wnt-1 (int-1) proto-oncogene is required for development of a large region of the mouse brain. Cell *62*, 1073-1085.

Mikels, A.J., and Nusse, R. (2006). Purified Wnt5a protein activates or inhibits beta-catenin-TCF signaling depending on receptor context. PLoS biology *4*, e115.

Miyoshi, H., Ajima, R., Luo, C.T., Yamaguchi, T.P., and Stappenbeck, T.S. (2012). Wnt5a potentiates TGF-beta signaling to promote colonic crypt regeneration after tissue injury. Science *338*, 108-113.

Montgomery, R.K., Carlone, D.L., Richmond, C.A., Farilla, L., Kranendonk, M.E., Henderson, D.E., Baffour-Awuah, N.Y., Ambruzs, D.M., Fogli, L.K., Algra, S.*, et al.* (2011). Mouse telomerase reverse transcriptase (mTert) expression marks slowly cycling intestinal stem cells. Proc Natl Acad Sci U S A *108*, 179-184.

Munoz, J., Stange, D.E., Schepers, A.G., van de Wetering, M., Koo, B.K., Itzkovitz, S., Volckmann, R., Kung, K.S., Koster, J., Radulescu, S.*, et al.* (2012). The Lgr5 intestinal stem cell signature: robust expression of proposed quiescent '+4' cell markers. Embo J *31*, 3079-3091.

Murga-Zamalloa, C.A., Atkins, S.J., Peranen, J., Swaroop, A., and Khanna, H. (2010). Interaction of retinitis pigmentosa GTPase regulator (RPGR) with RAB8A GTPase: implications for cilia dysfunction and photoreceptor degeneration. Human molecular genetics *19*, 3591-3598.

Nachury, M.V., Loktev, A.V., Zhang, Q., Westlake, C.J., Peranen, J., Merdes, A., Slusarski, D.C., Scheller, R.H., Bazan, J.F., Sheffield, V.C.*, et al.* (2007). A core complex of BBS proteins cooperates with the GTPase Rab8 to promote ciliary membrane biogenesis. Cell *129*, 1201-1213.

Najdi, R., Proffitt, K., Sprowl, S., Kaur, S., Yu, J., Covey, T.M., Virshup, D.M., and Waterman, M.L. (2012). A uniform human Wnt expression library reveals a shared secretory pathway and unique signaling activities. Differentiation; research in biological diversity *84*, 203-213.

Nusse, R., Fuerer, C., Ching, W., Harnish, K., Logan, C., Zeng, A., ten Berge, D., and Kalani, Y. (2008). Wnt signaling and stem cell control. Cold Spring Harb Symp Quant Biol *73*, 59-66.

Okamoto, M., Udagawa, N., Uehara, S., Maeda, K., Yamashita, T., Nakamichi, Y., Kato, H., Saito, N., Minami, Y., Takahashi, N.*, et al.* (2014). Noncanonical Wnt5a enhances Wnt/beta-catenin signaling during osteoblastogenesis. Scientific reports *4*, 4493.

Pan, C.L., Baum, P.D., Gu, M., Jorgensen, E.M., Clark, S.G., and Garriga, G. (2008). C. elegans AP-2 and retromer control Wnt signaling by regulating mig-14/Wntless. Dev Cell *14*, 132-139.

Pinto, D., Gregorieff, A., Begthel, H., and Clevers, H. (2003). Canonical Wnt signals are essential for homeostasis of the intestinal epithelium. Genes Dev *17*, 1709-1713.

Polakis, P. (2007). The many ways of Wnt in cancer. Curr Opin Genet Dev *17*, 45-51.

Port, F., Kuster, M., Herr, P., Furger, E., Banziger, C., Hausmann, G., and Basler, K. (2008). Wingless secretion promotes and requires retromer-dependent cycling of Wntless. Nat Cell Biol *10*, 178-185.

Powell, A.E., Wang, Y., Li, Y., Poulin, E.J., Means, A.L., Washington, M.K., Higginbotham, J.N., Juchheim, A., Prasad, N., Levy, S.E.*, et al.* (2012). The pan-ErbB negative regulator Lrig1 is an intestinal stem cell marker that functions as a tumor suppressor. Cell *149*, 146-158.

Radice, G., Lee, J.J., and Costantini, F. (1991). H beta 58, an insertional mutation affecting early postimplantation development of the mouse embryo. Development *111*, 801-811.

Reya, T., and Clevers, H. (2005). Wnt signalling in stem cells and cancer. Nature *434*, 843-850.

Rezaie, T., Child, A., Hitchings, R., Brice, G., Miller, L., Coca-Prados, M., Heon, E., Krupin, T., Ritch, R., Kreutzer, D.*, et al.* (2002). Adult-onset primary open-angle glaucoma caused by mutations in optineurin. Science *295*, 1077-1079.

Rodriguez, O.C., and Cheney, R.E. (2002). Human myosin-Vc is a novel class V myosin expressed in epithelial cells. J Cell Sci *115*, 991-1004.

Roelink, H., and Nusse, R. (1991). Expression of two members of the Wnt family during mouse development--restricted temporal and spatial patterns in the developing neural tube. Genes Dev *5*, 381-388.

Rojas, R., van Vlijmen, T., Mardones, G.A., Prabhu, Y., Rojas, A.L., Mohammed, S., Heck, A.J., Raposo, G., van der Sluijs, P., and Bonifacino, J.S. (2008). Regulation of retromer recruitment to endosomes by sequential action of Rab5 and Rab7. The Journal of cell biology *183*, 513-526.

Roland, J.T., Lapierre, L.A., and Goldenring, J.R. (2009). Alternative splicing in class V myosins determines association with Rab10. J Biol Chem *284*, 1213-1223.

Romagnolo, B., Berrebi, D., Saadi-Keddoucci, S., Porteu, A., Pichard, A.L., Peuchmaur, M., Vandewalle, A., Kahn, A., and Perret, C. (1999). Intestinal dysplasia and adenoma in transgenic mice after overexpression of an activated beta-catenin. Cancer research *59*, 3875-3879.

Roth, S., Franken, P., Sacchetti, A., Kremer, A., Anderson, K., Sansom, O., and Fodde, R. (2012). Paneth cells in intestinal homeostasis and tissue injury. PLoS One *7*, e38965.

Sahlender, D.A., Roberts, R.C., Arden, S.D., Spudich, G., Taylor, M.J., Luzio, J.P., Kendrick-Jones, J., and Buss, F. (2005). Optineurin links myosin VI to the Golgi complex and is involved in Golgi organization and exocytosis. The Journal of cell biology *169*, 285-295.

Sakamori, R., Das, S., Yu, S., Feng, S., Stypulkowski, E., Guan, Y., Douard, V., Tang, W., Ferraris, R.P., Harada, A.*, et al.* (2012). Cdc42 and Rab8a are critical for intestinal stem cell division, survival, and differentiation in mice. J Clin Invest *122*, 1052-1065.

Sakamori, R., Yu, S., Zhang, X., Hoffman, A., Sun, J., Das, S., Vedula, P., Li, G., Fu, J., Walker, F.*, et al.* (2014). CDC42 Inhibition Suppresses Progression of Incipient Intestinal Tumors. Cancer research *74*, 5480-5492.

Salminen, A., and Novick, P.J. (1987). A ras-like protein is required for a post-Golgi event in yeast secretion. Cell *49*, 527-538.

San Roman, A.K., Jayewickreme, C.D., Murtaugh, L.C., and Shivdasani, R.A. (2014). Wnt secretion from epithelial cells and subepithelial myofibroblasts is not required in the mouse intestinal stem cell niche in vivo. Stem cell reports *2*, 127-134.

Sangiorgi, E., and Capecchi, M.R. (2008). Bmi1 is expressed in vivo in intestinal stem cells. Nat Genet *40*, 915-920.

Sato, N., Meijer, L., Skaltsounis, L., Greengard, P., and Brivanlou, A.H. (2004). Maintenance of pluripotency in human and mouse embryonic stem cells through activation of Wnt signaling by a pharmacological GSK-3-specific inhibitor. Nature medicine *10*, 55-63.

Sato, T., Iwano, T., Kunii, M., Matsuda, S., Mizuguchi, R., Jung, Y., Hagiwara, H., Yoshihara, Y., Yuzaki, M., Harada, R.*, et al.* (2014). Rab8a and Rab8b are essential for several apical transport pathways but insufficient for ciliogenesis. J Cell Sci *127*, 422-431.

Sato, T., Mushiake, S., Kato, Y., Sato, K., Sato, M., Takeda, N., Ozono, K., Miki, K., Kubo, Y., Tsuji, A.*, et al.* (2007). The Rab8 GTPase regulates apical protein localization in intestinal cells. Nature *448*, 366-369.

Sato, T., van Es, J.H., Snippert, H.J., Stange, D.E., Vries, R.G., van den Born, M., Barker, N., Shroyer, N.F., van de Wetering, M., and Clevers, H. (2011). Paneth cells constitute the niche for Lgr5 stem cells in intestinal crypts. Nature *469*, 415-418.

Sato, T., Vries, R.G., Snippert, H.J., van de Wetering, M., Barker, N., Stange, D.E., van Es, J.H., Abo, A., Kujala, P., Peters, P.J.*, et al.* (2009). Single Lgr5 stem cells build crypt-villus structures in vitro without a mesenchymal niche. Nature *459*, 262-265.

Schulte, G. (2010). International Union of Basic and Clinical Pharmacology. LXXX. The class Frizzled receptors. Pharmacol Rev *62*, 632-667.

Schulte, G., and Bryja, V. (2007). The Frizzled family of unconventional G-protein-coupled receptors. Trends Pharmacol Sci *28*, 518-525.

Schwartz, S.L., Cao, C., Pylypenko, O., Rak, A., and Wandinger-Ness, A. (2007). Rab GTPases at a glance. J Cell Sci *120*, 3905-3910.

Seabra, M.C., Mules, E.H., and Hume, A.N. (2002). Rab GTPases, intracellular traffic and disease. Trends in molecular medicine *8*, 23-30.

Seaman, M.N. (2005). Recycle your receptors with retromer. Trends in cell biology *15*, 68-75.

Silhankova, M., Port, F., Harterink, M., Basler, K., and Korswagen, H.C. (2010). Wnt signalling requires MTM-6 and MTM-9 myotubularin lipid-phosphatase function in Wnt-producing cells. Embo J *29*, 4094-4105.

Stefater, J.A., 3rd, Lewkowich, I., Rao, S., Mariggi, G., Carpenter, A.C., Burr, A.R., Fan, J., Ajima, R., Molkentin, J.D., Williams, B.O.*, et al.* (2011). Regulation of angiogenesis by a non-canonical Wnt-Flt1 pathway in myeloid cells. Nature *474*, 511-515.

Stenmark, H. (2009). Rab GTPases as coordinators of vesicle traffic. Nature reviews Molecular cell biology *10*, 513-525.

Sun, Y., Chiu, T.T., Foley, K.P., Bilan, P.J., and Klip, A. (2014). Myosin Va mediates Rab8A-regulated GLUT4 vesicle exocytosis in insulin-stimulated muscle cells. Molecular biology of the cell *25*, 1159-1170.

Takada, R., Satomi, Y., Kurata, T., Ueno, N., Norioka, S., Kondoh, H., Takao, T., and Takada, S. (2006). Monounsaturated fatty acid modification of Wnt protein: its role in Wnt secretion. Dev Cell *11*, 791-801.

Takeda, N., Jain, R., LeBoeuf, M.R., Wang, Q., Lu, M.M., and Epstein, J.A. (2011). Interconversion between intestinal stem cell populations in distinct niches. Science *334*, 1420-1424.

Tamai, K., Semenov, M., Kato, Y., Spokony, R., Liu, C., Katsuyama, Y., Hess, F., Saint-Jeannet, J.P., and He, X. (2000). LDL-receptor-related proteins in Wnt signal transduction. Nature *407*, 530-535.

Tanaka, K., Kitagawa, Y., and Kadowaki, T. (2002). Drosophila segment polarity gene product porcupine stimulates the posttranslational N-glycosylation of wingless in the endoplasmic reticulum. J Biol Chem *277*, 12816-12823.

Tanaka, K., Okabayashi, K., Asashima, M., Perrimon, N., and Kadowaki, T. (2000). The evolutionarily conserved porcupine gene family is involved in the processing of the Wnt family. European journal of biochemistry / FEBS *267*, 4300-4311.

Tetteh, P.W., Farin, H.F., and Clevers, H. (2014). Plasticity within stem cell hierarchies in mammalian epithelia. Trends in cell biology.

Thomas, K.R., and Capecchi, M.R. (1990). Targeted disruption of the murine int-1 proto-oncogene resulting in severe abnormalities in midbrain and cerebellar development. Nature *346*, 847-850.

Tian, H., Biehs, B., Warming, S., Leong, K.G., Rangell, L., Klein, O.D., and de Sauvage, F.J. (2011). A reserve stem cell population in small intestine renders Lgr5-positive cells dispensable. Nature *478*, 255-259.

Tsang, W.Y., Bossard, C., Khanna, H., Peranen, J., Swaroop, A., Malhotra, V., and Dynlacht, B.D. (2008). CP110 suppresses primary cilia formation through its interaction with CEP290, a protein deficient in human ciliary disease. Dev Cell *15*, 187-197.

Vaibhava, V., Nagabhushana, A., Chalasani, M.L., Sudhakar, C., Kumari, A., and Swarup, G. (2012). Optineurin mediates a negative regulation of Rab8 by the GTPase-activating protein TBC1D17. J Cell Sci *125*, 5026-5039.

van Amerongen, R., and Berns, A. (2006). Knockout mouse models to study Wnt signal transduction. Trends Genet *22*, 678-689.

van de Wetering, M., Sancho, E., Verweij, C., de Lau, W., Oving, I., Hurlstone, A., van der Horn, K., Batlle, E., Coudreuse, D., Haramis, A.P.*, et al.* (2002). The beta-catenin/TCF-4 complex imposes a crypt progenitor phenotype on colorectal cancer cells. Cell *111*, 241-250.

van den Heuvel, M., Harryman-Samos, C., Klingensmith, J., Perrimon, N., and Nusse, R. (1993). Mutations in the segment polarity genes wingless and porcupine impair secretion of the wingless protein. Embo J *12*, 5293-5302.

van der Flier, L.G., and Clevers, H. (2009). Stem cells, self-renewal, and differentiation in the intestinal epithelium. Annual review of physiology *71*, 241-260.

van Es, J.H., Haegebarth, A., Kujala, P., Itzkovitz, S., Koo, B.K., Boj, S.F., Korving, J., van den Born, M., van Oudenaarden, A., Robine, S.*, et al.* (2012a). A critical role for the Wnt effector Tcf4 in adult intestinal homeostatic self-renewal. Molecular and cellular biology *32*, 1918-1927.

van Es, J.H., Sato, T., van de Wetering, M., Lyubimova, A., Nee, A.N., Gregorieff, A., Sasaki, N., Zeinstra, L., van den Born, M., Korving, J.*, et al.* (2012b). Dll1+

secretory progenitor cells revert to stem cells upon crypt damage. Nat Cell Biol *14*, 1099-1104.

van Es, J.H., van Gijn, M.E., Riccio, O., van den Born, M., Vooijs, M., Begthel, H., Cozijnsen, M., Robine, S., Winton, D.J., Radtke, F.*, et al.* (2005). Notch/gamma-secretase inhibition turns proliferative cells in intestinal crypts and adenomas into goblet cells. Nature *435*, 959-963.

Wassmer, T., Attar, N., Bujny, M.V., Oakley, J., Traer, C.J., and Cullen, P.J. (2007). A loss-of-function screen reveals SNX5 and SNX6 as potential components of the mammalian retromer. J Cell Sci *120*, 45-54.

Wehrli, M., Dougan, S.T., Caldwell, K., O'Keefe, L., Schwartz, S., Vaizel-Ohayon, D., Schejter, E., Tomlinson, A., and DiNardo, S. (2000). arrow encodes an LDL-receptor-related protein essential for Wingless signalling. Nature *407*, 527-530.

Willert, K., Brown, J.D., Danenberg, E., Duncan, A.W., Weissman, I.L., Reya, T., Yates, J.R., 3rd, and Nusse, R. (2003). Wnt proteins are lipid-modified and can act as stem cell growth factors. Nature *423*, 448-452.

Willert, K., and Nusse, R. (2012). Wnt proteins. Cold Spring Harb Perspect Biol *4*, a007864.

Wong, H.C., Bourdelas, A., Krauss, A., Lee, H.J., Shao, Y., Wu, D., Mlodzik, M., Shi, D.L., and Zheng, J. (2003). Direct binding of the PDZ domain of Dishevelled to a conserved internal sequence in the C-terminal region of Frizzled. Mol Cell *12*, 1251-1260.

Wong, V.W., Stange, D.E., Page, M.E., Buczacki, S., Wabik, A., Itami, S., van de Wetering, M., Poulsom, R., Wright, N.A., Trotter, M.W.*, et al.* (2012). Lrig1 controls intestinal stem-cell homeostasis by negative regulation of ErbB signalling. Nat Cell Biol *14*, 401-408.

Wu, C.H., and Nusse, R. (2002). Ligand receptor interactions in the Wnt signaling pathway in Drosophila. J Biol Chem *277*, 41762-41769.

Yan, K.S., Chia, L.A., Li, X., Ootani, A., Su, J., Lee, J.Y., Su, N., Luo, Y., Heilshorn, S.C., Amieva, M.R.*, et al.* (2012). The intestinal stem cell markers Bmi1 and Lgr5 identify two functionally distinct populations. Proc Natl Acad Sci U S A *109*, 466-471.

Yang, P.T., Lorenowicz, M.J., Silhankova, M., Coudreuse, D.Y., Betist, M.C., and Korswagen, H.C. (2008). Wnt signaling requires retromer-dependent recycling of MIG-14/Wntless in Wnt-producing cells. Dev Cell *14*, 140-147.

Yin, X., Farin, H.F., van Es, J.H., Clevers, H., Langer, R., and Karp, J.M. (2014). Niche-independent high-purity cultures of Lgr5+ intestinal stem cells and their progeny. Nat Methods *11*, 106-112.

Yu, H.M., Jin, Y., Fu, J., and Hsu, W. (2010). Expression of Gpr177, a Wnt trafficking regulator, in mouse embryogenesis. Developmental dynamics : an official publication of the American Association of Anatomists *239*, 2102-2109.

Yu, J., Chia, J., Canning, C.A., Jones, C.M., Bard, F.A., and Virshup, D.M. (2014). WLS retrograde transport to the endoplasmic reticulum during Wnt secretion. Dev Cell *29*, 277-291.

Zhai, L., Chaturvedi, D., and Cumberledge, S. (2004). Drosophila wnt-1 undergoes a hydrophobic modification and is targeted to lipid rafts, a process that requires porcupine. J Biol Chem *279*, 33220-33227.

Zhang, P., Wu, Y., Belenkaya, T.Y., and Lin, X. (2011). SNX3 controls Wingless/Wnt secretion through regulating retromer-dependent recycling of Wntless. Cell Res.

Appendix 1

Immunofluorescent staining of intestinal paraffin sections from adult mice

Day 1

1. Dewax tissue slides by warming the slides at 55̊C for 30 minutes

   Prepare blocking solution (1X PBS containing 2% BSA, 2% serum and 0.1% Triton X-100) in the mean time
2. Wash slides in Xylene twice for 10 minutes and 5 minutes respectively
3. Wash slides in 100% ethanol twice for 5 minutes and 2 minutes respectively
4. Wash slides in 95 %, 90%, 80% and 70% ethanol sequentially for 1 minute each
5. Wash slides in water for 1 minute
6. Hold slides in 1X PBS
7. Boil 800ml of 0.01N Citric acid buffer (pH 6) for 5 minutes. Make sure to cover the container with saran wrap while heating it to avoid evaporation
8. Immerse slides in pre-boiled Citric acid solution and boil them for additional 15 minutes
9. Let the slides cool down to ~ 40̊C
10. Rinse slides in running water
11. Put slides in 1X PBS
12. Use pap-pen to enclose the tissue sections of each slide
13. Block the slides in blocking solution for 1.5 hours at room temperature (RT)

14. Incubate the slides in primary antibody (1:200, made in blocking buffer) over night at 4C

Day 2

Protect the slides from exposure to light after application of secondary antibody

1. Wash slides three times in 1X PBS for 10 minutes each
2. Apply secondary antibody (1:200, made in blocking solution) for 2 hours at RT in dark
3. Wash the slides in 1X PBS for 10 minutes each
4. Incubate slides in nuclear stain (Topro-3, 1:300, made in 1X PBS) for 30 minutes
5. Wash slides three times in 1X PBS for 10 minutes each
6. Shake off the PBS from the slides and let the slides dry in dark
7. Mount the slides with Prolonged gold aqueous mounting media

Appendix 2

Immunofluorescent staining of intestinal cryo sections from adult mice

Day 1

1. Thaw the cryo-sections at RT for 15 minutes
2. Wash slides twice with 1X PBS for 5 minutes each
3. Permeabilize tissue sections for 15 minutes with 0.1% Triton X-100 in 1X PBS (PBST) at RT
4. Block slides with 0.1% PBST + 2% BSA + 10% serum at RT for 1 hour
5. Incubate slides in primary antibody (1:200, made in blocking solution) over night at 4̊C

Day 2

Protect slides from exposure to light after application of secondary antibody

1. Wash slides three times in 1X PBS for 10 minutes at RT
2. Apply secondary antibody (1:200, made in blocking solution) for 2 hours in dark at RT
3. Wash slides three times in 1X PBS
4. Add Topro-3 (1:300, made in 1X PBS) for 15 minutes at RT
5. Wash slides twice in 1X PBS for 10 minutes
6. Dry slides and mount with Prolonged gold aqueous mounting media

Appendix 3

GFP tagged protein expression and immunofluorescence staining of cells

Day 1 Seeding

1. Seed Hela or Caco2 cells in wells/chambers or on coverslips (within wells) with MEM, Eagle (10% FBS without P/S) and incubate at 37°C overnight

Day 2 Transfection

1. If/when cells are ~70-80% confluent, proceed to step 2
2. Change the medium (without P/S) of the seeded cells to get rid of the dead cells
3. Transfect cells with the required plasmid using Lipofectamine 2000 (Invitrogen)
4. Allow the cells to grow at 37°C overnight

Day 3 Incubation

1. Change medium (without P/S) for the transfected cells to get rid of the dead cells
2. Allow cells to grow for 24-36 hours (After this period ~ 5% -10% of the cells are mitotic cells)

Day 4 Primary antibody staining (All steps in dark to protect GFP signal)

1. Thaw fresh 4% PFA (pH=7.4) to 37°C in waterbath
2. Remove medium completely from the 4 wells of the chamber. Do not wash the cells

3. Add 500µl of 4% PFA (pH=7.4) directly to each well and incubate at RT in dark for 10 minutes
4. Wash each well with 500µl of 1X PBS twice for 5 minutes each
5. Add 200µl of (PBS+0.1% Triton X-100) to each well and incubate at RT in dark for 10 minutes
6. Add 200µl of (PBS+10% serum) to each well and incubate them at RT in dark for 30 minutes. Do not wash cells
7. Add 200µl of 1:200 dilution of the primary antibody in (1X PBS+10% serum) to each well and incubate overnight at 4°C in dark

Day 5 Secondary antibody staining (All steps performed in dark)

1. Wash each well with 500µl of 1X PBS three times for 5 minutes each
2. Add 200µl of 1:200 dilution of secondary antibody in (1X PBS+10% serum) to each well and incubate for 2 hours at RT in dark
3. After 2 hours of secondary antibody incubation, remove secondary antibody solution from each well in dark. Do not wash the cells
4. Add 200µl of the nuclear stain (Topro-3, 1:300 in 1X PBS) in dark
5. Incubate nuclear stain with the cells for 15 minutes at RT in dark
6. Wash each well with 500µl of 1X PBS three times in dark for 5 minutes each
7. After the third wash keep the chamber slide upside-down onto a paper towel to get rid of the excess PBS. Let it dry in dark

8. Mount the slide/chamber/coverslip with prolonged gold aqueous mounting medium in dark. Seal with nail polish. Keep the slides in cold room in dark, until imaged

Appendix 4

Immunofluorescent staining of intestinal organoids from adult mice

Reagents

- PBS/glycine: 130mM NaCl, 7mM Na_2HPO_4, 3.5mM NaH_2PO_4, 100mM glycine
    - To make 50 ml: dissolve 375mg glycine in 50ml of 1XPBS
    - Filter sterilize the solution
- PBST: 0.5% Triton X-100 in 1X PBS
    - To make 50ml: 250µl of 100% Triton X-100 in 50ml 1X PBS
- 4% paraformaldehyde: 4% PFA in 1X PBS, pH=7.4
    - Freshly prepared immediately prior to each use
- IF Buffer: 130mM NaCl, 7mM Na_2HPO_4, 3.5mM NaH_2PO_4, 7.5mM (0.05%) NaN_3, 0.1% bovine serum albumin, 0.2% Triton X-100, 0.05% Tween-20
    - Filter sterilize the solution
- To make 100ml: 0.1g BSA, 0.2ml of 100% Triton X-100, 50µl of 100% Tween-20, 50µl of 100% NaN_3; bring up the volume with 1X PBS
- Goat serum
- Primary (1:200) and Secondary (1:200) antibodies of choice, antibodies are diluted in blocking solution

All reagents should be used at room temperature and under sterile conditions

Day 1

1. Fix organoids with 4% PFA for 10 minutes at room temperature
2. Rinse wells with PBS/glycine for 5 minutes at RT twice
3. Permeabilize with PBST for 10 minutes at room temperature
4. Block with IF buffer + 10% serum for an hour at room temperature
5. Apply primary antibody in IF buffer + 10% goat serum at room temperature for overnight

Day 2

Following application of secondary antibody, all steps should be performed in dark

1. Wash three times with IF buffer for 10 minutes at RT
2. Add ~120µl of secondary antibody to each well
3. Incubate for 2 hours at RT
4. Wash three times with IF buffer for 10 minutes at RT
5. Add ~120µl of Topro-3 (1:300 in 1X PBS) to each well
6. Incubate in nuclear stain (Topro-3, 1:300 in 1X PBS) for 30 minutes at
7. Wash twice with 1X PBS for 5 minutes each at RT
8. Mount using aqueous based prolonged gold mounting media

Appendix 5

Immunohistochemical staining of intestinal paraffin sections from adult mice

Reagents

- Blocking Buffer (0.1% Triton-X100, 2% BSA in 1xPBS)
- HRP conjugated Vectastain PK-6100 (30µl Reagent A and 30µl Reagent B mixed in 1.5ml blocking buffer)
- Vector 3,3' Diaminobenzidine (DAB) Mixture (2 drops Buffer, 4 drops DAB, 2 drops H2O2 in 5ml MilliQ water)

Day 1

1. Dewax tissue by heating the slides in 55° C for at least 15minutes
2. Wash slides in Xylene solution twice for at least 15minutes and 10 minutes each
3. Rinse slides with 100% ethanol solution twice for at least 5minutes each
4. Rinse slides in 95% ethanol solution for 2 minutes
5. Rinse slides sequentially in 90%, 80% and 70% ethanol, distilled water (DI) and 1X PBS solution for 1 minute each
6. Immerse slides into quenching buffer (2.5ml H_2O_2 in 250ml Methanol), incubate at RT for 20minutes
7. Wash under running DI water for 5 minutes
8. Incubate in 1xPBS for 2 minutes
9. Boil 800ml of 0.01N Citric acid buffer (pH6) for 5minutes, then immerse the slides into pre-boiled citric acid buffer (pH 6) for 15minutes

10. Leave slides in the buffer at RT and let them cool down to about 40C
11. Wash slides in running DI water for 5minutes
12. Give slides a quick rinse in 1xPBS
13. Block slides with Blocking buffer with 2% serum at RT for at least 2 hours
14. Incubate the slides in primary antibody overnight at 4C

Day 2

1. Wash slides in 1X PBS 3 times for 10 minutes each
2. Add secondary antibody (biotinylated anti-Rb IgG 1:200, Vector, 200ul/slide), incubate the slides at RT for at least 2 hours
3. Wash slides in 1X PBS for 3 times for 10 minutes each
4. Apply HRP conjugated Vectastain PK-6100 to the slides and incubate the slides at RT for 2 hours
5. Wash the slides in 1X PBS 3 times for 10 minutes each
6. Develop the stain with DAB buffer by checking under light microscope
7. Wash in running DI water for 5minutes
8. Immerse the slides sequentially into 70%, 80%, 90%, 95% and 100% ethanol solution for 2minutes each
9. Leave the slides in 100% ethanol for additional 2 minutes
10. Immerse slides in Xylene solution twice for 5 minutes each
11. Let the slides dry and mount the slides with xylene based mounting media

Appendix 6

Lentiviral knockdown of genes in mammalian cells

Reagents/Materials

*Endofree plasmid DNA for***:**

- psPAX2
- pVSVG
- hairpin-pLKO.1 vector

Transfection Reagents:

- Lipofectamine 2000 (Invitrogen)
- OPTI-MEM serum-free media (Invitrogen)
- 293T packaging cells (recommended: passage number < 10)

Cell seeding media: Low-antibiotic 293T growth media (DMEM + 10% FBS + 0.1x Pen/Strep)

- 500 ml DMEM (Dulbecco's Modification of Eagle's Medium; e.g. Mediatech)
- 50 ml FBS (heat-inactivated Fetal Bovine Serum; e.g. Sigma)
- 0.5 ml 100x Pen/Strep (10,000 IU/ml penicillin, 10,000 µg/ml streptomycin; e.g. Invitrogen)

Viral harvest media: High-BSA 293T growth media (DMEM + 10% FBS + 1.1g/100ml BSA + 1x Pen/Strep)

- 500 ml DMEM

- 50 ml FBS
- 16 ml 35g/100ml BSA stock (cell culture-grade Bovine Serum Albumin; Sigma)
- 5 ml 100x Pen/Strep

Alternative viral harvest media: High-serum 293T growth media (DMEM + 30% FBS + 1x Pen/Strep)

- 500 ml DMEM
- 200 ml FBS
- 5 ml 100x Pen/Strep

10 cm tissue culture plates

Polypropylene storage tubes

12ml Ultracentrifuge tube (Beckman)

<u>Lentiviruses packaging and harvest</u>

1. Seed 293T packaging cells at 2x105 cells/ml (10 ml per plate) in low-antibiotic growth media (DMEM + 10% FBS + 0.1x Pen/Strep) in 10 cm plates.

2. Incubate cells for 12 hours (37 °C, 5% CO2). After about 12 hours, the cells should be 80~90% confluent.

3. Transfect packaging cells by following procedure.

a. Prepare a mixture of the 3 transfection plasmids:

- Reagent per 10 cm plate

- packaging plasmid (psPAX2) 2.7 ug
- envelope plasmid (e.g. VSV-G/pMD2.G) 300 ng
- hairpin-pLKO.1 vector 3 ug
- OPTI-MEM to total volume 250 ul

b. Dilute 18ul Lipofectamine 2000 in 230ul OPTI-MEM, Incubate 5 minutes at room temperature.

c. Add the 3 plasmid mix to the diluted Lipofectamine 2000 and mix gently by swirling the tip.

d. Incubate the transfection mix for 20 minutes at room temperature.

e. Carefully transfer the transfection mix to the packaging cells (in low-antibiotic growth media).

The packaging cells can be sensitive to perturbation - take care not to dislodge the cells from the plate. The total volume of transfection mix should be 500ul per plate.

4. Incubate cells for 12 hours (37 °C, 5% CO2).

5. Change media to remove the transfection reagent and replace with 12 ml high-BSA growth media or high serum growth media for viral harvests.

6. Incubate cells for 36 hours (37 °C, 5% CO2).

7. Harvest media containing lentiviruses at 48 hours post-transfection. Transfer media to a polypropylene storage tube. Replace with 12 ml high-BSA growth media or high serum growth media for viral harvests.

8. Repeat viral harvesting every 12-24 hours and replace with 12 ml high-BSA growth media or high serum growth media for viral harvests. Viral titer tends to decrease in later harvests; we typically collect a total of 2-3 time points. After the final harvest, discard the packaging cells. The viral harvests may be pooled as desired.

9. Centrifuge the supernatant containing viruses at 4000 rpm for 10 minutes to pellet any packaging cells that were collected during harvesting. Transfer the supernatant to a sterile polypropylene storage tube.

10. Virus may be stored at 4 °C for short periods (hours to days), but should be frozen at -20 °C or -80 °C for long-term storage. To reduce the number of freeze/thaw cycles, aliquot large-scale virus preps to smaller storage tubes prior to long-term storage.

If increasing the viruses' titer, the supernatant can be ultra-centrifuged (30,000 g) for 2 hours at 4 °C. After ultracentrifugation, the pellet needs to be dissolved into a small volume of blank DMEM (50µl) (4°C, Overnight).